HIDG

CERN/SPSC 87-52
SPSC/T 27
01.12.1987

PERSPECTIVES FOR ULTRA-RELATIVISTIC NUCLEUS-NUCLEUS PHYSICS AT CERN IN THE 1990's

Report to the CERN SPS Committee by the Heavy Ion Discussion Group

Editors: G.W. London (Saclay/SPSC), N.A. McCubbin (RAL/SPSC), R. Stock (GSI/Frankfurt)

TABLE DES MATIERES

I- INTRODUCTION

In the summer of 1986 the CERN SPS Committee (SPSC) established several working-groups, in some cases jointly with the CERN PS Committee, to review and report on a variety of physics topics and how they might be studied at CERN in the next 5 years.

This document is the report on ultra-relativistic nucleus-nucleus physics, which is a new field of study at CERN. It has come into being thanks to the generosity of the Gesellschaft fur Schwerionenforschung (GSI) of the Federal Republic of Germany, and of the Lawrence Berkeley Laboratory, USA, who paid for the source, built by R. Geller (Grenoble), and the radio-frequency quadrupole pre-accelerator (RFQ). The project also relied on the usual wizardry of the CERN accelerator teams who were able to couple this source into an old Linac (Linac 1) and thence into the PS-SPS complex.

The project was approved as an exploratory one of two 17-day running periods, one in December 1986 and the second in the fall of 1987. The original source was capable of producing O^{16} ions which were then accelerated up to 200 GeV/nucleon. The running in 1986 was done mainly at this energy, a smaller fraction being devoted to 60 GeV/nucleon. For the 1987 run, which is just finished at the time of writing, the source was upgraded to S^{32}.

Physicists have shown enormous interest in this field. More than 300 physicists are participating in the experiments, a substantial number coming from the field of low energy heavy ion physics, and so are newcomers to CERN. The experimental effort consisted of five large experiments, and a host of smaller ones which usually involved emulsions. A further major experiment, using the Omega spectrometer, was approved for 1987.

The two members of the SPSC charged with reviewing the future of heavy ions proceeded by convening a series of meetings with representatives of the heavy ion community. A list of those who participated in these meetings, the Heavy Ion Discussion Group, is given in Appendix I. It should be noted that this group first started meeting before the 1986 run had taken place. The first results from O^{16} beams are now available, and so conjectures and extrapolations are on a more solid basis.

The aim of this program is the study of the space-time development of partonic/hadronic interactions in nuclear volumes under extreme conditions of energy density and baryon density. Bigger nuclei and higher energies enable us to explore these two variables over a very wide range selectively, exploring non-equilibrium and equilibrium aspects of nuclear matter. While we have studied the strong interaction of elementary particles over a large energy domain, we have not yet studied in parallel strongly interacting systems at high energy density and high baryon density. The thermodynamics of very dense matter is largely an unexplored field.

One may ask what happens when nuclear matter is compressed to a density far higher than that of normal nuclear (or hadronic) matter. Given that we know that nucleons are composite objects of quarks, anti-quarks and gluons, one might anticipate that at some point a description in terms of nucleons would break down. Experimentally, the only way to achieve a high density is through sufficiently violent collisions between nuclei.

These conjectures have been put on a firmer theoretical foundation in the framework of lattice QCD calculations [I.1]. QCD in fact predicts two "phase transitions" from normal hadronic matter. One is the transition to a "quark deconfinement" phase in which large numbers of quarks, anti-quarks, and gluons exist in an extended volume without being bound into normal hadrons. This is the state of no hadronic identity alluded to above. The second transition is to a state of "chiral symmetry" in which all quarks become effectively massless. Calculations suggest that these two transitions in fact coincide, or nearly so.

Furthermore, there are two independent routes to high energy density. One is simply to compress nuclear matter, thus increasing also the baryon density, and the other is to pump energy into it, i.e. to heat it. The theoretician's standard phase diagram for strongly interacting matter is shown in Fig. I.1. It is described by two independent variables, the baryo-chemical potential, μ, related to the net (i.e. baryons - antibaryons) baryon density, and by a temperature T which is related to the energy density, ϵ, by $\epsilon \propto T^4$. Lattice gauge calculations give a deconfinement temperature $\simeq$ 200 MeV (at zero net baryon density) with an error of perhaps 20%, and so an energy density which is good to about a factor of 2. The estimates for the critical net baryon density (at zero temperature) vary between 4 and 10 times the nucleon density in ordinary nuclear matter.

Once deconfinement is achieved in a given volume, it is instructive to look at the time evolution of the system. The results of a calculation [I.2] based on the hydrodynamical model including transverse expansion are displayed in Fig. I.2. For purposes of the discussion, suppose that $T_c/T_i = \frac{1}{2}$ (c=confinement, i=initial). At t=1 fm/c, the transverse radius of the deconfining volume is about 8 fm. At subsequent times, this radius decreases and the volume ceases to exist between t=7 and t=10 fm/c.

It is worth noting that the quark deconfinement phase, usually referred to as the quark-gluon plasma, has an analogue in the phenomenon of Debye screening in atomic solids. In Debye screening the usual Coulomb interaction between a nucleus and electron becomes exponentially damped as the total charge density increases, and the electron becomes "free" or deconfined.

It should also be pointed out that modern ideas on the origin of the universe suggest that the universe passed through the quark-gluon plasma phase at some 10^{-6} seconds after the Big Bang. Heavy ion collisions offer therefore the exhilarating possibility of recreating the early universe in a "little bang".

The exploration of the QCD vacuum could have other consequences. In particular, it has been suggested [I.3] that the reason that many conservation laws are only approximate can be attributed to the mechanism of spontaneous symmetry breaking [I.4]. The source of this breaking is most naturally a macroscopic vacuum state and one could consequently be able to change some conservation laws in a volume by varying the energy density in it. A natural way to do this would be with heavy ion collisions.

Of course, from the point of view of an experimentalist, the question is what new physics can be observed when we achieve very high densities over large (i.e. nuclear) volumes. To study this, it is necessary to find some way to connect the measured spectra to the energy density and, eventually, to the temperature, and to connect $d(p-\bar{p})/dy$ to a measure of the chemical potential, where p and $\bar{p}$ refer to protons and anti-protons.

All this argues for a systematic study of ultra-relativistic nucleus-nucleus interactions. In the first place, the present program needs to be extended beyond 1987. In the longer term, continuing from the Oxygen and Sulfur studies at CERN energies, we need to extend the range up to very heavy projectiles, such as Lead, and eventually to much higher energies (Large Hadron Collider, LHC).

In the next chapter of this report we shall review what has been learnt from the experiments so far. In chapter III we describe how the parameters controlling the formation of the quark-gluon plasma depend on the atomic number, A_p, of the projectile nucleus for unequal A collisions. The conclusion is that a significant gain is achieved by having the largest A_p possible. Accordingly, in chapter IV some brief preliminary comments are made on how the original five major experiments are considering tackling Pb beams. Finally, chapter V describes how an injector for Pb beams might be realised.

The proposed Pb injector is of course a substantial item. It involves a new ion-preaccelerator-Linac structure to replace the existing Linac 1 complex. The injector is equipped with a new high charge state ECR (Electron Cyclotron Resonance) source capable of delivering beams up to A about 200 (Pb). No major modifications of the PS or SPS are required. The total cost is about 30 MSfr.

If the LHC were built, then Pb-Pb collisions at 3.2 TeV/nucleon in the centre of mass are perfectly feasible, but this would require a different front-end structure costing approximately an additional 20 MSfr.

We are of course aware of the proposed Relativistic Heavy Ion Collider (RHIC) at BNL, with colliding beams at about 100 GeV/nucleon. However it is not expected that RHIC would be operational before about 1994-95 [I.5], and the fixed-target Pb beam programme could be operational well before that (about 1991) at modest cost. Since the international community interested is this field is finite, it is crucial that the start-up of the CERN Pb beam programme be as soon as possible to exploit fully this new tool. We therefore have an

a) Transverse energy

The violence of the collision is also measured by the transverse energy which is related to the number of participating beam and target nucleons. Very large transverse energy indicates not only that all the beam nucleons have interacted but also that an unusually large number of target nucleons have interacted. These events determine the tail of the ET distribution. It is important to realize that the geometry of the collisions of nuclei plays a large rôle in determining the ET distribution. One can use the well-measured nuclear density distribution of protons, $\rho(r)$, to calculate the overlap integral, $\int (\rho_1+\rho_2)\, dS$, as a function of the number of participating nucleons, assuming the neutron distribution to be similar to the proton. This integral is calculated by IRIS and is displayed in Fig.II.4 for O-W interactions. As we shall see, this figure reflects the main features of the data: a rather flat plateau region until the colliding objects fully overlap, corresponding to central collisions. If one uses the measured density distributions, the tail falls off more gradually, since the tungsten nucleus is non-spherical [II.7]; this effect is not yet in IRIS.

The cross-section, $d\sigma/dET$, has been measured for different targets in the backward hemisphere (Fig.II.5a) [II.8], in the central region (Fig.II.5b) [II.9], and in the forward region (Fig.II.5c) [II.6]. In comparing the predictions to the data, one must remember that there is in general a systematic ET-scale experimental error of the order of 10%.

In addition to comparisons with IRIS, Fig.II.5b shows a comparison to p-Pb data measured in the same apparatus, convoluted 16 times to simulate a central collision. This is of course approximate since the pPb collisions are averaged over all impact parameters while the OPb central collisions are averaged over impact parameters less than the Oxygen radius. One sees that the data are well reproduced; to a certain extent, ET scale errors are minimized.

To determine whether high ET events are due primarily to an increase in multiplicity, as indicated in section II.2., or to an increase also in ET/particle, the latter has been measured in the backward region, near the peak of the ET distribution (vs η). In Fig.II.6a [II.8], the charged multiplicity is plotted vs ET (charged + neutral). We see that there is a linear relationship. This is seen also in the central region, Fig.II.6b [II.6]. The charged contribution to ET is 59% as given by the IRIS physics generator. No striking dependence on ET is observed, giving an $\langle ET \rangle$/charged particle $\simeq$ 350 MeV.

The experimental $1/\langle ET \rangle\, dET/d\eta$ distributions in the backward hemisphere are approximately independent of ET (Fig. II.7). In the tail of the ET distribution for the W target, $(dET/d\eta)_{max} \simeq 100$ GeV at $\eta = 2.4$. A version of the Bjorken formula [II.10], $\varepsilon_{BJ}=(dET/d\eta)/\pi R^2\tau$, can be used to estimate the energy density to be about 3.8 GeV/fm^3, assuming the thermalization time = 1 fm. However, it should be noted that the cylindrical volume used and the thermalization time assumed have large uncertainties.

b) Interaction volume and thermalization

One can measure the hadronization volume by hadronic interferometry which involves the measurement of the normalized one- and two-particle inclusive distributions $P_1(p)$ and $P_2(p_1,p_2)$ for indistinguishable hadrons produced in a reaction. The correlation function, $C(p_1,p_2)=P_2(p_1,p_2)/P_1(p_1)P_1(p_2)$, is then constructed and the small relative-momentum ($|p_1-p_2|\to 0$) correlations are analyzed in terms of a space-time picture of the dynamics. For a distributed source, $\rho(x)$, one has $C \propto \int dx_1 dx_2 \rho(x_1)\rho(x_2)\ P_2$. Using the parametrization of [II.11], one has $\rho(x) \propto \exp(-r^2/R^2)\exp(-t^2/\tau^2)$ where one assumes separable space and time gaussian variables. R and τ are parameters which characterize the space-time emitting volume. Changing to the momentum representation, one has:

$$C(q,q_0) \propto 1 + \lambda \exp(-q^2R^2/2) \exp(-q_0^2\tau^2/2) \quad (II.2)$$

where λ is an empirical parameter which is 1 for an ideal chaotic source, i.e. the complex amplitudes for the two particles have zero expectation value. This parameter can be different from 1 if dynamical effects are present [II.12]. To the extent that λ approaches one, one approaches an equilibrated system.

Since II.2 is no longer Lorentz-invariant, one specifies the frame as the rest system of the number of participating nucleons for average central collisions (N_{proj}=16, N_{targ}=55, see Fig.II.4), y≃2.4. One separates the qR term into perpendicular and longitudinal parts relative to the beam, $(q_pR_p)^2 + (q_1R_1)^2$. This has been fitted [II.3] for central events for negative particles, assumed π^-, in different regions of rapidity, see Fig.II.8 and Table II.1. The maximum likelihood contours for R_p and R_1 show no correlation and are clearly distinct in the two rapidity intervals, Fig.II.9. It must be recalled that the dimensions measured here are those at which the π^- no longer interact.

TABLE II.1. Summary of pion interferometry results in different rapidity intervals

	all y	0.5<y<2	2<y<3
R_p(fm)	4.9 (+0.3)(-0.5)	4.5 +/- 0.5	8.3 +/- 1.2
R_1(fm)	2.7 +/- 0.5	2.8 +/- 0.7	7.0 +/- 1.8
τ(fm/c)	0.1 (+0.8)(-0.1)	0.1 (+1.6)(-0.1)	0.0 (+4.5)(-0.0)
λ	0.41 +/- 0.04	0.47 +/- 0.07	0.89 +/- 0.20

The general trend is towards a large, spherical, chaotic (i.e. thermalized) system in the region of highest energy density ($2<y<3$). It will be interesting to study the trend as a function of the centrality of the collision, in particular in the ET tails.

3 - Possible signatures for plasma formation

It has been conjectured [II.13] that the rising <pT/particle> as a function of dN/dy (or ET) already observed in JACEE cosmic ray events [II.14] would reach a plateau signifying a phase transition, above which <pT> would continue to rise due to a higher initial temperature. Indeed, this relationship is regarded as a possible signature for the existence of a quark-gluon plasma.

Another proposed signal for the quark-gluon plasma is that of strange particles, where hyperons and especially anti-hyperons could be in large relative abundance [II.15]. If the temperature of the this plasma is high enough so that chemical equilibrium is obtained, states containing any number of strange quarks should be equally common. For example the ratio of anti-Ξ^- to antiprotons could be one!

A promising signal for the quark-gluon plasma is the reduction of the Ψ production rate relative to the continuum rate [II.16]. This arises from the inability of charmed quarks in the quark-gluon plasma to form bound states, and the large mass of the Ψ prevents it from being formed later. In addition, there is an argument [II.17] that the suppression is Ψ-momentum dependent since produced $c\text{-}\bar{c}$ pairs which are slow will preferentially reach the Ψ radius <u>within</u> the plasma and therefore not produce the Ψ, while fast pairs have a chance to produce the Ψ outside the plasma.

Preliminary results on these signatures are now presented.

a) <u>pT spectra for charged particles and photons</u>

If there is thermalization, the transverse momentum spectrum, parametrized as $\exp(-pT/T)$, should reflect the temperature at which the particles become non-interacting. For hadrons, and γ from neutral hadron decay, this temperature is that after hadronization and reflects the latter stages of the interaction which are somewhat independent of the early stages. This implies for example that T(hadrons) should be approximately independent of ET. On the other hand, for direct or virtual photons T should reflect more strongly the early stages of the interaction, giving a strong dependence on ET.

In Fig.II.10 [II.8], we observe the transverse momentum spectra (dN/dpT^2) of a) positive and b) negative particles, in the region $1\leq\eta\leq2$, compared to the IRIS prediction for charged pions. A non-exponential behaviour is observed. The negative particle distribution is

dominated by π^-, though some K^- and/or $\bar{p}$ are perhaps present. The positive particle distribution includes perhaps π^+ and K^+, and certainly protons. The flatter distribution is probably due to the latter. The distributions are quite similar to those (not shown) for p-W interactions in the same apparatus.

We are only in the very beginning phase of this type of analysis which clearly requires hadron identification.

In Fig.II.11a, one compares the pW and OW photon pT distributions in the rapidity range $1<y<2$ [II.8]. They are quite similar. In Fig.II.11b, the O-Au and O-C photon pT distributions are shown for a somewhat different rapidity interval, $1.7<y<2.4$ [II.6]. A non-exponential behaviour is observed, like that for the charged particles. The difference in shape between the IRIS prediction, arbitrarily normalized, and the data is puzzling in that IRIS predicts the π^0 distribution quite well as we shall see later.

The comparision of the pT-distribution for photons in this rapidity region with that for π^- is delicate for two reasons: 1) the photons come from neutral hadron decays in a larger rapidity interval than the charged hadrons and 2) the neutral hadron parents include not only π^0 (like π^-) but also η, ω etc. These effects have not yet been taken into account.

In Fig.II.12a, one sees that π^0 are well reconstructed but no η signal is observed; IRIS predicts $\eta/\pi \simeq 7\%$. The resulting π^0 pT distributions, Fig.II.12b, resemble that of charged particles [II.6]. As mentioned above, IRIS reproduces the distribution quite well, with a relative normalization. It was far from obvious that π^0 reconstruction could be done in this high multiplicity environment.

In Fig.II.13 [II.8] the average transverse momentum of positive and negative particles as a function of ET ($-0.1 \leq \eta \leq 2.9$) is plotted. The variation of $\langle pT \rangle$ with ET is less than 10%. No sign of a plateau is visible.

b) Strange particle production

At the time of the writing of this report, one can only say that strange particles are being reconstructed; for example, a clear Λ peak is seen with good resolution in Fig.II.14 (again not obvious a priori) [II.3]. We await further results on this important issue.

c) Ψ suppression

As in the past, the usefulness of electromagnetic probes for new phenomena may be repeating itself.

In Fig. II.15 [II.18], we see the dimuon spectrum where the Ψ peak is quite apparent for events with a) $ET^{em}<28$ GeV and b) $ET^{em}>50$ GeV, where ET^{em} is the transverse energy measured in the electromagnetic calorimeter. A fit is made to the spectrum (1.7-5.3 GeV/c^2) and the

Ψ/continuum ratio is determined for the mass interval, 2.7-3.5 GeV/c^2. A ratio of ratios gives

$$R = [\Psi/\text{continuum}]_{high} / [\Psi/\text{continuum}]_{low} = 0.64 \pm 0.06$$

This reduction in Ψ production relative to the continuum goes in the direction of [II.16]. Such a reduction is not seen in p-U data (not shown) taken with the same apparatus.

The analysis has been made as a function of the dimuon transverse momentum. In Fig.II.16, we see the ratio of dN/dpT vs pT for the Ψ mass region for the two ET samples. The reduction seems most pronounced at low transverse momentum as expected [II.17]. This reduction is not seen in the mass interval from 1.7 GeV/c^2, excluding the Ψ, nor in p-U data in the Ψ region. Though the error bars are large, the effect appears more pronounced at small x_F than at large x_F (not shown).

It must be noted that the A dependences of Ψ and continuum production are different for proton-induced reactions [II.19]. To the extent that these dependences do not change as a function of the ET of the event, we appear to have a real suppression. However, the two ET samples of events are quite different in their average impact parameter. The target nucleus is much more perturbed in the high ET case and thus Ψ absorption could be changed, especially at low pT.

It is thus too early to conclude definitely on this very sensitive and important point.

4 - Tentative conclusions

We are at the beginning of the analysis of the 1986 Oxygen data. The kinds of measurements that have been made are quite varied and the progress has been very rapid.

The measurements which have just been described are relatively straight-forward, allowing the preliminary results to be obtained in a short time. However, the quantities which are sensitive to the the nature of the state are more difficult to measure and results are not yet all available. It is therefore premature to draw definitive conclusions.

The predictions of IRIS have been given in Figs.II.1-3, 5-7 and 10-13. One observes that these data are reproduced quite satisfactorily within the expected 10 to 15%. Most of the first preliminary results seem to be mere extrapolations of p-nucleus physics with additional geometrical effects.

However, the collective effects necessary for thermalization have begun to be observed. The simplest understanding of the experimental Ψ suppression at high ET is that of plasma formation.

In general, we must extend our analysis into the ET tails. This is an exciting and hopefully rewarding task.

Data have just been taken with a Sulfur beam. Compared to the 1986 program, two large experiments should extend the studies to charged hyperons and anti-hyperons.

The systematic study should continue beyond 1987, with similar projectiles in the short run, and with much heavier projectiles in the long run.

III- RELEVANT A-DEPENDENCES IN NUCLEUS-NUCLEUS INTERACTIONS

From the considerations outlined in Chapter 1, it is clear that the formation of the quark-gluon plasma in nucleus-nucleus collisions requires that:

- Sufficient initial longitudinal energy must be deposited in the interaction volume to provide the necessary heating and compression. From lattice gauge theory calculations, the energy density, ε, required for plasma formation is estimated to be $\simeq$ 1.5 - 5 GeV fm^{-3}, a range which reflects theoretical uncertainties and allows some spread in the value of the baryo-chemical potential, μ. This estimate for ε may be compared with the 0.15 GeV fm^{-3} of normal nuclear matter.

- The interaction volume should be large on the scale of the inter-quark distance, the scattering length, and the "screening" distance - in analogy to Debye screening. To observe a phase transition, a property of infinite systems, finite size effects should be made as small as possible.

- The energy pumped into the interaction volume should be confined long enough for a global phase transition to occur.

It is clear then that we are interested in collisions in which the two nuclei collide essentially "head-on", with a large fraction of the initial nucleons being involved in the collision. These collisions are usually referred to as "central" collisions, and, as explained in Chapter II, a convenient signature is a large amount of ET. Collisions at large impact parameter imply a smaller interaction volume, and are thus of less interest.

In Chapter II we mentioned that data from the 1986 Oxygen running has already reached $\varepsilon \simeq 3.8$ GeV fm^{-3} in the tail of the ET distribution, albeit with some model uncertainty. This could already be in the interesting range, but of course energy density is only one of the requirements for plasma formation, i.e. it is necessary but not sufficient.

The uncertainties in the predicted critical energy density and critical net baryon density lead one to the conservative approach that factors of two can be quite important in achieving the necessary conditions with a reasonable cross section.

In this chapter, we shall give the arguments which demonstrate the interest of nuclear beams with large atomic mass even at a small sacrifice of beam momentum/nucleon. We shall try to estimate how the various parameters governing the plasma formation depend on the

projectile mass, A_p. In particular an estimate of the A_p-dependence of the initial energy density, the net baryon density, the initial temperature, and the plasma and mixed phase lifetimes will be given. Specifically we shall be interested in comparing O-Pb, S-Pb, and Pb-Pb collisions.

1 - Simulation of Pb-Pb events and comparison to O-Pb and S-Pb

The Monte-Carlo generator IRIS has already been described. It is worth stressing that the parameters for IRIS are tuned using data from e+e- and pp collisions, and subsequent predictions for p-A_t and A_p-A_t collisions are absolute, with no free parameters, except for the description of the nucleus. It was seen that it gave a good overall description of the main features of the Oxygen data reported so far. Its predictions for S and Pb collisions, in the absence of new physics, can then be treated with some confidence.

TABLE III.1: Comparision of O-Pb, S-Pb and Pb-Pb generated events

	O-Pb	S-Pb	Pb-Pb
ALL IMPACT PARAMETERS with parent hadron decays			
<beam participants>	8	14	53
<target participants>	20	28	53
<ET> GeV	70	115	350
<N charged>	140	220	680
N charged for 1%σ	430	800	3050
dN(charged)/dy at y*=0	35	60	210
<Nbaryons>	30	42	105
CENTRAL COLLISIONS with no parent hadron decays			
% of events	20	16	2
dN(total)/dy at y*=0	100	200	1160
d(B-$\bar{B}$)/dy at y*=0	3.6	7.5	60

Events were generated for O-Pb and S-Pb interactions at 200 GeV/nucleon and Pb-Pb interactions at 160 GeV/nucleon, reflecting the smaller Z/A. To give some feeling for the

experimental difficulties and opportunities, we present in Table III.1 some of the characteristics of the events. Central collisions (cc) are defined as those in which the beam participants > 90% beam nucleons.

In comparing the above results with those for O-Al and O-Ag (not shown), one obtains the empirical formulae

$$[dN/dy]_{cc} = 11.9\ A_t^{0,4} + 7.7\ A_p^{0,94} - 104 \qquad \text{(III.1a)}$$

$$[d(B-\bar{B})/dy]_{cc} = 0.2\ A_t^{0,54} + 0.18\ A_p^{1,09} - 3.7 \qquad \text{(III.1b)}$$

One should note that for $A_p = A_t \geq 90$, $[dN/dy] \propto A^1$, as expected.

Since we are comparing different projectiles with the same heavy target, we shall use the following:

$$[dN/dy]_{cc} \propto A_p^{\ 1} \qquad \text{(III.2a)}$$

$$[d(B-\bar{B})/dy]_{cc} \propto A_p^{\ 1,1} \qquad \text{(III.2b)}$$

2 - Dependence of plasma formation parameters on projectile mass

a) Temperature-time scenario

Let us recall the standard temperature-time scenario (see Fig.III.1):

- the interaction occurs at proper time $\tau \equiv 0$ and the partons are formed at τ_p (which does not appear in the figure since a temperature is not yet defined)
- the partons interact (one must use kinetic theory as a description) and thermalize at τ_i with temperature T_i.
- If this temperature is greater than to the confinement temperature, T_c, the partons remain unconfined. The temperature falls mainly via the longitudinal expansion which can be described by hydrodynamics. This is the pure plasma phase.

- The partons begin to be confined at τ_c (and T_c) via a first order transition and enter the mixed phase. During this phase, further longitudinal expansion occurs, as well as some transverse expansion, at least for Oxygen. See section III.2i.

- At the end of this mixed phase, at τ_h, the partons have all hadronized and we enter the interacting hadron phase.

- At some later time (τ_f) and temperature (T_f), the hadrons are "free-streaming" and are ready to enter our detectors. In this idealized picture, the transverse momentum distribution of the hadrons should reflect T_f, and interferometry should measure the space-time volume at τ_f. In contrast, the pT distribution of real and virtual photons should reflect their formation temperature.

To make use of this scenario we need some dynamical model. Of the various options, we shall use the hydrodynamical model [III.1], noting that the parton model [III.2] and the flux tube model [III.3] give the same A-dependences.

b) Assumptions of the hydrodynamical model

We list the assumptions which we have used to compare different projectiles on the same heavy target (note that [III.1] treated only the equal nuclei case at "infinite energy"):

- identification of the transverse dimensions with the projectile ($\leq$ size of target)

- thermalization

- cylindrical symmetry

- neglect of transverse expansion

- conservation of entropy, i.e. no particle production from τ_i to τ_f

At the end of this chapter, we shall make some comments on these assumptions.

In the next sections, we shall make an estimate of the A-dependences of the initial net baryon density and energy density, of τ_i, T_i, the plasma phase lifetime ($\tau_c - \tau_i$), and the mixed phase lifetime ($\tau_h - \tau_c$).

c) A-dependence of thermalization time and initial temperature

A simple calculation (see Appendix III.1), assuming entropy conservation and neglecting the transverse expansion, gives

$$T_i^3 \tau_i \propto A_p^{**1/3} \qquad \text{(A.III.1)}$$

T_i and τ_i are sensitive to quantum fluctuations which can be ignored if $T_i \tau_i \gg \hbar$. More important for our purposes, the product already has the dimensions of $\hbar$ and is therefore independent of A (∝volume), and a model! Thus $T_i^2 \propto A_p^{**1/3}$ and

$$T_i \propto A_p^{**1/6} \qquad \text{(III.3a)}$$

$$\tau_i \propto A_p^{**-1/6} \qquad \text{(III.3b)}$$

Since the energy density is proportional to T^4, its A_p-dependence is $A_p^{**2/3}$. However, from an earlier analysis [III.6], in which the energy density was given by $(dN/dy)\langle p_t\rangle/\pi R^2 \tau_i$, the A-dependence of the energy density was A**1/3 from $(dN/dy) \propto A$ and $R \propto A^{**1/3}$. The difference is due to the A_p-dependence of τ and $\langle p_t \rangle$ ($\propto A^{**1/6}$) [III.2], which Bjorken took as A-independent.

In specific models [III.4-III.6], one gets $T_i \equiv T_0$ A**1/6 ≃(140-200) A**1/6 MeV and $\tau_i \equiv \tau_0$ A**-1/6 ≃(0.2-1.4) A**-1/6 fermi, which gives for Oxygen, Sulfur and Lead beams, taking the conservative values T_0=140 MeV and τ_0=1.4 fm:

TABLE III.2: Model-dependent values for temperature and proper time at thermalization

	Oxygen	Sulfur	Lead
initial temperature, T_i (MeV)	220	250	340
thermalization time, τ_i (fm)	0.9	0.8	0.6

One must remember that the thermalization times can be limited by kinematics as indicated in section III.2h, in particular for the case of Lead.

d) A-dependence of initial net baryon density

The two independent variables of the phase diagram (Fig.I.1) are temperature and net baryon density. For the latter we make an estimate relative to the ordinary nucleon density in nuclear matter: $n_o \simeq 1/7$ nucleons/fm^3. A simple calculation gives for the central region (see Appendix III.2):

$$d(B-\bar{B})/dV \propto A^{**}0.6 \qquad \text{(A.III.2)}$$

This gives a factor of 4.6 (1.5) for Pb-Pb (S-Pb) relative to O-Pb. For central Pb-Pb collisions, the net baryon density relative to the nucleon density in ordinary matter is

$$d(B-\bar{B})/dV*(1/n_0) = 7 * 60/\pi\tau_i(7.1)^2 = 2.7/\tau_i \qquad \text{(see Table III.1)}$$

Thus for values of $\tau_i \leq 1$ fm (see Table III.2), the baryon density for central Pb-Pb interactions in the central region is at least 2.7 times the ordinary nucleon density.

e) A-dependence of lifetimes of plasma and mixed phases

A simple calculation (see Appendix III.3-4), assuming entropy conservation and neglecting the transverse expansion, gives a plasma lifetime, $\tau_{plasma} \equiv \tau_c - \tau_i$,

$$\tau_{plasma} = \tau_0[(T_0/T_c)^3 A_p^{**}1/3 - A_p^{**}-1/6] \qquad \text{(A.III.3)}$$

Comparing two different nuclei for their plasma lifetimes, we have

$$R \equiv \frac{\tau_{plasma}(A_p)}{\tau_{plasma}(A_p')} \geq (A_p/A_p')^{**}1/3 \quad \text{(neglecting the } A_p^{**}-1/6 \text{ term)}$$

In particular, R_{min}=2.4 (1.3) for A_p=208 (32) and A_p'=16.

The mixed phase lifetime, $\tau_{mixed} \equiv \tau_h - \tau_c$, is

$$\tau_{mixed} \propto A_p^{**}1/3 \qquad \text{(A.III.4)}$$

f) A-dependence of mean free path

The mean free path, $\lambda=1/\sigma n$, is inversely proportional to the parton cross section and the number density of the partons. This is to be compared to the transverse dimension, $R \propto A_p^{**}1/3$. Since $n \propto T^3$, we have therefore (see Appendix III.5)

$$\lambda/R \propto A_p^{**}(-5/6) \qquad \text{(A.III.5)}$$

This gives a reduction of 8.5 (1.8) in the parton mean free path relative to the size of the system in going from Oxygen to Lead (Sulfur) beams.

g) Implications for the di-lepton signal

The production of dileptons is very sensitive to the initial conditions. This is because of the exponential Maxwell-Boltzmann factor exp[-E/T(t)] which must be integrated over the time evolution of the temperature (see Appendix III.6).

Within the context of a given hydrodynamical model [III.6], this type of integral was performed. As we can see in Fig.III.2, the production of dileptons, e.g. around 2 GeV/c^2, is particularly sensitive. At this mass, the plasma phase production dominates the mixed phase by a factor of 4 to 20 depending on initial conditions.

h) Relationship among beam momentum/nucleon, longitudinal beam size and minimal thermalization time

Theoretical treatments have generally considered the case of extreme energies where the γ_{cm} is very high. One then worries about quantum fluctuations, "wee" partons and minimal formation times not given by the geometry [II.8]. However, at CERN energies we are in a regime where geometry still plays a rôle. The beam momentum/nucleon is Z/A 400 GeV/c which gives 200 GeV/nucleon for beam projectiles up to Ca and 160 GeV/nucleon for Lead beams. The γ factors are 10 and 9, respectively, in the nucleon-nucleon system, with longitudinal dimensions of R/γ = 0.3 (Oxygen), 0.4 (Sulfur) and 0.8 fm (Lead). These dimensions give the minimal thermalization time for a plasma formed in A-A collisions at these energies.

i) Comments on assumptions: work to be done

Even though we have restricted ourselves in general to A_p-dependences, there are a number of points which would repay further study:

- Is there thermalization? Some work has begun on this difficult problem in the context of kinetic theory [III.7].

- What is the effect of a lack of plateau in the central region? Perhaps the cylindrical symmetry should be replaced by spherical symmetry as another extreme case. See the pion interferometry results of the previous chapter. It appears [III.8] that for relatively short times, the cooling is slower in the spherical case.

- How does the transverse expansion influence the mixed phase? The setting in of the transverse expansion occurs at a time equal to the radius of the system divided by the speed of sound, which for an ideal gas = $1/\sqrt{3}$, or at $\Delta\tau$=5.2, 6.6 and 12.3 fm for Oxygen, Sulfur and Lead, respectively. Thus the increase is 2.4 for Lead relative to Oxygen.

- What is the effect of entropy production, especially in the mixed phase?

- What is the influence of the limitation on the formation time given by the beam momentum?

- What signals other than di-leptons are affected "exponentially" by increases in the plasma and mixed phases?

- What signals are affected by the large net baryon density?

3 - Conclusion

In Table III.3, we collect all the A_p-dependences discussed in the previous section.

TABLE III.3: Summary of A-dependences for central collisions in the central region

	α for $A^{**}\alpha$	O/Pb factors	S/Pb factors
initial net baryon density	0.6	1.5	4.6
energy density	2/3	1.6	5.5
initial temperature	1/6	1.1	1.5
plasma lifetime	>1/3	>1.3	>2.4
mixed phase lifetime	1/3	1.3	2.4
thermalization time	-1/6	0.89	0.65
confinement time	1/3	1.3	2.4
hadronization time	1/3	1.3	2.4
relative mean free path	-5/6	0.56	0.12
onset of transverse expansion	1/3	1.3	2.4

Whilst the gain from any one of these factors is maybe not overwhelming, they are all trends in the right direction, and, taken together, suggest that a Lead beam will enhance greatly the chance for plasma formation in ordinary central collisions.

IV- EXPERIMENTAL CONSIDERATIONS

1 - Introduction

The primary motivation for the study of ultra-relativistic nucleus-nucleus collisions is the search for a new state of matter: the quark-gluon plasma. However, there is unfortunately no dramatic new particle whose observation can confirm the existence of this plasma. Rather, the expected observable signatures are in terms of the spectra of "old" particles.

The experimental problem is to discern these signatures in collisions which produce hundreds and even thousands of particles. Furthermore, since the laboratory frame is the target rest frame, one centre-of-mass hemisphere is boosted forward to a cone of a few degrees in the laboratory frame. On the other hand, a nice feature of Pb-heavy target collisions is that the beam and target are symmetric, or nearly so. Hence, for general spectra, it suffices to measure in one centre-of-mass hemisphere only, and the backward hemisphere is fanned out over a large solid angle in the laboratory, which eases the experimental problems in a high multiplicity environment.

From the discussion in Chapter III, a physics generator of O-Pb and Pb-Pb events suggests that parameters such as mean multiplicity, transverse energy, dN/dy, etc. increase by a factor of about 5 for 'minimum bias' collisions, and by a factor of about 10 for average 'central' collisions. For example, the mean charged multiplicity in the tail of the transverse energy distribution is estimated to be about 3000 in Pb-Pb collisions, Table III.1. To 'zeroth' order one can say that calorimetry continues to work (the gains may have to be lowered), and tracking detectors, which are already being pushed to the limit in Oxygen collisions, will have to be retracted so that they see an acceptable particle density. This is reflected in the comments from the experiments made below.

Five major experiments have been installed for the exploratory studies of 1986 and 1987. (A sixth large experiment using the Omega spectrometer was approved. It will not be considered further in this chapter.) With the exception of NA38, which is a dedicated di-muon experiment, all the experiments are capable of measuring the general features of heavy-ion collisions in terms of energy flow and multiplicity distributions. In particular they can trigger on "central" collisions by requiring large transverse energy, or roughly equivalently, a low

amount of forward energy. The experiments differ in how they choose to identify and measure particles away from the high density forward cone.

Overviews of the apparatus are shown in Fig.IV.1, and the main features of the experiments are summarized in Tables IV.1 and IV.2. Further details can be found in 'Experiments at CERN 1986' and references therein.

In addition to these five major detectors, a host of small emulsion based experiments has been carried out with Oxygen beams. Some emulsions would surely be exposed to Pb beams, but, since the emulsion technique is not susceptible to significant change, such experiments are not discussed further here.

Obviously the experimental groups have been very busy with the assembly and commissioning of their detectors and the analysis of the first data. It is therefore clear that at this stage their ideas on how to meet the challenge of Pb beams are only beginning to be thought about as the experience of the Oxygen and Sulfur running is absorbed. It is in this spirit that the comments made below should be viewed.

Furthermore, although discussions with representatives of these experiments have made it clear that there is great enthusiasm for Pb beams, nothing written here should be construed as implying any kind of formal commitment by the Institutes involved in the experiments at the present time.

TABLE IV.1: Summary of general features of detectors

Exp	Calorimetry	Chgd Det	Tracking+Magnet	Special Det	Comments
WA80	$\Theta<8$, $\Delta\Phi=2\pi$ granularity 20x20cm2	$1<\Theta<160$	none	Plastic Ball scintillator: measures low energy target fragments $30<\Theta<160$	
	$10<\Theta<20$, $\Delta\Phi=80$ granularity 3.5x3.5cm2				
	$11<\Theta<20$, $\Delta\Phi=10$ granularity 20x20cm2			photons (lead glass)	
HELIOS NA34/2	$6>\Theta$, $\Delta\Phi=2\pi$ granularity 15x15mm2 strips and towers	$\Theta<45$	muon spectrometer behind hadron absorber	emulsion photons (conversion method)	
	$6<\Theta<100$, $\Delta\Phi=2\pi$ granularity 20x20cm2		spectrometer with hadron identification $15<\Theta<45$, $\Delta\Phi=5$		
NA35	$\Theta<12$, $\Delta\Phi=2\pi$ granularity $\Delta\eta=0.2$		streamer chamber in magnetic field		neutral strangeness
NA36	$\Theta<8$, $\Delta\Phi=2\pi$ granularity 5x5cm2		TPC in magnetic field+downstream chambers		charged and neutral strangeness
NA38	$\Theta<45$, $\Delta\Phi=2\pi$ e.m. only granularity $\Delta\eta=0.4$		spectrometer downstream of hadron absorber for muons		high trigger capability $>10^7$/sec

TABLE IV.2: Summary of the Capabilities of the Experiments

	target λ	ET,E flow	Eveto	$\mu\mu$	chgd mult	γ	identified particles
WA80	.005	$2.4<\eta<5.5$ $-1.6<\eta<1.6$	$\pm 0.3°$		$\eta<4.4$	$1.7<y<2.4$	$y<1.6$ π^+p,d,.. $-1.6<y<2.2$ chgd
NA34	.01-.001 x10	$-0.1<\eta<6$	$\pm 1.4°$	$3<y<6$	$0.9<\eta<5$	$1<y<2$	$0.7<y<2$ π,K $.2<y<1.5$ p,$\bar{p}$
NA35	.01	$2.25<\eta<5.9$	$\pm 0.3°$		$0<\eta<3$	$2.3<y<3.5$	$0<y<3$ π^-,Λ,K_s
NA36	.001 x10	$2.3<\eta$ e.m.			$1<\eta<4$		$1<y<4$
NA38	.01 x10	$1.8<\eta<4$ e.m.		$3<y<4$			
EMU					4π		

2 - Preliminary ideas from the experiments

a) WA80

Photon detection in the angular region $10°<\Theta<15°$ is one of the main features of WA80. In order to cope with the increased multiplicity of Pb collisions whilst preserving their single photon resolution, WA80 are considering retracting their photon detector to a distance some 2 to 3 times further away from the target. This detector would also be enlarged appropriately to cover the same solid angle. Given the arrangement of the apparatus this change in the photon detector would then entail pushing back the forward calorimetry by a similar factor and building more modules.

As an alternative, WA80 are considering, in conjunction with other groups, a completely new experiment combining the measurement of low mass di-muons ($M \leq J/\Psi$), forward calorimetry, and tracking in the backward centre-of-mass hemisphere.

b) HELIOS (NA34/2)

The HELIOS experiment would keep the basic design of the experiment, but add new devices to tackle the detection of electron-positron pairs. A RICH device to cover the region $1 \leq \eta \leq 2$ is being studied in prototype version, and could be ready for 1989. For the forward region ($3 \leq \eta \leq 6$) ideas for a "super-TRD" are being discussed, but this could not be ready before 1990.

c) NA35

NA35 would continue to focus on the study of events with the highest energy density, and their calorimetry detectors could be used for Pb beams with no significant change. However, the streamer chamber would be swamped in its present position, and would have to be retracted so that it covers particle production in the 'mid-rapidity' ($\eta \leq 3$) region. Particle identification is feasible in this region and would be added, using scintillator hodoscopes. A Si-strip detector to measure the charge multiplicity distribution is currently under construction for the 1987 run, and would be retracted and enlarged for Pb beams.

NA35 are also considering a completely new experiment in the framework of a larger collaboration.

d) NA36

NA36 have a similar problem to NA35, in that their tracking detector (TPC) must be moved to avoid being swamped. In addition some of the downstream tracking chambers could be upgraded to planar TPCs. The feasibility of a strangeness trigger would be investigated. The coverage of the forward calorimetry would also be increased.

e) NA38

NA38 would aim to preserve the two prominent features of their present di-muon spectrometer: compactness and high-rate capability. The di-muon background from π and K decay goes like the square of the multiplicity, whilst the genuine signal, at least at the Ψ, does not grow as fast. However, in Oxygen collisions NA38 have observed that the background is only 2-3% at and above the Ψ, and so should be manageable even in Pb collisions. (The background to signal might increase to 20-30%.)

NA38 are considering some extensions to the detector in the target region, together with other groups.

V- ACCELERATION OF HEAVY NUCLEI IN THE SPS AND LHC

1 - Basic Requirements and Boundary Conditions

The scheme [V.1] proposed in this chapter for the acceleration of nuclear beams up to mass A=208 (Pb) is an extension of the present nuclear beam acceleration program [V.2]. The pre-accelerator components are:

- High charge state electron cyclotron resonance (ECR) source, made by R. Geller, Grenoble. A first source delivered Oxygen ions for the 1986 run, and the present source produced Oxygen and Sulfur ions for the 1987 run.
- Low velocity transport system, provided by GSI.
- Radio-frequency quadrupole (RFQ) pre-accelerator, supplied by LBL.
- Refurbished CERN Linac I.

At the exit from Linac I ions with Q/A=0.5 have been accelerated to 11.6 MeV/A, and are then injected into the PS Booster, and thence into the PS and SPS.

It should be noted that the present scheme respects two important boundary conditions which serve to minimize cost, effort, and time:

- All pre-accelerator components fit within the space confines of the Linac I area.
- Modifications to the accelerators (Booster, PS, and SPS) are minimized.

As will be seen, the scheme proposed for Lead beams also respects these conditions.

The major constraint on the present solution results from using the old proton Linac 1 which, ideally, can accept only fully stripped ions, such as $^{16}O(8+)$, $^{32}S(16+)$ or $^{40}Ca(20+)$, with Q/A=0.5. In practice a 30% increase of the RF acceleration voltage permits one to accelerate incompletely stripped ions, O(6+), S(12+), Ca(15+), although at the limit of stable Linac 1 operation. These are still very high charge states which, at the required high currents

(about 30μA), represent the state of the art of source technology. Above mass 40 such intensities at Q/A>0.35 cannot be attained. Note that although the number of circulating charges is low ($\simeq 10^9$) in the synchrotrons, the small injection duty factor Linac to Booster ($\simeq 5\times10^{-5}$) and the low transmission source to Booster (0.2) lead to a high instantaneous source current requirement.

The acceleration of heavy projectiles thus calls for replacement of Linac 1 by a structure accelerating ionic species of about 0.15<Q/A<0.2. This range corresponds to Pb(30+) to Pb(40+); it may require some further development of the ECR source technology which is in progress [V.3], and a new RFQ. The new Linac structure constitutes the major cost factor, resulting in the overall option for a high charge state source and a correspondingly short Linac, of about 40-55 MV total acceleration voltage gradient, which will fit into the available space without new building construction. Injection into the PS-Booster will take place at 8 MeV/A, and both the Booster and PS synchrotrons will have to accelerate incompleteley stripped ions. This requires an average vacuum level of 10^{-9} Torr which is available at the PS after the present upgrade program, but calls for a similar effort at the Booster. At the SPS, no additional effort will be required other than implementation of a rebunching (change of RF harmonics) acceleration mode. The top SPS extraction energy for ^{208}Pb will be 175 GeV/A. The new facility will provide external beams of all lighter nuclei as well, with a maximum energy of 225 GeV/A for nuclei up to ^{40}Ca, and external beam intensities of about 5×10^8 ions (Ca) to 10^7 ions/s (Pb). The total cost is about 30 MSF.

The pre-accelerator, Linac, accelerator, and stripping phases are described in more detail in section 2. A possible injector layout and cost are given in section 3, and a possible schedule in section 4. Finally, in section 5 we look rather further into the future, and discuss very briefly the additional requirements on the pre-accelerator for achieving Pb-Pb collisions in the LHC at 3.2 TeV per nucleon in the centre of mass.

2 - Lead Beams in the SPS

As already indicated, in order to fit into the space confines of the Linac I area, a high charge state, relatively low intensity source/injector has to be used in order to keep the Linac structures short and cheap. In other words: no kind of "Unilac" type structure, with low charge state, high current, several stripping stages, various Linac structures etc. may be employed. In the present proposal we assume that the further development of the Geller ECR source should soon produce ionic species like Xe(25+) and Pb(37+) at the level of 50μA instantaneous current (for 150μs). The resulting external beams would thus not exceed an intensity of about 5×10^7 ions/s for Pb, but higher intensities are hardly compatible with

the radiation limitations in the North and West area external beam systems. Furthermore, higher intensities would very quickly saturate the data acquisition rates of the present set of experiments. Higher effective luminosities could still be employed with internal SPS targets, if necessary, because the internal beam luminosity is higher by 5×10^4. Also the external beam intensity could be higher for lighter projectiles, reaching 10^8 ions/s for the Xe isotopes, and about 5×10^8 for Ca.

The total length of Linac structures is then fixed: on the one hand by the input ionic Q/A, and on the other by the minimum energy per nucleon at which the Booster can be injected. Two considerations govern this energy: firstly the stripping efficiency to higher charge states, Ca(20+) to Pb(60+), at injection, and secondly the incident velocity which, with the available RF frequency swing, should produce a reasonable top energy of the Booster acceleration. The latter constraint is not very stringent if one considers the option of re-bunching (change of RF harmonics) in the Booster. The resulting Linac top energy is 6-8 MeV/A. For 8 MeV/A, the required total Linac voltage gradient for Pb (35+) acceleration is 46 MV, resulting in a length of about 20 to 25m. For the Linac, the technical solution could be an Alvarez structure [V.4] or the "pig" structure [V.5]. A superconducting solution, like the Argonne type [V.6] might also be considered. We favour the Alvarez solution (see next section).

A sketch of the injector structure is given in Fig.V.1. The ECR source is followed by a 90° charge state analyzing magnet, a low energy beam line focusing into an RFQ-preaccelerator, and a re-bunching section injecting the Linac. This design is analogous to the presently employed ^{16}O-^{32}S injector but it may require a high RF frequency (perhaps 20 GHz) ECR and certainly a new RFQ designed for the Q/A range of 0.15 to 0.20 encountered in Xe(25+) and Pb(35+) acceleration. Of course, all lighter ions can also be handled by this RFQ in the appropriate charge states, such as Ca(8+).

The Linac is broken up into two sub-units for construction convenience. Furthermore, a future upgrade of this design, to accomplish an order of magnitude intensity increase in connection with LHC (see sect. 5), would imply a different front end structure. This would be matched to the acceptance of the second Linac section, thus maintaining the major element of the first phase.

At the end of the Linac a foil stripper changes the charge state to Xe(44+) and Pb(60+). This beam is injected into the Booster which accelerates the Xe and Pb ions to about 120 to 150 MeV/A. The injection rigidity is above that of 50 MeV protons, in both cases. The extraction rigidity corresponds to that of 1.8 GeV/c protons. The final velocity is $\beta \approx 0.5$. The Booster vacuum has to be upgraded to about 10^{-9} Torr in order for the incompletely stripped ions to survive acceleration with less than 10% loss due to change of charge state [V.7]. This requires conventional measures only (outgassing in situ, more pumps, leak searches etc).

Injecting into the PS at β=0.5 implies using the maximum PS RF frequency swing of about 2. Stripping before injection makes sense for the Xe ions where the efficiency of complete stripping to Xe(54+) is about 50%. For Pb, however, 120 MeV/A is insufficient for complete stripping, and the intensity loss due to distribution over about 6 intensely populated charge states is too high. One will therefore choose not to strip at this stage. The PS vacuum system will be improved in 1987 to about 10^{-9} Torr, and the Xe(42+) and Pb(60+) beams could be accelerated with no more than 10% loss [V.7].

We note here that due to the PS vacuum requirement of 10^{-9} Torr it will be unlikely that heavy ion running could be maintained during the LEP filling periods. The dynamical recovery of the PS vacuum, from the reduced level of electron cycles back to 10^{-9}, is too long for imbedding ions into the SPS LEP filling supercycle. This implies a down-time of about 0.5 hours every 4 hours, assuming that it takes ½ hour to fill LEP and that this is required every four hours.

At extraction from the PS, the rigidity of 24 GeV protons corresponds to energies of 7.7 GeV/A for Xe and 7.0 GeV/A for Pb. These beams will then be transferred to the SPS after complete stripping (>95% efficiency). However, this injection energy is too low for the standard SPS acceleration scheme: the limited SPS RF swing requires 10 GeV/A at injection. A rebunching (change of harmonics) mode of acceleration has to be developed in order to reach the top energies for the heaviest projectiles: 187 GeV/A for Xe and 177 GeV/A for Pb. No rebunching will be required for the lighter ions because they can be accelerated to above 10 GeV/A in the PS. The SPS vacuum is not critical.

The overall pattern of beam intensity in the various acceleration stages may be illustrated for Pb acceleration:

- Source output = 35μA (one ion is 35+)
- Linac transmission 0.5
- Stripping efficiency at 8 MeV/u: 0.17 to Pb(60+)
- Booster injection 60 μs $\simeq 6\times10^{-5}$ efficiency
- Ions in Booster: 3×10^{7}
- Booster, PS, transfer to SPS overall efficiency: 0.5
- 4 PS cycles injected into SPS

---> Final yield: 6×10^{7} ions per SPS cycle

For ^{40}Ca acceleration, an estimated 40μA output of the same source for Ca(8+), and a better stripping efficiency at 8 MeV/u to Ca(20+) - no further stripping occurring - leads to $\geq 5\times10^{8}$ ions per SPS cycle.

SPS extraction energies for Pb will range from about 50 to 177 GeV/A, with about 2 s spill length at the top, and about 8 s at the bottom energy in a 14.5 s supercycle. The

transport of these ions in secondary beam lines appears to pose no problems; see the note by P. Grafstrom in Appendix V.1.

3 - Injector Layout and Cost

For a detailed technical solution of the structure sketched in Fig.V.1 we adopt the study of Haseroth, Lombardi and Weiss [V.4] of CERN which is attached as Appendix V.2 to this chapter. Its main components are an advanced ECR source, an RFQ preaccelerator and an Alvarez Linac.

ECR source: The key to improving the yield for high charge state ions in the ECR is to increase the RF frequency. Stepping up from 10 GHz (present ^{16}O source) to 16 GHz, R.Geller [V.3] obtained an increase of the $^{32}S(12+)$ yield from about 1 to 30 charge μA. Ionic outputs in the Pb region have not been analyzed yet. The present study assumes a source with 30 charge μA output for Pb(35+). RF frequencies of at least 20 GHz will be required to match this goal but overall the intended solution can be considered [V.3] as "state of the art".

RFQ: The RFQ accelerates $^{208}Pb(35+)$ from 15 keV/u up to 0.3 MeV/u. The effective acceleration voltage therefore is 1.8 MV. A 200 MHz solution leads to a length between 3 and 6 meters, indicating the most likely final solution will consist of two or more subsections. Depending on the final choice of Alvarez design, a shorter RFQ section, for 0.15 MeV/u top energy, may also be opted for.

Alvarez: A possible layout is indicated in Fig.V.2 of Appendix V.2: a 2 m RFQ injects at 0.15 MeV/u into a first 7m Alvarez section operating in $2\beta\gamma$ mode, which accelerates Pb(35+) to 1 MeV/u. It is followed by a $\beta\gamma$ structure of 18m length taking the beam up to 8 MeV/u. Both structures operate at 200 MHz, with an accelerating field of 2.5 MV/m. In view of our intention to stay compatible with a possible later "stage 2" solution (for LHC injection) it would be more appropriate to extend the $2\beta\gamma$ part up to 1.5-2 MeV/u or, equivalently, start the $\beta\gamma$ sector at this energy rather than at 1 MeV/u. The reason: in stage 2 one would most likely replace the RFQ and $2\beta\gamma$ structures by a system accelerating high currents of low charge state, Pb 5+ to 10+. Stripping to the range 30^+ to 35^+ with high yield requires about 1.5-2 MeV/u. The $\beta\gamma$ Alvarez - the most expensive component of stage 1 - could then be employed again.

This solution would exceed somewhat the 30m total length limitation imposed by available space at the old Linac 1. However, one might consider to fold up the structure behind the $2\beta\gamma$ section, thus fitting into the space.

The option for 200 MHz implies re-using the existing RF equipment of Linac 1. The total cost of the above design can then be estimated to amount to:

20 GHz ECR..... 3 MSF

200 MHz RFQ (150 keV/u)..... 3

2 $\beta\gamma$ Linac (7 m)..... 6

$\beta\gamma$ Linac (18 m).....14

Booster vacuum upgrade..... 2

---

28 MSF

This estimate is rather conservative because the Linac lengths refer to a 30+ instead of a 35+ charge state of Pb. At this level there is a finite possibility that the 1987 ECR (for ^{32}S) already yields the required 30μ of Pb(30+), eliminating the need for a new source. The "phase 2" compatible solution (Linac break at 1.5 MeV/u) might require an additional 4 MSF.

A superconducting solution could also be developed based on the structures described by Bollinger and Shepard [V.6] for the upgrade of the ANL "Atlas" heavy ion Linac. This design is similar in its use of a high charge state ECR source, which is followed by a sequence of superconducting structures tailored to the increasing ionic velocity [V.8]. We have not pursued this approach in detail because with its average acceleration field of 2-3 MV/m it does not offer significant length saving and, hence, no better cost-effectiveness. Furthermore, the ANL structures are designed for a DC acceleration of an average ionic current of about Q/eμA whereas the injector considered here would only have to deliver this intensity for 100-200 μs, with a 1s repetition rate. The effective RF power dissipation is thus lower by orders of magnitude, which again makes a conventional Alvarez approach simpler and probably more cost and effort-effective.

4 - Possible Schedule

The CERN management and committees should manifest their encouragement to this program by the end of 1987 [V.9]. During 1988, the experiments will continue their analyses of the 1986 Oxygen data and should demonstrate the interest in the extrapolation to higher A_p through their analyses of the 1987 Sulfur data. During this same year, the proposed funding of the Pb injector should become clear. A proposal will be made and the CERN management will then be asked to approve the project. If approved, construction of the various elements should be accomplished during 1989-1990. The first Pb beam for SPS fixed target experiments should be available by 1991.

5 - Nuclear Beams in the Large Hadron Collider (LHC)

A preliminary outlook [V.10] can already be given concerning the possibility to collide nuclei in the LHC at 3 to 4 TeV per nucleon in the center of mass.

Considering a luminosity of $2 \times 10^{26} cm^{-2} sec^{-1}$ to be the minimum reasonable goal, the following scenario might be suggested:

- Provide 10^8 circulating ions per PS cycle
- Inject 15 PS cycles into the SPS at flat bottom
- Transfer 4 such SPS fillings to each LHC ring
- Employ bunched LHC beams, about 30 m bunch spacing (100ns), about 30 cm bunch width. This increases the average luminosity by 100, and is of no importance to the instantaneous event rate because the average number of events per bunch crossing is far below unity.

The stability and life-time of the collider mode (about 20 hrs for protons) has not been calculated yet. See Fig.V.3 for a possible relationship between beam lifetime and luminosity. Of key importance will be the Weizsacker-Williams process of electromagnetic nuclear excitation [V.11]. For Pb on Pb at 3 TeV/A the corresponding nuclear fragmentation cross section has been estimated [V.12] to be of the order of magnitude of 500 barn, i.e. of atomic cross section size, and about 100 times higher than the strong interaction total inelastic cross section. At $L=2 \times 10^{26}$ the beam is thus lost with a rate of 10^5 ions/s due to this process. The number of circulating ions being about 5×10^9, one then expects to reach a lifetime of several hours duration.

The 10^8 PS ions per PS cycle, forseen in this outlook, can be easily obtained from the injector discussed in the previous sections for $A < 100$ nuclei. For Pb collisions in the LHC the injector current has to be increased by a factor of 5 or 10. Alternatively, one might also consider the possibility of RF stacking in the PS, thus accomodating 10 extractions from the Booster. In order not to lose too many ions during the prolonged PS flat bottom period, the PS vacuum might then have to be improved slightly beyond 10^{-9} Torr.

A higher injector current, about 10^8 to 2×10^8 Pb ions per Booster filling, requires a different front-end and, in particular, an additional stripping stage at low energy (with the unavoidable loss of 80-85%) because it is inconceivable that the output of ECR sources could be further increased for $30^+ - 35^+$.

Thus, a source with an output of about 30 particle-μA is required, with a low charge state like 5+. Acceleration to 1.5 MeV/u would require 62.5 MV total voltage, and foil stripping to 30+ at this energy would match to the main ($\beta\gamma$ Alvarez) part of the Linac corresponding to phase I. Obviously, the product of source ionic charge and required additional Linac voltage and length is constant. An appropriate solution [V.13] could consist of a series of Q/A RFQ's, up to 0.2 MeV/u, followed by the Munich IH-type Linac [V.5], which offers highly cost-effective low-β acceleration. The additional cost can be estimated to be 20 MSF.

VI- CONCLUSIONS

As explained in Chapter I, the study of ultra-relativistic nucleus-nucleus collisions is in its infancy. However, we already know from the first results with Oxygen (see Chapter II) that:

- there is nothing very surprising in the gross features of the data except perhaps in the photon pT spectrum in the central region
- the energy densities attained in the central region seem sufficient to produce the quark-gluon plasma, at least in rare events
- there is a tendency towards thermalization in the central region
- the experimentally established suppression of the Ψ relative to the continuum goes in the direction of plasma formation.

These are preliminary results and definite conclusions cannot yet be made. Continuing analyses of the 1986 run and analysis of the 1987 Sulfur run are obviously important. Runs beyond 1987 will surely be necessary.

In Chapter III, we have indicated how the various parameters which govern the plasma formation vary with increased projectile mass. In particular, it has been shown that Pb beams would be significantly better for each of the important parameters, and would therefore offer an enormous advantage overall. We demonstrated this in the context of a specific model, but all models give essentially similar factors. Further confidence will be gained for the scaling laws when the comparison between Oxygen and Sulfur is made.

Lead beams present specific experimental challenges. A first rapid look at the problems posed by Pb interactions indicates that these are not insurmountable.

A specific proposal has been put forth in this document for a Pb injector which looks quite feasible technically, with little necessary R & D, and which represents excellent value for money.

We realize that it may seem somewhat premature to be proposing a significant upgrade at this stage, but the realization of Pb beams will take some time, and if a start is not made soon the opportunity may, effectively, be lost. But the cost is relatively modest, the

advantages of Pb overwhelming, and the time is very ripe. We believe it is a chance which must be seized.

We would like to acknowledge the important contributions of the members of the Heavy Ion Discussion Group, composed of various members of the five major electronics experiments as well as emulsion representatives. In addition we would like to thank J.-P. Blaizot and H.Haseroth.

VII- APPENDIX I: HIDG participants

R. Bock, GSI, FRG, NA35/WA80

M. Faessler, Munich, FRG, NA34

S. Garpman, Lund, Sweden, WA80

P. Grafstrom, CERN, Switzerland, PS

H. Gutbrod, GSI, FRG, WA80

L. Kluberg, Ecole Polytechnique, France, NA38

G.W. London, Saclay, France, NA34 and SPSC

N.A. McCubbin, RAL, UK, SPSC

G. Neuhofer, Vienna, Austria, NA36

A. Oskarsson, Lund, Sweden, WA80

A. Poskanzer, LBL, USA, WA80

G. Romana, Roma, Italy, NA34

A. Sandoval, GSI, FRG, NA35

R. Santo, Munster, FRG, WA80

T. Siemiarasuk, GSI, FRG, WA80

P. Sonderegger, CERN, Switzerland, NA38

H.J. Specht, Heidelberg, FRG, NA34

R. Stock, Frankfurt, FRG, NA35

G. Veneziano, CERN, Switzerland, Theory

C. Voltolini, Strasbourg, France, NA36

W.J. Willis, CERN, Switzerland, NA34

VIII- APPENDIX II: IRIS event generator

IRIS [II.1] is a Monte Carlo generator of nucleon-nucleus and nucleus-nucleus interactions at high energy (≥50 GeV per nucleon for the projectile on a fixed target). The physics basis of the generator is the exchange of colour with a long formation time for hadrons.

The main goal of IRIS is the prediction of what to expect in nucleus-nucleus collisions as a result of a simple extrapolation from nucleon-nucleus collisions, i.e. the situation in which there is no new physics, for the various signals suggested for detecting the quark-gluon plasma: (1)$<p_t>$ of the produced particles; (2)rapidity density fluctuations; (3)lepton pairs; (4)strangeness production, as well as the E_T distribution, considered to measure the centrality of the collision. The predictions of the data have to be done with a single set of parameters.

In IRIS, a nucleus-nucleus collision is an incoherent superposition of elementary collisions at the parton level. Individual collisions are described by the exchange of colour and emission of gluons.

The starting point is the Dual Parton Model as developed by A. Capella and J. Tran Thanh Van. The hadronization of colorless strings is done with the LUND program. To this description of non-diffractive inelastic processes, we have added the diffractive process and hard processes.

There are obvious parameters such as the atomic number, the charge and the momentum of the initial state particles. The other parameters are: a) the total and inelastic p-p cross sections used to compute the number of participating nucleons and the p-nucleus and nucleus-nucleus cross sections. b) the QCD parameter Λ; c) the non perturbative cutoff, Q_0, of Odorico's program; d) the coefficients of the structure functions for low p_t physics; e) the quark and gluon masses; f) the intrinsic p_t of quarks and gluons, important for the E_T distributions; g) the cutoffs for hard scattering; h) the coefficients of the structure functions for hard scattering; i) the parameters of the hadronization are those obtained from the study of e+e- → hadrons at PETRA and are considered to be fixed, except for the diquark production which has been roughly adjusted in order to reproduce the production rate of antiprotons in the central region at the ISR.

IRIS continues to be developed and there are probably ≃10% prediction errors.

It is important to realize that the parameters are quite constrained and unchanged once set by e+e- and p-p collisions.

IX- APPENDIX III: A-dependences in the context of the hydrodynamical model

Let us calculate the number density of non-interacting massless bosons at temperature T. The average number with energy E is $1/[\exp(\beta E)-1]$ where $\beta=1/kT$, k being the Boltzmann constant. The number of states in volume V is $V\, d^3p/h^3$. This gives a density:

$$dn = d(N/V) = d^3p/(hc)^3\ 1/[\exp(\beta E)-1]$$

Integrating, we get

$$n = 4\pi/(hc)^3 \int p^2\, dp/[\exp(\beta E)-1] \qquad \text{or}$$

$$n = 4\pi/(hc)^3\ T^3 \int_0^\infty x^2\, dx/[\exp(x)-1]$$

where the integral is the Riemann zeta function 2! $\zeta(3)$. Therefore

$$n = T^3\ \zeta(3)/\ [\pi^2(\hbar c)^3] \text{ where } \hbar=h/2\pi$$

In the following table, we have listed similar useful relations, derived in the same manner.

TABLE III.4: Some useful thermodynamic relations

per degree of freedom	number density, n	energy density, ε	entropy density, s
non-interacting massless bosons	$\dfrac{\zeta(3)T^3}{\pi^2(\hbar c)3}$	$\dfrac{3\zeta(4)T^4}{\pi^2(\hbar c)3}$	$\dfrac{4\zeta(4)T^3}{\pi^2(\hbar c)3}$
non-interacting massless fermions	$\dfrac{c(3)T^3}{\pi^2(\hbar c)3}$	$\dfrac{3c(4)T^4}{\pi^2(\hbar c)3}$	$\dfrac{4c(4)T^3}{\pi^2(\hbar c)3}$

As can be seen, the zeta function, $\zeta(n)$, for bosons is replaced by a modified function for fermions, $c(n)$. Some values are $\zeta(3)\simeq 1.2$, $c(3)\simeq 0.9$, $\zeta(4)=\pi^4/90\simeq 1.08$ and $c(4)=7\pi^4/720\simeq 0.947$.

For the following, we have taken the gluon degrees of freedom = 16 (8 color states x 2 spin states), the quark degrees of freedom = 24 (3 color states x 2 spin states x 2 flavors x 2 for quarks and anti-quarks) and the hadron degrees of freedom = 3 for pions (surely an underestimate, but unimportant for the A-dependence). Thus, for example, the energy density for a massless parton gas is

$$\varepsilon = \frac{3\zeta(4)T^4}{\pi^2(\hbar c)^3} \quad [\ 16 + 24 \times 7/8\ ] \quad \text{where } 7/8 = c(4)/\zeta(4)$$

1 - A-dependence of thermalization time and initial temperature

For massless bosons, the entropy density is related to the particle density: $s=4n\zeta(4)/\zeta(3)=3.6n$. In particular, for a pion gas (i.e. the final state):

$$n(\pi) = s_f/3.6 \qquad \text{or}$$

$$dN/d\eta = (s_f/3.6)\ dV/d\eta \qquad \text{where } n = dN/dV$$

From cylindrical symmetry, we have $dV=\pi R^2 dz$ and, since $z=\tau_f \sinh\eta$, $dz/d\eta=\tau_f \cosh\eta\simeq\tau_f$ at $\eta\simeq 0$. Therefore

$$dN/d\eta = (s_f/3.6)\ \pi R^2 \tau_f$$

From entropy conservation we have $s_f\tau_f=s_i\tau_i$ and therefore

$$dN/d\eta = \pi R^2 s_i \tau_i/3.6 \qquad \text{or}$$

$$dN/d\eta \propto R^2\ T_i^{\,3}\ \tau_i \qquad \text{since } s \propto T^3$$

For central collisions, $dN/d\eta \propto A_p^{\,1}$, see III.1. Therefore ($R\simeq 1.2A^{**}1/3$):

$$T_i^{\,3}\ \tau_i \propto A_p{}^{**}1/3 \qquad \text{(A.III.1)}$$

2 - A-dependence of initial net baryon density

The initial net baryon density is related simply to the final net baryon rapidity density, which is a measureable quantity, if we again assume no particle production and only longitudinal expansion:

$$d(B-\bar{B})/dV = d(B-\bar{B})/dy * dy/dV$$

As above, we have ($\eta \simeq y$ in the central region):

$$d(B-\bar{B})/dV \simeq d(B-\bar{B})/dy * (1/\pi R^2 \tau_i)$$

$$\propto A_p{**}1.1/(A_p{**}2/3 * A_p{**}-1/6)$$

[for the A_p-dependence of $d(B-\bar{B})/dy$, see III.1]

or, $$d(B-\bar{B})/dV \propto A_p{**}0.6 \qquad \text{(A.III.2)}$$

3 - A-dependence of confinement time: lifetime of plasma phase

If entropy is conserved during the expansion and cooling from the time of initial thermalization to the confinement time, and if we neglect the transverse expansion, we have

$$\tau_i T_i^3 = \tau_c T_c^3$$

Since T_c is fixed, we have

$$\tau_c = \tau_0 (T_0/T_c)^3 A_p{**}1/3$$

where we have used the parametrization of III.2c for τ_i and T_i.

The conservative Oxygen, Sulfur and Lead confinement times are 1.2, 1.5 and 2.8 fm respectively (τ_0=1.4 fm, T_0=140 MeV and T_c=200 MeV)

The plasma lifetime, $\tau_{plasma} \equiv \tau_c - \tau_i$, is

$$\tau_{plasma} = \tau_0 [(T_0/T_c)^3 A_p{**}1/3 - A_p{**}-1/6] \qquad \text{(A.III.3)}$$

4 - A-dependence of hadronization time: lifetime of mixed phase

Likewise, if entropy is conserved during the mixed phase and the transverse expansion is neglected, we have $\tau_h\ s_h = \tau_c\ s_c$. The only difference between the entropy densities, at fixed temperature T_c, is the number of degrees of freedom. Therefore

$$\tau_h = \tau_c\ 37/3 \qquad \text{or}$$

$$\tau_h \propto A_p{**}1/3$$

and the mixed phase lifetime, $\tau_{mixed} \equiv \tau_h - \tau_c$

$$\tau_{mixed} \propto A_p{**}1/3 \qquad \text{(A.III.4)}$$

(Though our arguments do not depend on this, we remind the reader that the factor 37/3 is uncertain maybe by a factor 2.)

5 - A-dependence of mean free path

The mean free path, $\lambda=1/\sigma n$, is inversely proportional to the parton cross section and the number density of the partons, given by

$$n = \frac{\zeta(3)T^3}{\pi^2(\hbar c)^3}\ [\ 16 + 24 \times 3/4\ ] \quad \text{where } 3/4 = c(3)/\zeta(3)$$

This is to be compared to the transverse dimension, $R \propto A{**}1/3$. With $T \propto A{**}1/6$, we have therefore

$$\lambda/R \propto A_p{**}(-5/6) \qquad \text{(A.III.5)}$$

6 - Temperature-time evolution of the di-lepton signal

The exponential Maxwell-Boltzmann factor exp[-E/T(t)] must be integrated over the time evolution of the temperature. For example, in [III.8], an explicit form is given for this integral:

$$d\sigma/[d(P_Tc)^2\ dy\ d(M^2c^4)] = 2\pi\sigma_{in}\alpha^2F(Pc/Mc^2)\Sigma e_q{}^2/(hc)^4 \int V(\tau)\ \exp[-E/T(\tau)]\ d(c\tau)$$

where σ, M, P_T, y, E and P refer to the dilepton

σ_{in} = inelastic nucleus-nucleus cross section

$F(x) = [1 + \arctan(x)(1+x^2)/(2x)]/2$

$T(\tau)$ = time evolution of the temperature

$V(\tau)$ = time evolution of the volume = $\pi R^2 \tau$

α = fine structure constant

Σe_q^2 = sum over charges of different flavors

X- APPENDIX V.1: Note on the possibility to transport Lead ions in SPS secondary beams

Per Grafstrom, CERN

The extracted 200 GeV/nucleon Oxygen beam had a measured contamination of nuclear fragments, when reaching the experiment, on the level of 1-2% [V.14]. This agreed roughly with a calculation based on the flux of fragments produced in material traversed and on surfaces of septa [V.15]. This note addresses the question of contamination if Lead ions instead of Oxygen ions are transported in the secondary beamlines.

A basic ingredient in the calculation for the Oxygen beam was the cross section to create a fragment with Z/A=0.5 in interactions with material in the beamline. The unavoidable material, 2 g/cm^2 Carbon equivalent, is situated in the upstream part of the beamline and thus only fragments with the right Z/A will be transported to the experiments. In the case of Oxygen-Carbon collisions, a cross section of 1 barn was used. Clearly, the geometrical cross section in a Lead-Carbon collision is larger than in an Oxygen-Carbon collision. A simple estimate of the geometrical Lead-Carbon cross section gives roughly 3 barns. However this cross section has to be multiplied with the probability to create a fragment wit the same Z/A as Lead. In order to preserve the Z/A, the Lead nucleus cannot be broken up too much, and only interactions with the outer skin of the nucleus have to be considered. Assuming a skin thickness of 0.5 fm already reduces the geometrical cross section by a factor 10. The beamline can transport fragments with Z/A within a couple per thousand of the nominal Z/A. All other fragments will be lost. In the mass range 120<A<200 there are about 400 isotopes. Of those 400 there are about 30 with an acceptable Z/A. Thus one could guess that the probability is reduced by another factor 10.

From the argument above, it is clear from the point of view of contamination due to nuclear interactions, a Lead beam is even more favourable than an Oxygen.

At high energies and with high Z projectiles like Lead, it is not enough to consider the strong processes. The Coulomb dissociation cross section becomes important. For a 200 GeV/nucleon incident Au ion on a Au target, this cross section is 30 barns [V.15]. Assuming that the cross section for Lead ions is the same and scaling with Z^2 of the target nucleus, one gets a cross section of about 3 barns for Lead on stainless steel. There is 0.6 mm of stainless steel in the beamlines, the only high Z material present. This leads to an interaction probability of 2%. Thus concerning the material in the beamline, the Coulomb dissociation process does not cause a major problem.

Up to now, we have only considered the effect of material in the beamlines. There are also contributions from the surfaces of the septa used to split the beams. These contributions

were calculated for Oxygen [V.16] and found to be less than 1%. In the case of the contributions to fragmentation from strong interactions there is no reason to believe that the situation will be worse using Lead ions, the arguments being the same as developped above in connection with material in the beamlines. For Coulomb dissociation, the situation is however different. There one cannot strongly rely upon the reduction due to different Z/A of the daughter nucleus since the most frequent process is just one nucleon being lost. In the worst case, assuming that every Lead ion interacting with the surface of the septum gives an isotope with an acceptable Z/A, one would get a contamination of roughly 15%. On the other hand, is it of importance if 15% of the beam would be Pb^{207} instead of Pb^{208}?

To conclude, we do not see any major problem in transporting Lead ions in the secondary beamlines instead of Oxygen.

XI- APPENDIX V.2: Feasibility study concerning a possible layout for a Lead-ion injector for the CERN accelerator complex

H.Haseroth, A.Lombardi and M.Weiss, CERN [V.4]

Presented at the 1987 Particle Accelerator Conference

March 16-19, 1987, Washington DC, USA

1 - Abstract

A possible machine layout for acceleration of Lead ions is presented, based on the experience gained with the successful, but painful, acceleration of Oxygen ions in the CERN Linac 1 [V.17].

The scenario consists of an ECR source, an RFQ and an ALvarez Linac. One has tried to optimize the parameters within the restrictions of the space available, keeping in mind the requirements and desiderata of the subsequent machines.

2 - Introduction

After the successful acceleration of Oxygen ions in the complex of CERN accelerators, an interest for acceleration of heavier ions is growing among the community of physicists [V.1]. As a reasonable step forward, one envisages the acceleration of Lead ions, which are to be extracted from an Electron Cyclotron Resonance (ECR) ion source in a rather highly ionized state. The linear accelerators, which follow the ECR ion source must be designed for a charge to mass ratio $q/A^* \geq 1/7$, which means that one expects from the ion source Pb(30+) ions.

The CERN Linac 1 accelerates now O(6+) ions ($q/A^*=0.375$) for the CERN accelerator complex and protons (or H^-) for the LEAR machine. We propose to separate these two operations: for the accleration of Lead ions a special Linac should be built, whereas Linac 1 (or rather its first tank only) would serve exclusively LEAR from another location. The new Linac (Linac 3) could be housed in the old building of Linac 1, extending the possible range of q/A^* from 0.375 to 0.144. The boundary conditions for Linac 3 are:

1. overall length ≤ 35 m

2. final energy/nucleon ≃ 8 MeV/u (minimum energy for injection into the Booster)

3. operating frequency ≃ 200 MHz.

These conditions are imposed by the existing space and by cost effectiveness obtained by using available 200 MHz RF equipment.

3 - General Considerations

To facilitate the choice of parameters for the Pb linear accelerator complex, we proceed as follows:

1. establish a 'reference' layout by choosing some realistic main parameters. The reference layout we start with is schematically represented in Fig.V.4.

2. analyze the reference design by applying approximated analytic formulae (smooth, linear motion) to see the interdependence of various parameters. Change parameters until a reasonable set of values is found.

3. correct the reference layout for the new set of values.

The ECR ion source will be of a similar type like the one used for the O(6+) [V.18], however, the magnetic field will be increased as well as the RF frequency (up to about 30 GHz). The source will then be capable to deliver currents of 30 to 40 μA of Pb(35+) [V.3]. The extraction voltage will be pushed to about 100 kV to provide beams of 15 KeV/u. In what follows, a normalized emittance E_N=1π mm mrad is assumed.

The two accelerators which follow in our reference scheme are the RFQ and the Alvarez Linac. We analyze these accelerators with linear optimization programs, which contain essentially analytic formulae shown below. With a low q/A^* ratio, it is not trivial to find acceptable acceleration and focusing parameters by keeping E_s and B_m in reasonable limits (see formulae V.15 and V.16).

$$\sigma^2_{OT} = B^2/8\pi^2 - \tfrac{1}{2}\sigma^2_{OL} \qquad (V.1)$$

$$\sigma^2_{OL} = [\pi^2\ qe\ AV|\sin(\Phi_s)|]/[A^* m\beta^2 c^2] \qquad (V.2)\ \underline{RFQ}$$

$$B = [\lambda^2\ qe\ xV]\ /\ [c^2\ A^*\ m\ a^2] \qquad (V.3)$$

$$x = 1 - AI_0\ (\omega a/\beta c) \qquad (V.4)$$

$$V = xV + AV\ I_0\ (\omega a/\beta c) \qquad (V.5)$$

$$\Delta W/\Delta z = [\pi\ qe\ AV\ \cos(\Phi_s)]/(2A^*\beta\lambda) \qquad (V.6)$$

$$V^2/a \leq 5\ 10^{-2}\ (MV)^2 cm^{-1} \qquad (V.7)$$

$$\sigma^2_{OL} = [2\pi\ qe\ E_m\ T\ \lambda N^2|\sin(\Phi_s)|]/[A^* m\beta c^2] \qquad (V.8)\ \underline{Alvarez}$$

$$B = [\lambda^2\ qe\ N^2\ x\beta G]\ /\ [c\ A^*\ m\ ] \qquad (V.9)$$

$$+-: \quad x = 4/\pi\ \sin(\tfrac{1}{2}\pi\Lambda) \qquad (V.10)$$

$$++--: \quad x = 8/\sqrt{2}\pi\ \sin(\tfrac{1}{4}\pi\Lambda) \qquad (V.11)$$

$$++{+}{-}{-}{-}: \quad x = 8/\pi\ \sin(\pi\Lambda/6) \qquad (V.12)$$

$$a = SF\{([N\lambda E_N]/\sigma_{OT})\ (1+B/4\pi^2)/(1-B/4\pi^2)\}^{0,5} \qquad (V.13)$$

$$\Delta W = qe\ E_m T\ L\ \cos(\Phi_s)/A^* \qquad (V.14)$$

$$E_s = L_c\ E_m\ \ EF/g \qquad (V.15)$$

$$B_m = G\ (a + 1\ mm) \qquad (V.16)$$

Definitions

σ_{OL}: sync. phase advance/period

σ_{OT}: betatron phase advance/period

V: intervane voltage in RFQ

A: acceleration factor in RFQ

x: focusing factor

B: focusing parameter

a: minimum aperture radius

E_N: normalized beam emittance

I_0: zero order modified Bessel function

Λ: quad. filling factor

N: number of $\beta\lambda$/period

E_m: mean acc. field

T: transit time factor

B_m: magn. flux density at pole type ($\leq$ 1.3T)

L: accelerator length

L_c: cell length

g: gap length

E_s: maximum surface field ($\leq$ 25 MV/m)

SF: safety factor (1.25)

EF: enhancement factor (1.5)

4 - Analysis of the RFQ

We start analyzing the RFQ: low phase advances per period, σ_{0L} and σ_{0T}, are chosen because of the low q/A^*. However, we try not to descend below $\sigma_{0L}=\sigma_{0T}=10°$. The breakdown criterion which is applied is a semiempirical one (equation V.7), derived from [V.19].

The results of computations are presented in Table V.1. Several frequencies have been considered, but it is the 200 MHz which interests us mostly. In fact, with σ_{0T} and σ_{0L} below 15°, solutions can be found. It is interesting to see which portion of the intervane voltage V is needed for acceleration (AV) and which for focusing (xV): it is the latter which predominates; compare formulae V.2, V.3 and V.5.

TABLE V.1: RFQ Parameters

W_{in}=15 KeV/u; W_{out}=300 KeV/u

	f_r (MHz)	A	B	a (mm)	xV (MV)	AVIo (MV)	V (MV)	V^2/a (MV^2cm^{-1}) 10^{-2}	L (m)
σ_{0T}=15° σ_{0L}=15°	200	.39	2.8	3.2	.09	.06	.15	6.8	2.9
	150	.46	2.8	3.7	.06	.06	.12	4.2	4.1
	120	.52	2.8	4.2	.05	.06	.11	3.0	4.9
σ_{0T}=10° σ_{0L}=10°	200	.24	1.9	3.8	.09	.03	.11	3.2	6.3
	150	.29	1.9	4.4	.06	.03	.09	1.8	8.6
	120	.34	1.9	5.0	.05	.03	.08	1.2	10.3

5 - Analysis of the Alvarez

The situation is more complicated with the Alvarez. In order to fit in the available space, the Alvarez length should be $L_A \leq 25$ m. This gives for the accelerating field $E_m T \simeq$ 2.5 MV/m (Φ_s is taken as -30°).

The length of the period of betatron motion depends on the type of focusing: it is $N\beta\lambda$, with N=2(+-), 4(++--) or 6(+++---). The last type of focusing is unusual, but it has also been tried out.

The period of the synchrotron motion is $\beta\lambda$; however, the phase advances σ_{0L} quoted in following tables refer to the same length as σ_{0T}.

With $E_m T$=2.5MV/m one gets $\sigma_{0L} \simeq 30°$; the result for various σ_{0T} and types of focusing are presented in Table V.2. To facilitate the comparison of results, one has always kept the filling factor $\Lambda = \frac{1}{2}$ and the ratio $g/\beta\lambda = \frac{1}{4}$.

From Table V.2 we see that with W_{in}=300 KeV/u none of the solutions is satisfactory, although we came close with +++--- focusing. The situation would improve going to higher injection energies, but then the RFQ gets too long and complicated.

The same calculations are repeated for a lower frequency (150 MHz) and the results presented in Table V.3.

TABLE V.2: Alvarez parameters for f=200 MHz

W_{in}=300 KeV/u, W_{out}=8 MeV/u, E_mT=2.5 MV/m, L=25 m

	σ_{OT} (deg)	a (mm)	G_{in} (Tm^{-1})	B_m (T)	E_{s_1} (MVm^{-1})	T_{in}
	30	3.4	616	2.7	18.9	.79
+-	25	3.7	552	2.6	19.2	.78
	20	4.1	482	2.5	19.7	.76
σ_{OL}=30°	15	4.7	432	2.4	20.5	.73
	10	5.6	392	2.6	22.1	.67
	50	4.3	352	1.9	20.0	.74
++--	40	4.6	315	1.8	20.5	.73
	30	5.2	282	1.7	21.4	.69
σ_{OL}=60°	20	6.2	256	1.8	23.2	.63
	10	8.5	238	2.3	29.0	.51
	60	5.3	217	1.37	21.5	.69
+++---	50	5.6	202	1.33	22.1	.67
	40	6.2	188	1.35	23.1	.65
σ_{OL}=90°	30	7.0	177	1.41	24.9	.60
	20	8.4	168	1.59	28.7	.52

TABLE V.3: Alvarez parameters for f=150 MHz

W_{in}=300 KeV/u, W_{out}=8 MeV/u, $E_m T$=2.5 MV/m, L=25 m

	σ_{OT} (deg)	a (mm)	G_{in} (Tm^{-1})	B (T)	E_s (MVm^{-1})	T_{in}
	30	4.0	357	1.8	18.3	.81
+-	20	4.8	293	1.7	18.9	.79
σ_{OL}=36°	10	6.6	248	1.9	20.6	.78
	50	5.0	211	1.27	19.1	.78
++--	40	5.5	192	1.24	19.4	.77
	30	6.2	175	1.26	20.1	.74
σ_{OL}=72°	20	7.4	162	1.36	21.5	.69
	10	10.3	153	1.73	26.1	.57
	60	6.3	133	0.97	20.3	.74
++----	40	7.35	118	0.99	21.5	.69
σ_{OL}=108°	20	10.0	108	1.20	26.0	.57
	10	13.9	106	1.59	34.8	.43

As expected, with the ++---- focusing one is now comfortably within the limits imposed on B_m. The frequency could be raised somewhat, staying between 150-200 MHz.

A solution where the 200 MHz frequency could be kept is to start with an Alvarez operating in the 2 $\beta\lambda$ mode and returning to the $\beta\lambda$ mode at a somewhat higher energy [V.20]. Such a hybrid structure has been analyzed as follows:

- find lowest W_{in} for the $\beta\lambda$ structure with +- and ++-- focusing; E_s=20 and 25 MV/m, respectively. The bore hole radius a=6mm (a=SFxbeam radius, SF=1.25); $g/\beta\lambda$=¼
- find lowest W_{in} for 2 $\beta\lambda$ structure with +- focusing and other conditions as above
- repeat the two steps with a=7.5mm and SF=1.5. (It is a check how critical the choice of a and SF is.)

The results are grouped in Table V.4 which shows several solutions for Linac 3, one of which is shown in Fig.V.5.

TABLE V.4: Parameters of the hybrid structure

W_{out}=8 MeV(u)

	$2\beta\lambda$			$\beta\lambda$		
E_s (MV m^{-1})	W_{in} (KeV)	L (m)	foc.	W_i (KeV)	L (m)	L_A (m)
	a= 6 mm		SF=1.25			
25	140 140	6.3 3.2	+- ++--	950 550	17 19	23.3 22.2
20	110 110	8.5 4.3	+- ++--	850 480	21.6 24	30.1 28.3
	a= 7.5 mm		SF=1.5			
25	150 150	13.2 5.4	+- ++--	1500 700	15.7 18.5	28.9 23.4
20	120 120	15.8 6.4	+- ++--	1300 600	20.2 23.5	36. 29.9

6 - Discussion

The analysis which was carried out was only a feasibility study, from which it follows that a Pb(30+) Linac could be built in the frame of conditions imposed. This analysis is in a certain respect complementary to [V.1] where the effective shunt impedances ZT^2 for $\beta\lambda$ and 2 $\beta\lambda$ structures were considered. Due to our space limitations we have to find an optimum

compromise between ZT^2 (RF power) and ET (efficiency of acceleration); this has not yet been done. However, ZT^2, also in the worst case (2 $\beta\lambda$ structure at injection), was kept > 10MΩ/m.

To accelerate Pb ions in the CERN accelerator complex, only some minor improvements are necessary for the vacuum of the machines following the Linac 3, as PSB and PS.

It should also be mentioned that the feasibility study showed that $q/A^*=1/7$ is not so critical and that one could go even lower. This is particularly interesting if one requires higher beam intensities which could eventually be supplied by other sources having a lower charge to mass ratio.

7 - Acknowledgement

We thank P.Lapostolle and M.Vretenar for comments and help.

XII- REFERENCES

I.1. H. Satz, Nature 324 (1986) 116 and Asilomar Quark Matter Conference, Nucl.Phys. A461 (1987) 1c and references therein

I.2. G.Baym et al., Nucl.Phys. A407 (1983) 541

I.3. T.D.Lee, Particle Physics and Introduction to Field Theory, Harwood Academic Publishers (1981) 378

I.4. Y.Nambu, Fields and Quanta 1 (1970) 33

I.5. N.P.Samios, July 1987 AGS Users Newsletter

II.1. J.-P.Pansart, Nucl. Phys. A461 (1987) 521c and references therein.

II.2. E.O. Abdrahmanov et al., Z. Phys. C5 (1980) 1

II.3. NA35, Uppsala Conference on High Energy Physics (1987) and Quark Matter VI, Nordkirchen (1987)

II.4. NA36, submitted for publication

II.5. KLM Collaboration, preprint (May 1987)

II.6. WA80, Uppsala Conference on High Energy Physics (1987) and Quark Matter VI, Nordkirchen (1987)

II.7. F.Lamarche and H.H.Thodberg, private communication

II.8. HELIOS (NA34), Uppsala Conference on High Energy Physics (1987) and Quark Matter VI, Nordkirchen (1987)

II.9. A.Bamberger et al., Phys.Lett. B184 (1987) 271

II.10. J.D. Bjorken, Phys Rev D27 (1983) 140

II.11. F.B. Yano and S.E. Koonin, Phys. Lett. 78B (1978) 556

II.12. M. Gyulassy, Phys. Rev. Lett. 48 (1982) 454

II.13. L.Van Hove, Phys. Lett. 118B (1982) 138

II.14. T.H.Burnett et al., Phys. Rev. Lett. 50 (1983) 2062

II.15. P.Koch, B.Mueller and J.Rafelski, GSI 86-7 (1986)

II.16. T.Matsui and H.Satz, Phys. Lett. 178 (1986) 416

II.17. F.Karsch and R.Petronzio, CERN-TH 4699/87

II.18. NA38, Uppsala Conference on High Energy Physics (1987) and Quark Matter VI, Nordkirchen (1987)

II.19. J.Badier et al., Phys. Lett. 104 (1981) 335 and Z. Phys. C20 (1983) 101; P.Bordalo et al., CERN-EP/87-68

III.1. J.-P.Blaizot, Acta Phys. Pol. B18 (1987) 659

III.2. J.-P.Blaizot and A.Mueller, Nucl. Phys. B289 (1987) 861
III.3. A.Kerman, T.Matsui, B.Svetitisky, Phys.Rev.Lett. 56 (1986) 219
III.4. T.Matsui, Nucl.Phys. A461 (1987) 27c
III.5. R.Hwa, K.Kajantie, Phys.Rev.Lett 56 (1986) 696
III.6. P.V.Ruuskanen, Acta Phys. Pol. B18 (1987) 551
III.7. for example, G.Baym, Phys. Lett. 138B (1984) 18
III.8. J.Badier, G.W.London, M.Winter, Saclay preprint DPhPE 82-11 (1982); note that equations A.8 and A.9a must be multiplied by 2 and equation A.9b by 2π
V.1. R.Stock and R.Bock, Univ. Frankfurt preprint 1986
V.2. B.H.Wolf et al., GSI Report 86-2, 1986
V.3. R.Geller, CEN Grenoble, private communication
V.4. H.Haseroth, A.Lombardi, M.Weiss, CERN preprint PS28 (1987)
V.5. U.Ratzinger et al., Proc. 19854 Linac Conference, GSI-84-11, p.220
V.6. L.M.Bollinger and K.W.Shepard, ibid. p.217
V.7. B.Franzke, private communication
V.8. Atlas Uranium Upgrade Project, ANL Report 1986
V.9. See minutes of SPSC, CERN/SPSC 87-44
V.10. J.Gareyte, private communication
V.11. D.Olson et al., Phys. Rev. C24 (1981) 1529
V.12. A.Sandoval, private communication
V.13. N.Angert, private communication
V.14. H.W.Atherton et al., Contamination of nuclear fragments in a 200 GeV/nucleon Oxygen ion beam at CERN, CERN/SPS/87-11 (EBS)
V.15. H.W.Atherton et al., Considerations on providing ion beams to the SPS experimental areas, SPS/EBS/Note 84-8 and CERN/SPSC/84-65
V.16. M.T.Mercier et al., Electromagnetic Dissociation of Au by relativistic heavy ions, Phys. Rev. Lett. 52 (1984) 898
V.17. H.Haseroth et al., "Ion Acceleration in the CERN Linac I", Proc. of the 1986 Linac Acc. Conf. Stanford (USA), 1986
V.18. R.Geller et al., Proc of the 6th Int. Workshop on ECR Sources, Berkeley 1985, PUB-5143, LBL Berkeley, 1985
V.19. H.Daehne, "Sparking Experiments", Proc. of Acc. Aspects of Heavy Ion Fusion, Darmstadt, 1982
V.20. J.Ungrin and J.Klabunde, "A Heavy Ion Replacement for the First Tank of the Old CERN Linac, GSI, 1986

XIII- FIGURE CAPTIONS

Fig. I.1. Phase diagram from ref. [I.1]

Fig. I.2. Temperature distribution as a function of r for cylindrical transverse expansion coupled to longitudinal expansion. Each curve is labeled by the time in fm/c that has elapsed since the collision with τ_i=1.

Fig. II.1. NA35 and NA36: the inelastic nucleus-nucleus cross section as a function of projectile and target masses

Fig. II.2. KLM Collaboration: charged multiplicity vs pseudo-rapidity

Fig. II.3. WA80: a) charged multiplicity vs energy at "zero degrees" for different targets, and b) "zero degree" energy spectra

Fig. II.4. IRIS probability distribution of number of participants

Fig. II.5. ET distributions: a) HELIOS (backward hemisphere), b) NA35 (central region) and c) WA80 (forward region). Note that there are about 10% ET scale errors on the data

Fig. II.6. ET/particle distribution: a) HELIOS (backward region, scale errors about 10%) and (b) WA80 (central region)

Fig. II.7. HELIOS: $dET/d\eta$ vs ET for O-W interactions

Fig. II.8. NA35: Examples of the fits to the perpendicular extent of the pion source in different regions of rapidity (a) 2<y<3, (b) 0.5<y<2 and (c) all y, for Q_0, Q_L < 100 MeV/c.

Fig. II.9. NA35: Likelihood contours for the perpendicular and longitudinal extent of the pion source

Fig. II.10. HELIOS: pT distributions a) positive and b) negative particles

Fig. II.11. pT distributions of photons for a) HELIOS: 1<y<2 and b) WA80: 1.7<y<2.4

Fig. II.12. WA80: (a) π^0 reconstruction and (b) pT spectra for different targets

Fig. II.13. HELIOS: <pT> for charged particles vs ET

Fig. II.14. NA35: Λ mass spectrum

Fig. II.15. NA38: dimuon mass spectrum for a) low ET_{em} and b) high ET_{em}

Fig. II.16. NA38: dimuon pT spectrum for high ET_{em} relative to low ET_{em}

Fig. III.1. Standard temperature-time scenario

Fig. III.2. Sensitivity of di-lepton spectrum to the initial conditions

Fig. IV.1. Overviews of the 5 Major Experiments: a)HELIOS, b)NA35, c)WA80, d)NA36, e)NA38

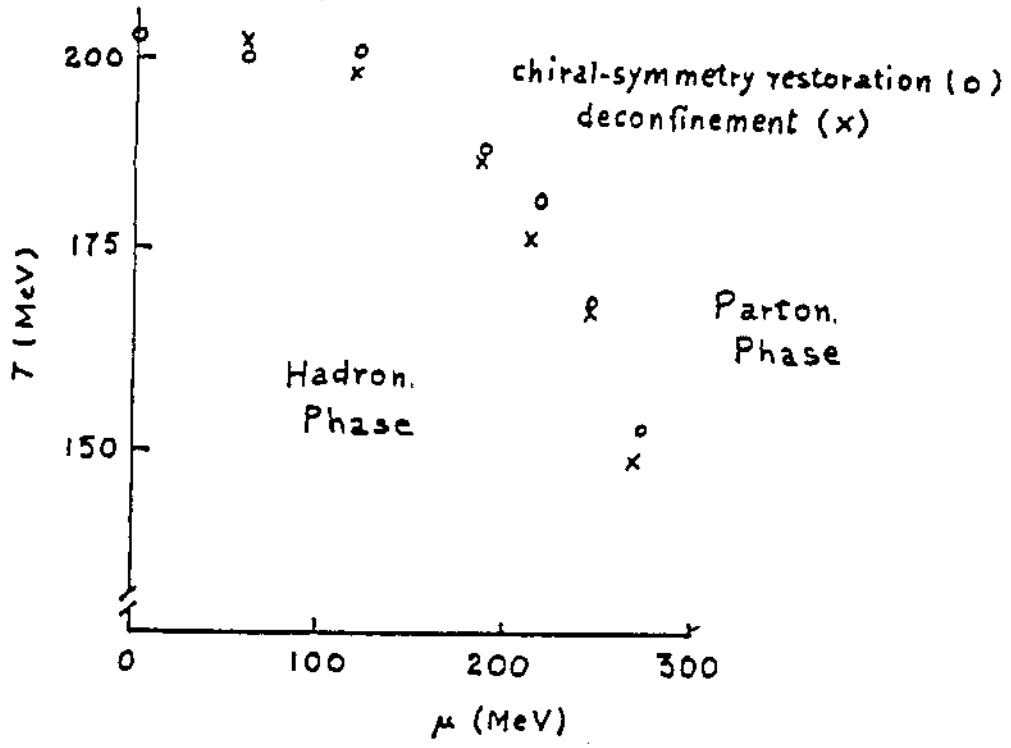
200
175
150
T (MeV)
0
100
200
300
μ (MeV)
chiral-symmetry restoration (o)
deconfinement (x)
Hadron.
Phase
Parton.
Phase

FIGURE I.1.

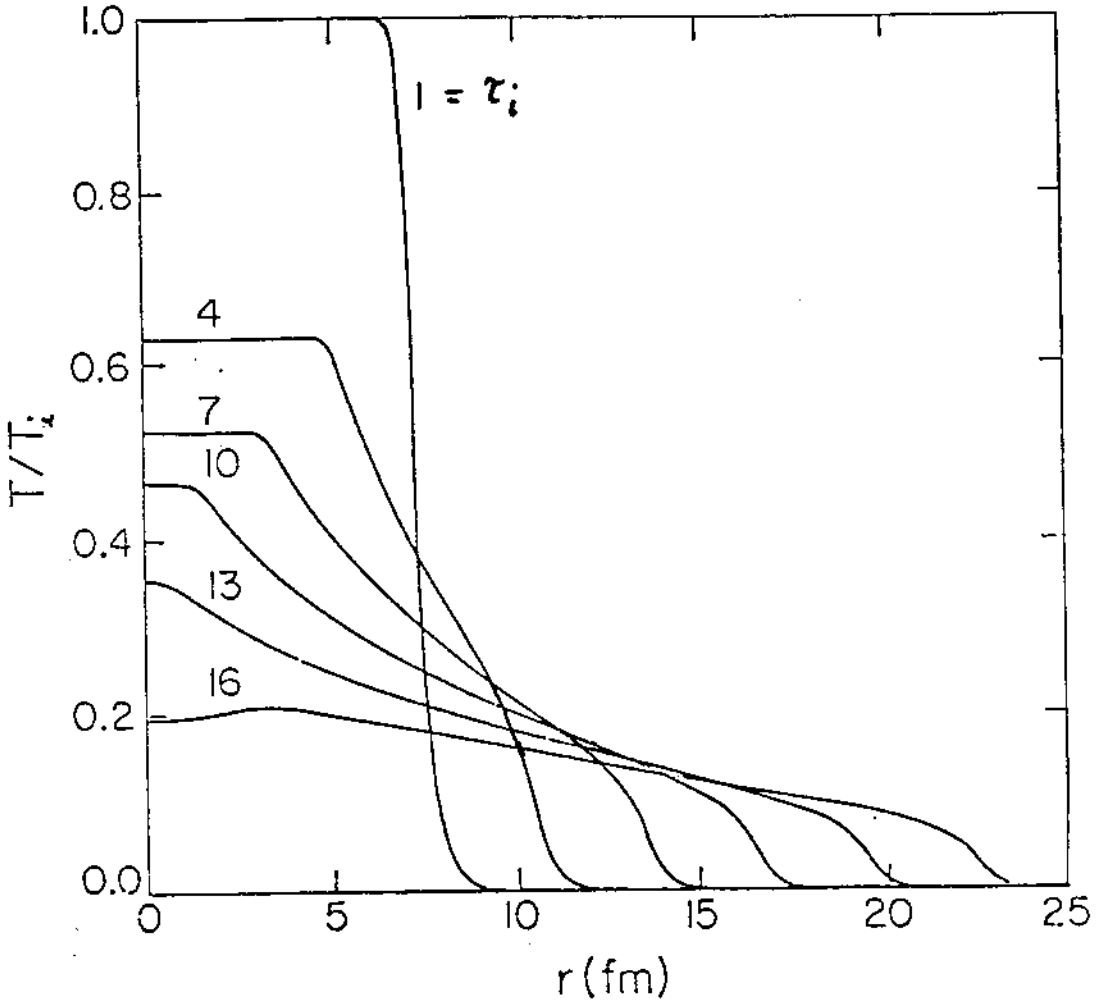

FIGURE I.2.

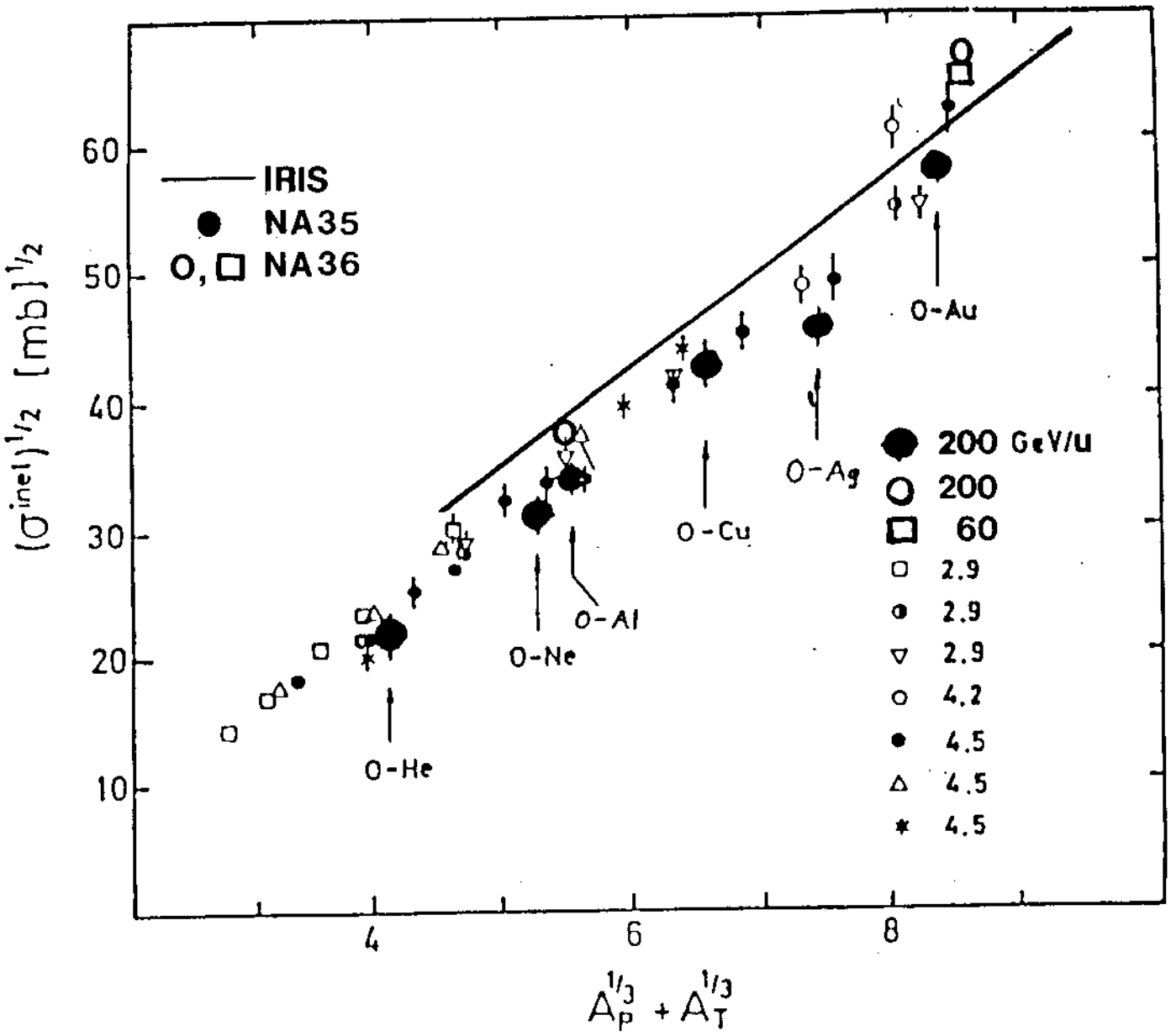
IRIS
NA35
O, NA36
O-He
O-Ne
O-Al
O-Cu
O-Ag
O-Au
200 GeV/u
200
60
2.9
2.9
2.9
4.2
4.5
4.5
4.5
$(\sigma^{inel})^{1/2}$ [mb]$^{1/2}$
$A_p^{1/3} + A_T^{1/3}$
10
20
30
40
50
60
4
6
8

FIGURE II.1.

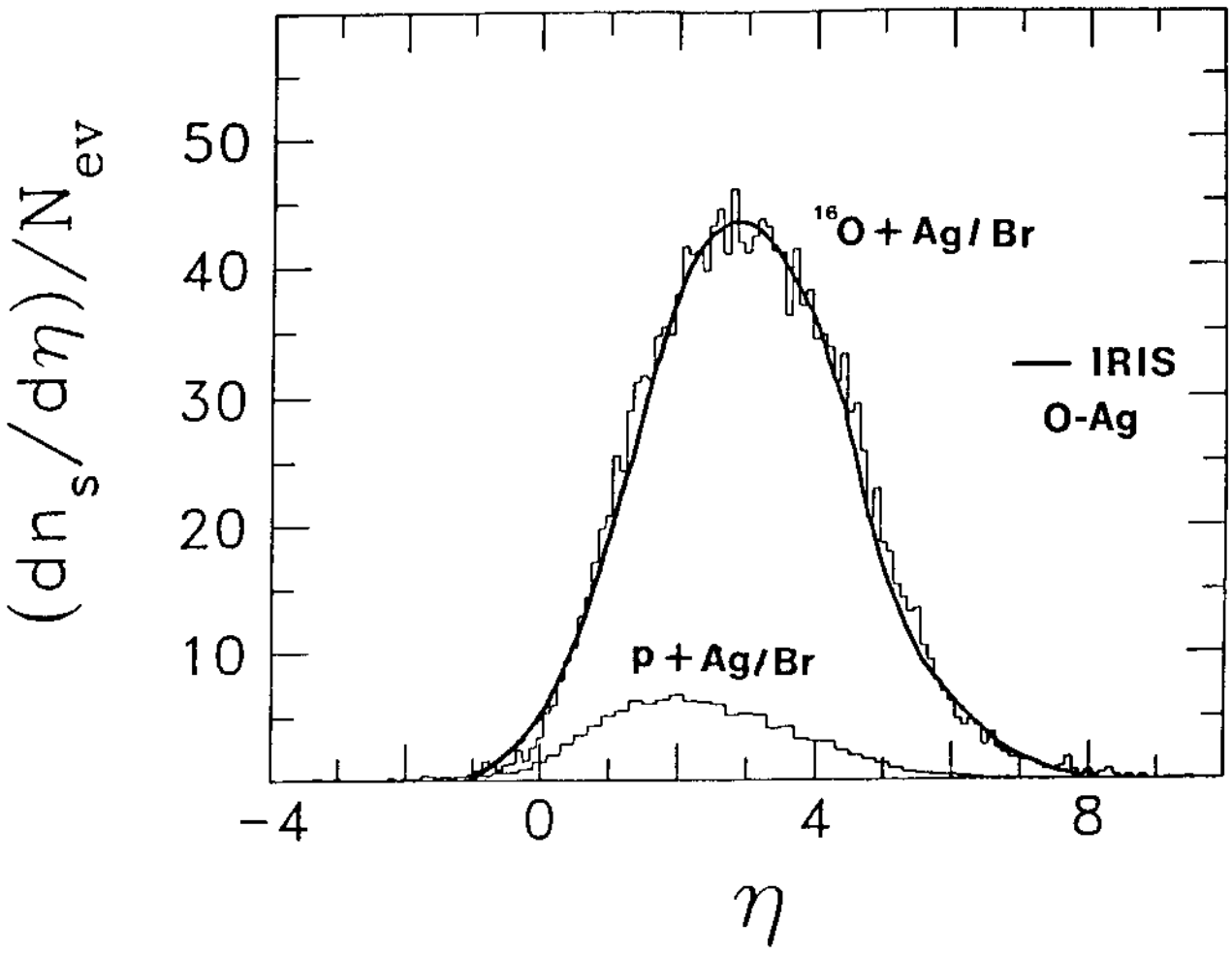

FIGURE II.2

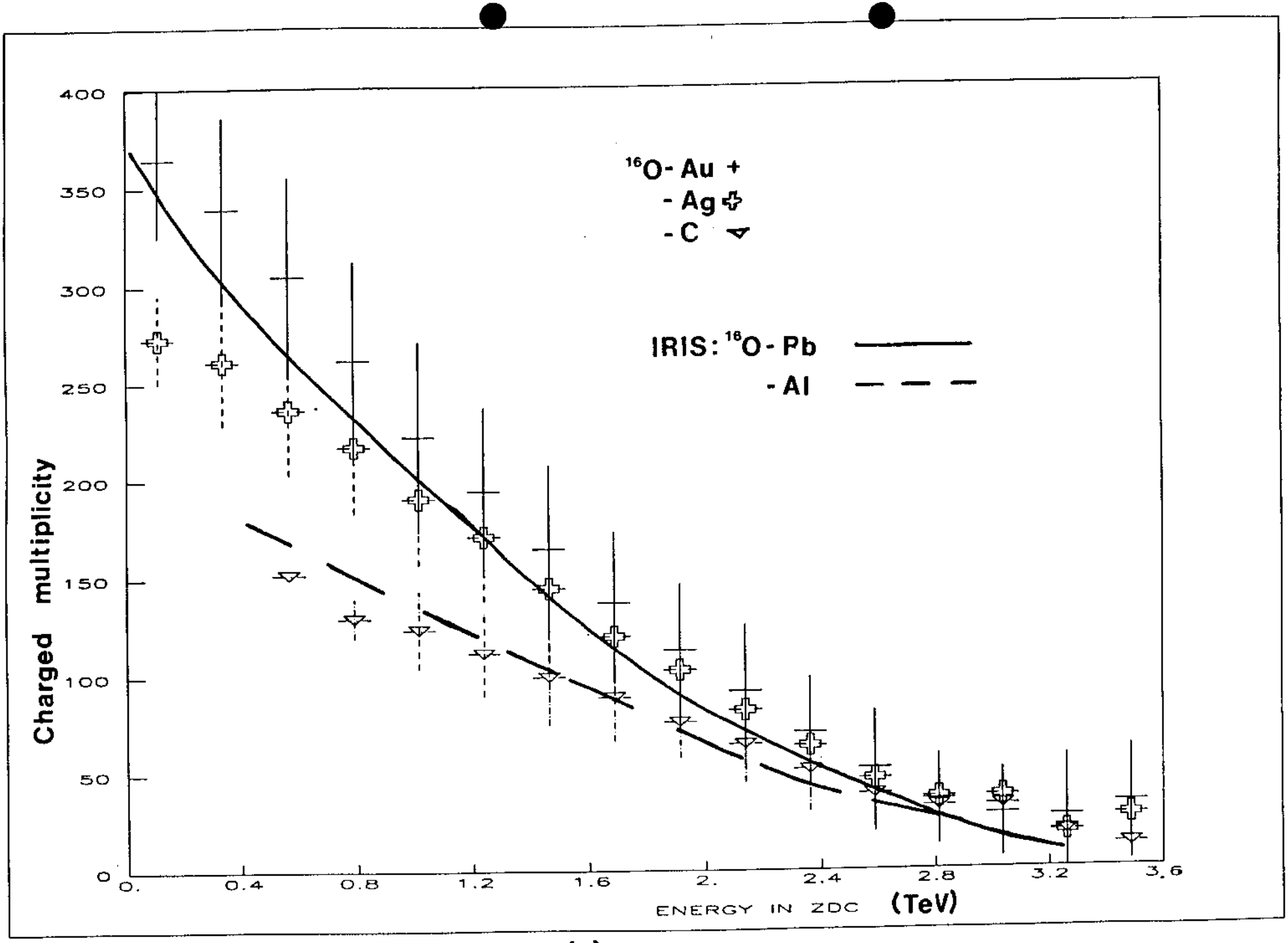
400
350
300
250
200
150
100
50
0
Charged multiplicity
^{16}O- Au +
- Ag
- C
IRIS: ^{16}O- Pb
- Al
0.
0.4
0.8
1.2
1.6
2.
2.4
2.8
3.2
3.6
ENERGY IN ZDC (TeV)

FIGURE II.3. (a)

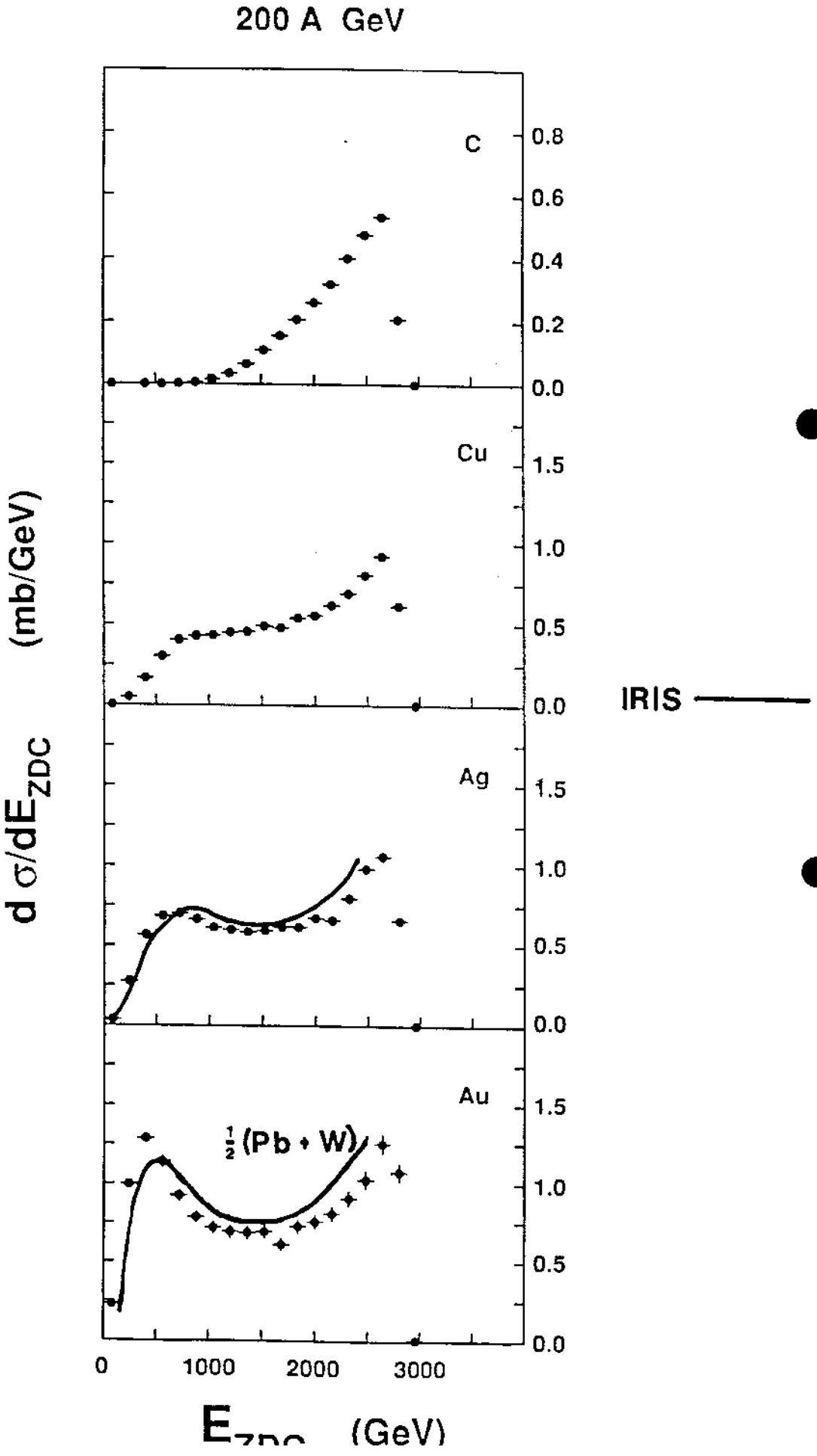
200 A GeV
C
Cu
Ag
Au
0.8
0.6
0.4
0.2
0.0
1.5
1.0
0.5
0.0
½(Pb + W)
IRIS
0
1000
2000
3000
d σ/dE_ZDC (mb/GeV)
E_ZDC (GeV)

^{16}O-W interactions

IRIS PROBABILITY DISTRIBUTION

OF NUMBER OF PARTICIPANTS, P

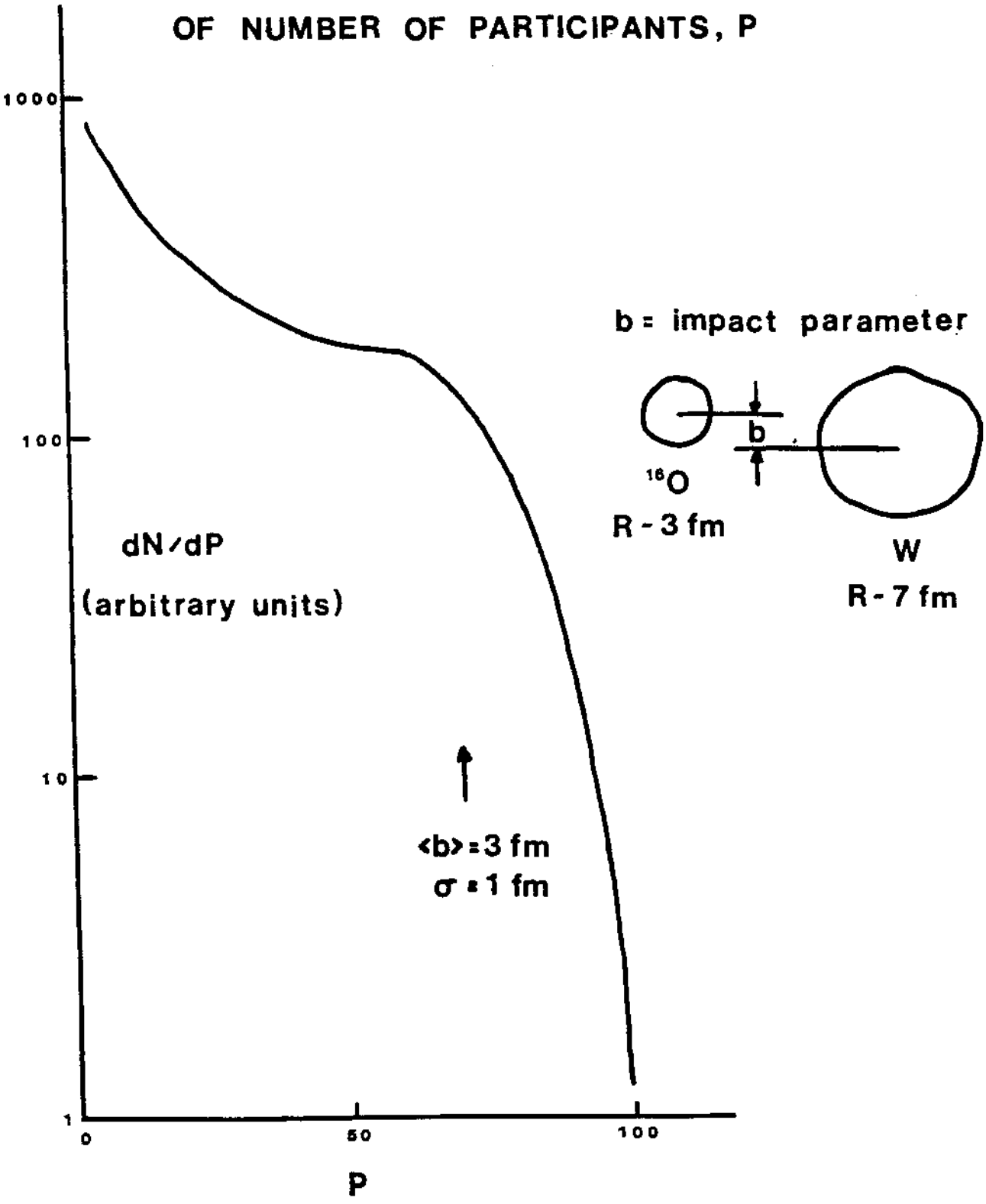

FIGURE II.4

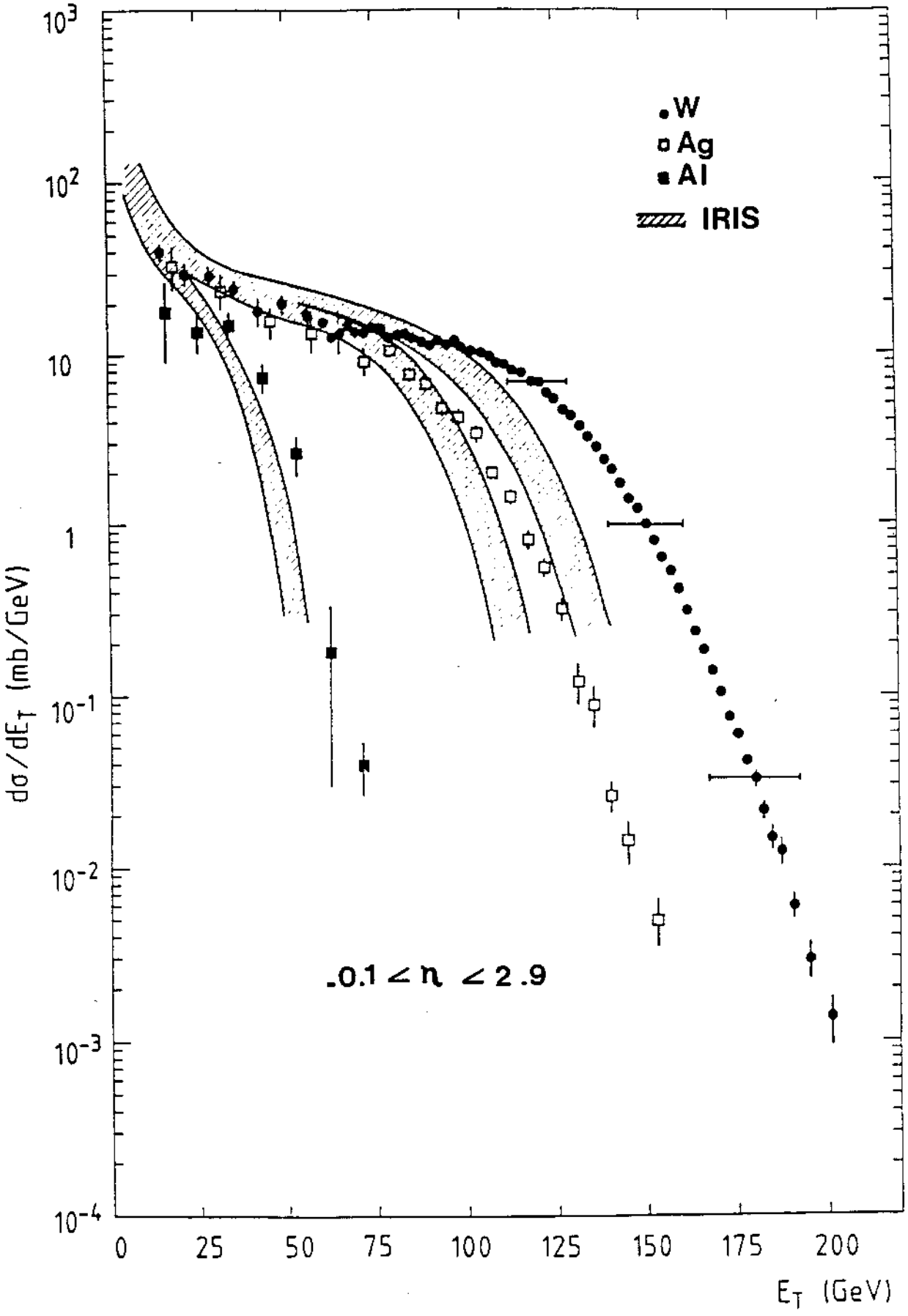
W
Ag
Al
IRIS
10^3
10^2
10
1
10^{-1}
10^{-2}
10^{-3}
10^{-4}
$d\sigma/dE_T$ (mb/GeV)
0
25
50
75
100
125
150
175
200
E_T (GeV)
$-0.1 < \eta < 2.9$

(a)

FIGURE II.5

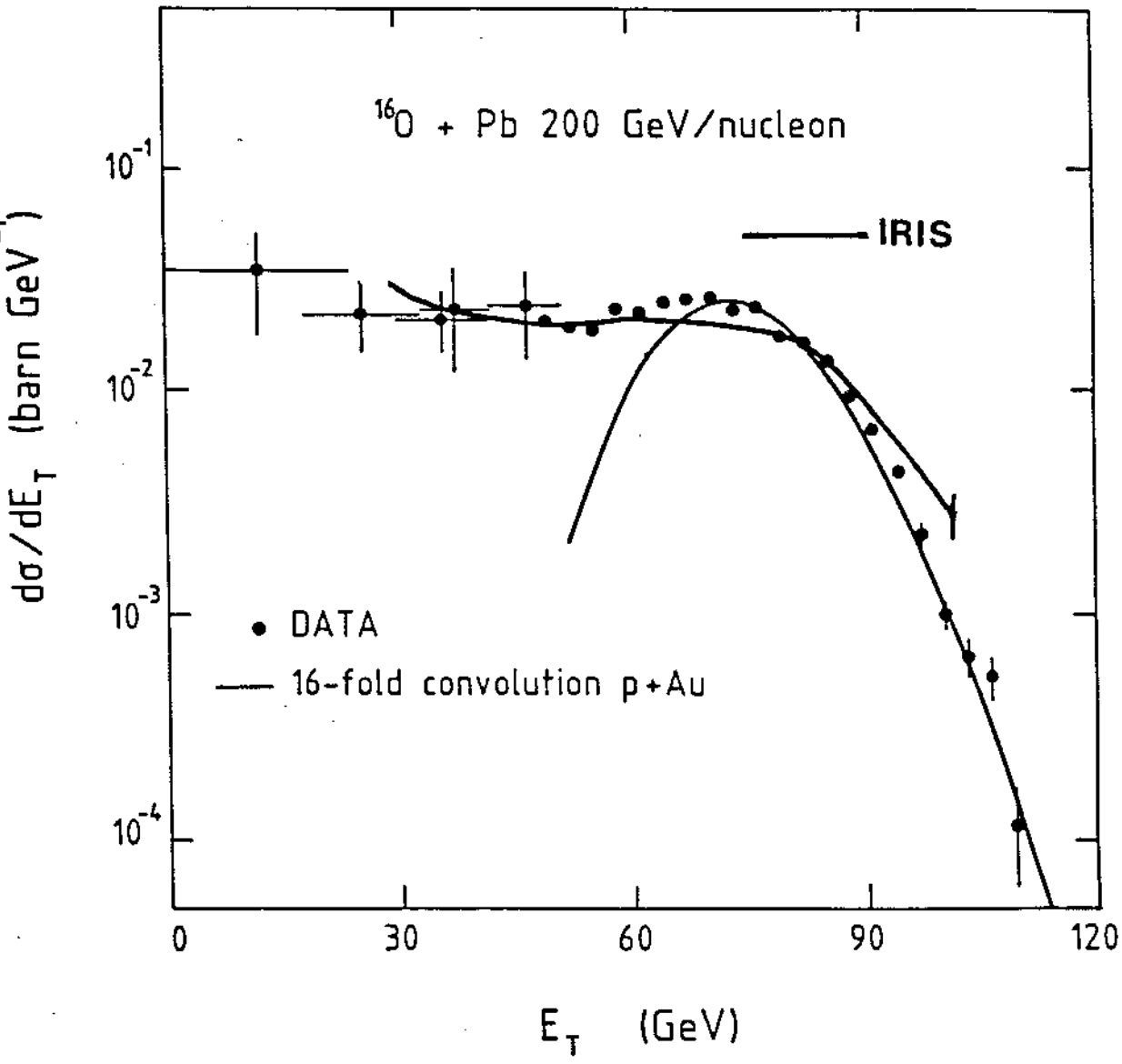
^{16}O + Pb 200 GeV/nucleon
IRIS
DATA
16-fold convolution p+Au
$d\sigma/dE_T$ (barn GeV^{-1})
10^{-1}
10^{-2}
10^{-3}
10^{-4}
0
30
60
90
120
E_T (GeV)
$2.25 \leq \eta \leq 3.8$

(b)

FIGURE II.5.

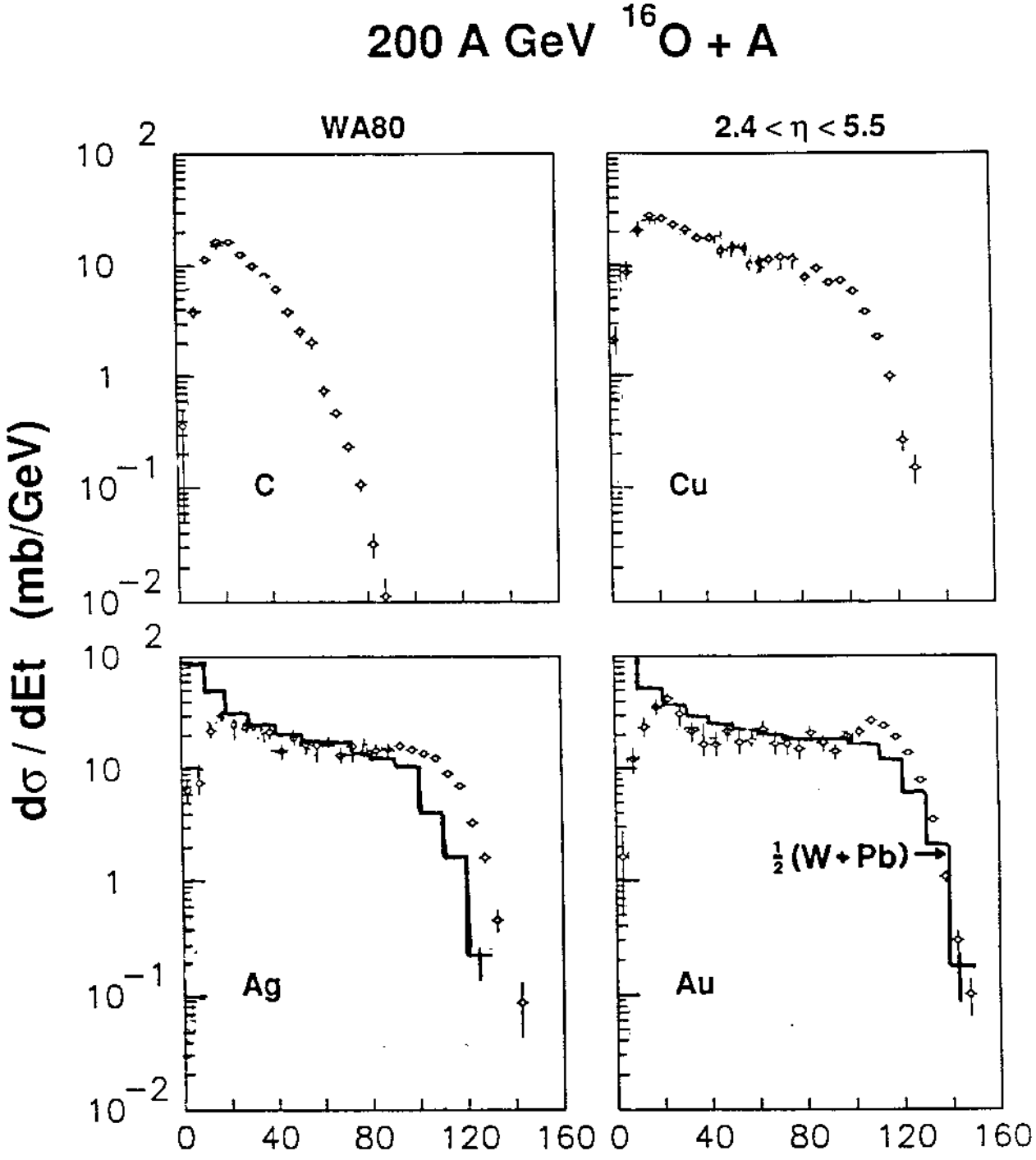
200 A GeV ^{16}O + A
WA80
2.4 < η < 5.5
C
Cu
Ag
Au
½ (W + Pb)
dσ / dEt (mb/GeV)
Transverse Energy (GeV)
o: WA80 data
: IRIS

(c)

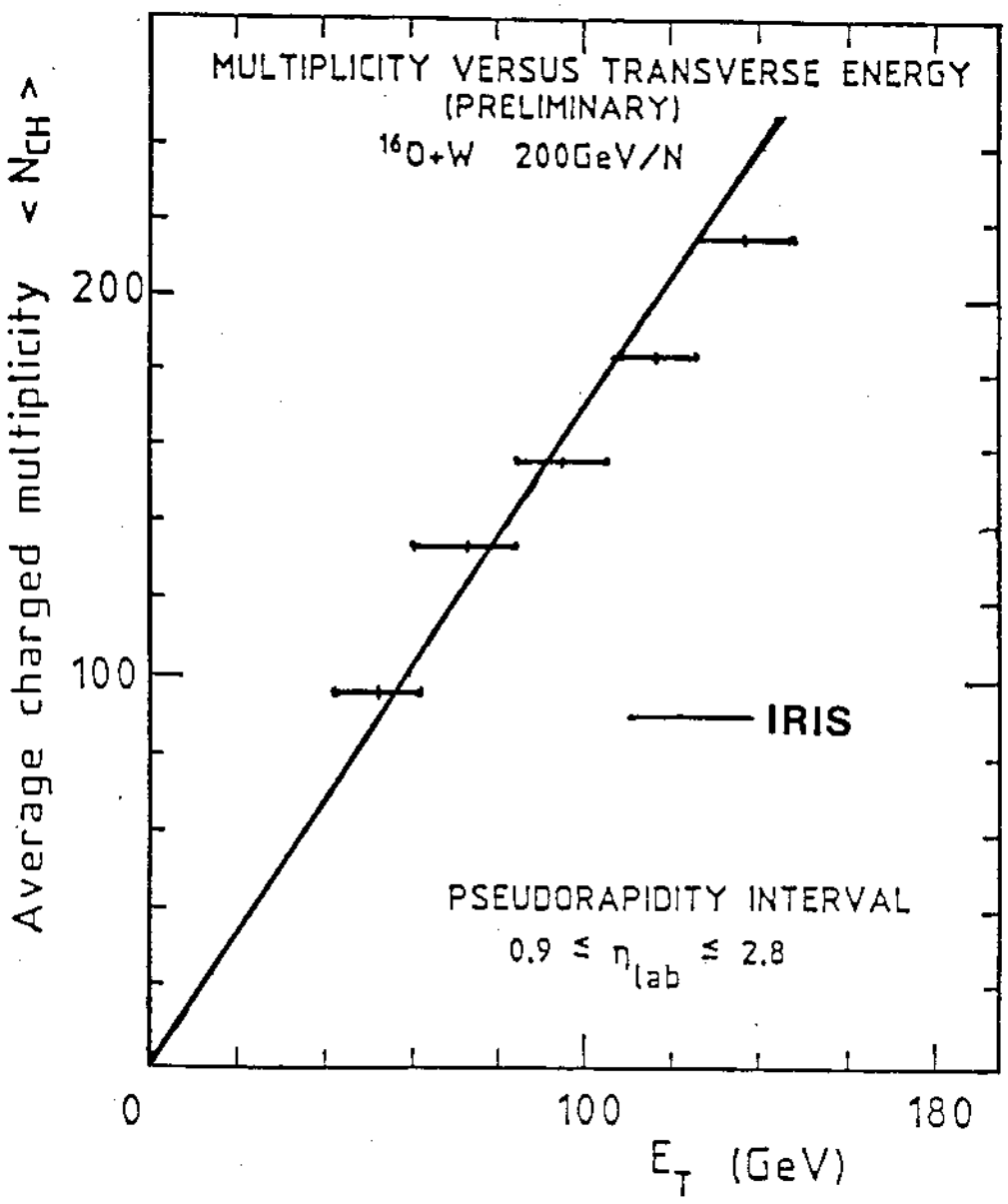
MULTIPLICITY VERSUS TRANSVERSE ENERGY
(PRELIMINARY)
16O+W 200GeV/N
IRIS
PSEUDORAPIDITY INTERVAL
0.9 ≤ η lab ≤ 2.8
Average charged multiplicity < NCH >
200
100
0
100
180
ET (GeV)

(a)

FIGURE II.6.

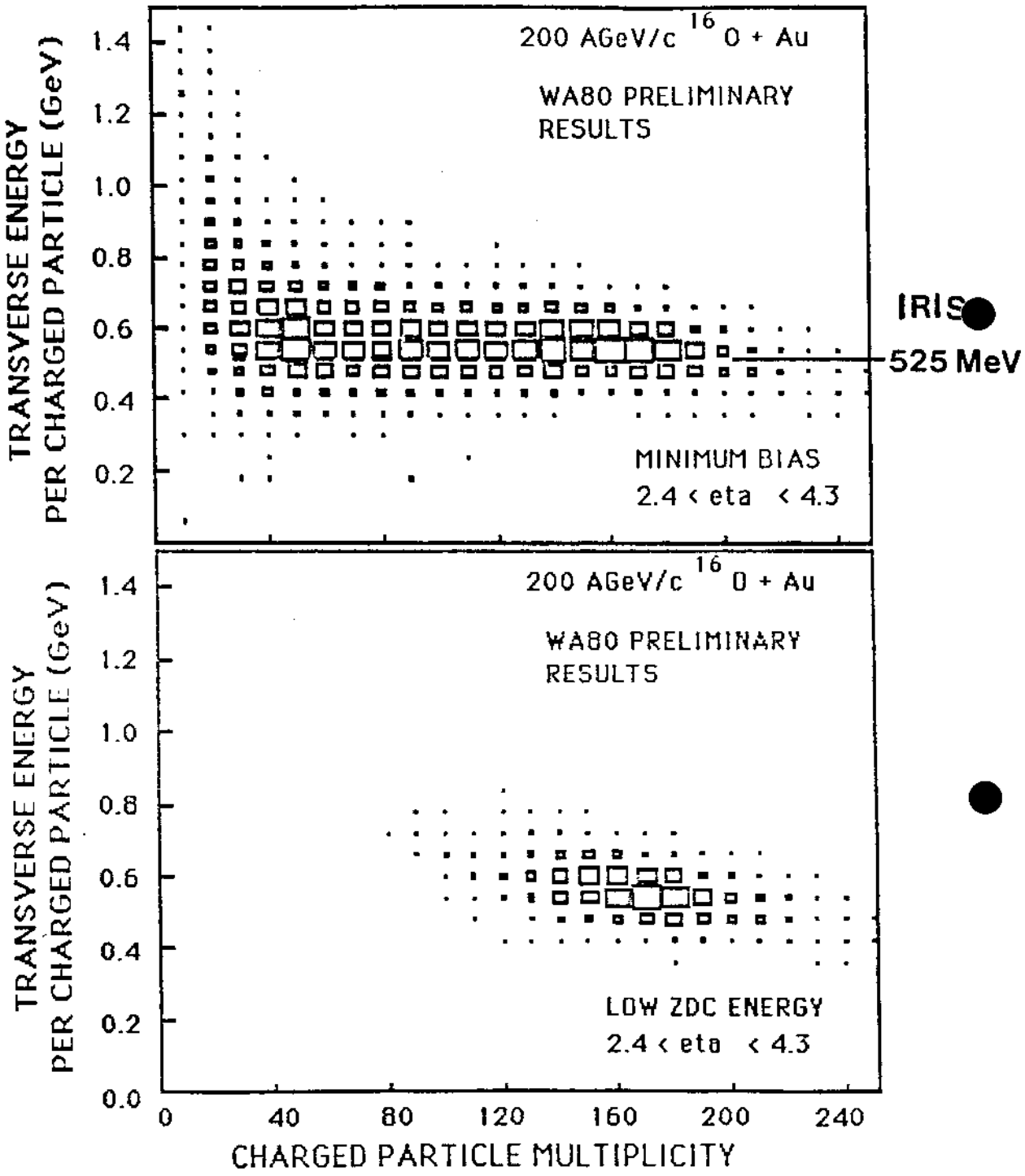
200 AGeV/c 16 O + Au
WA80 PRELIMINARY
RESULTS
MINIMUM BIAS
2.4 < eta < 4.3
IRIS
525 MeV
TRANSVERSE ENERGY
PER CHARGED PARTICLE (GeV)
200 AGeV/c 16 O + Au
WA80 PRELIMINARY
RESULTS
LOW ZDC ENERGY
2.4 < eta < 4.3
TRANSVERSE ENERGY
PER CHARGED PARTICLE (GeV)
0.0
0.2
0.4
0.6
0.8
1.0
1.2
1.4
0
40
80
120
160
200
240
CHARGED PARTICLE MULTIPLICITY

(b)

FIGURE II.6.

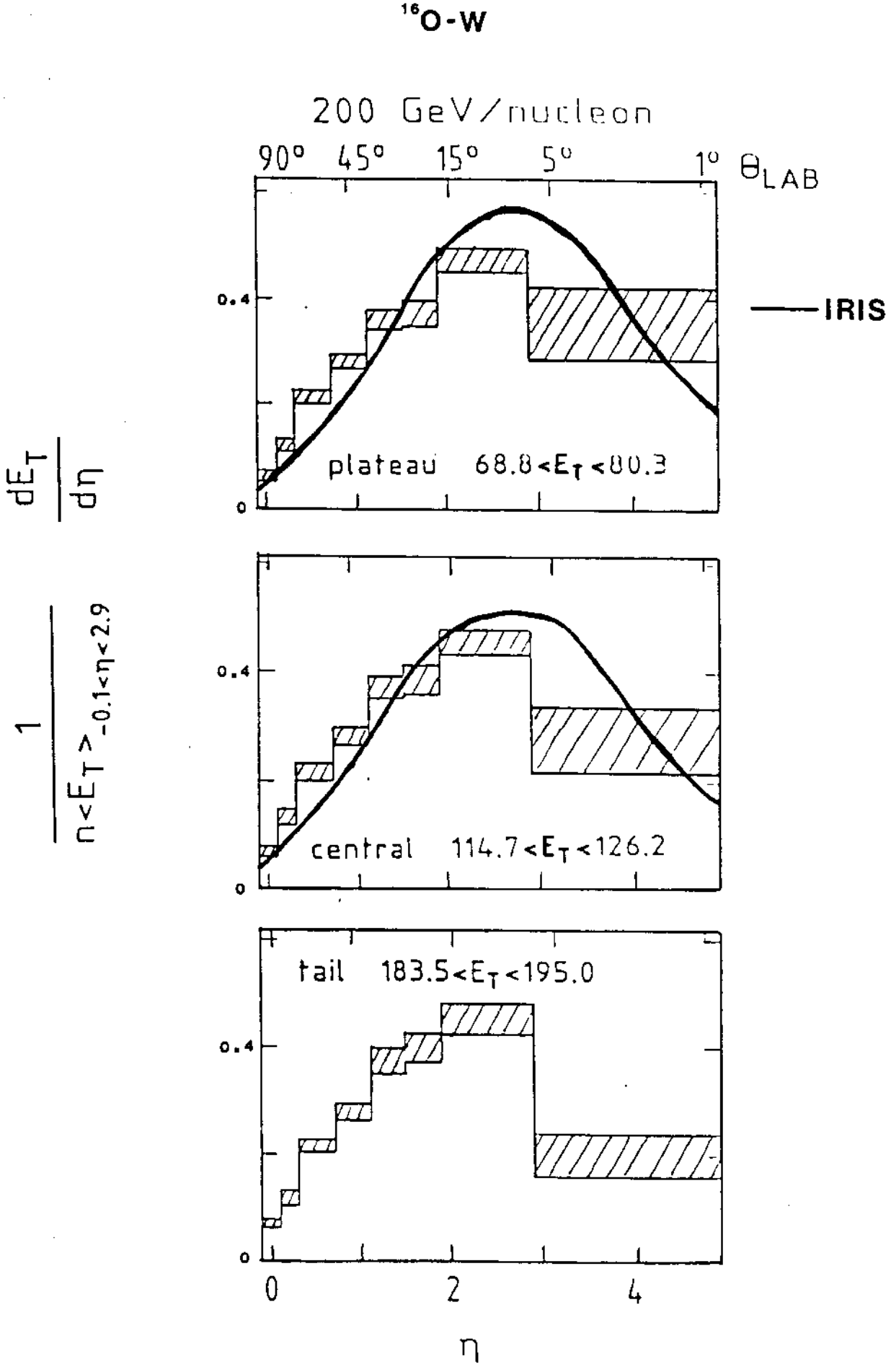
^{16}O-W
200 GeV/nucleon
90° 45° 15° 5° 1° θ_{LAB}
IRIS
plateau 68.8<E_T<80.3
central 114.7<E_T<126.2
tail 183.5<E_T<195.0
0.4
0
0
2
4
η
$\frac{dE_T}{d\eta}$
$\frac{1}{n<E_T>_{-0.1<\eta<2.9}}$

FIGURE II.7.

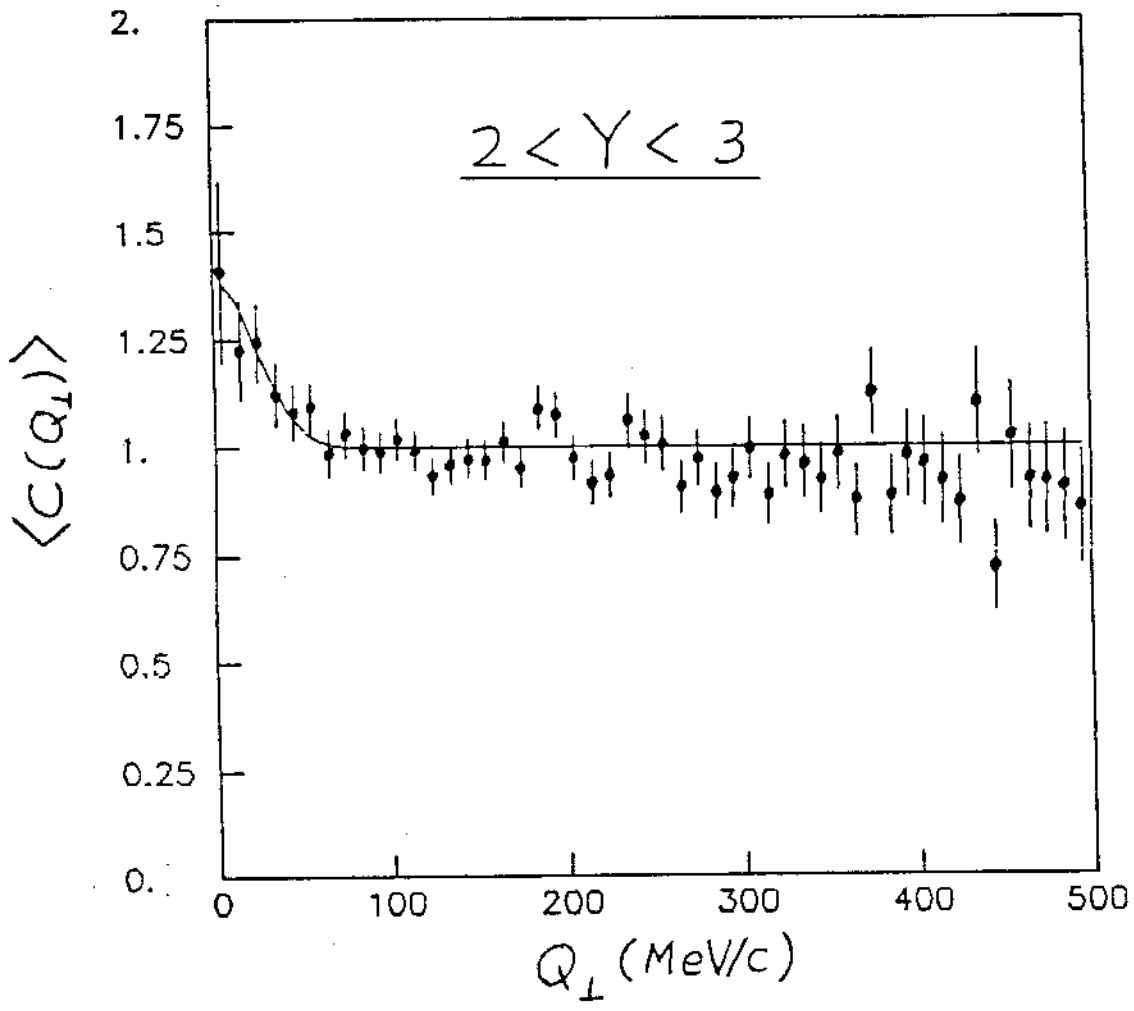

(a)

FIGURE II.8.

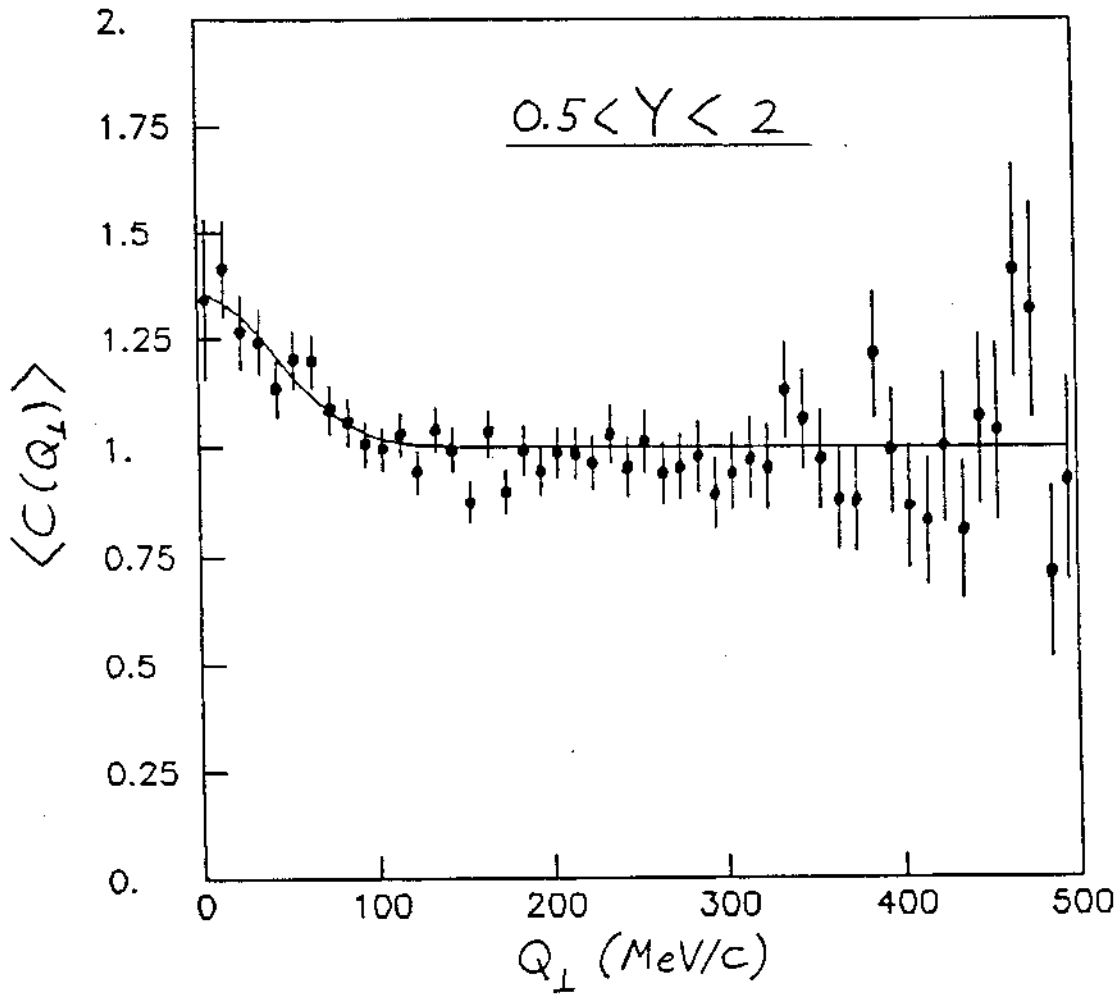
0.5<Y<2
2.
1.75
1.5
1.25
1.
0.75
0.5
0.25
0.
0
100
200
300
400
500
$\langle C(Q_\perp)\rangle$
$Q_\perp$ (MeV/c)

(b)

FIGURE II.8.

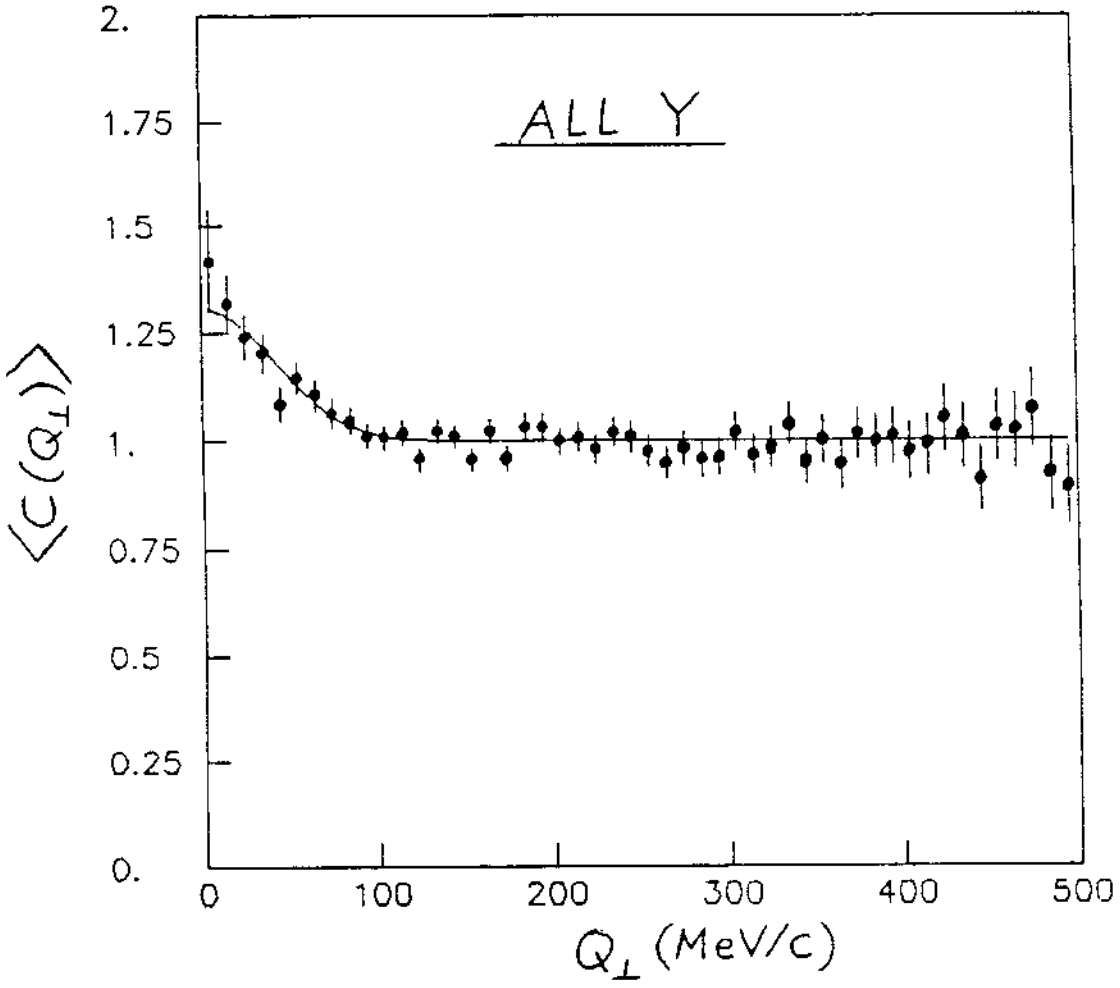
ALL Y
2.
1.75
1.5
1.25
1.
0.75
0.5
0.25
0.
0
100
200
300
400
500
$\langle C(Q_\perp)\rangle$
$Q_\perp$ (MeV/c)

(c)

FIGURE II.8.

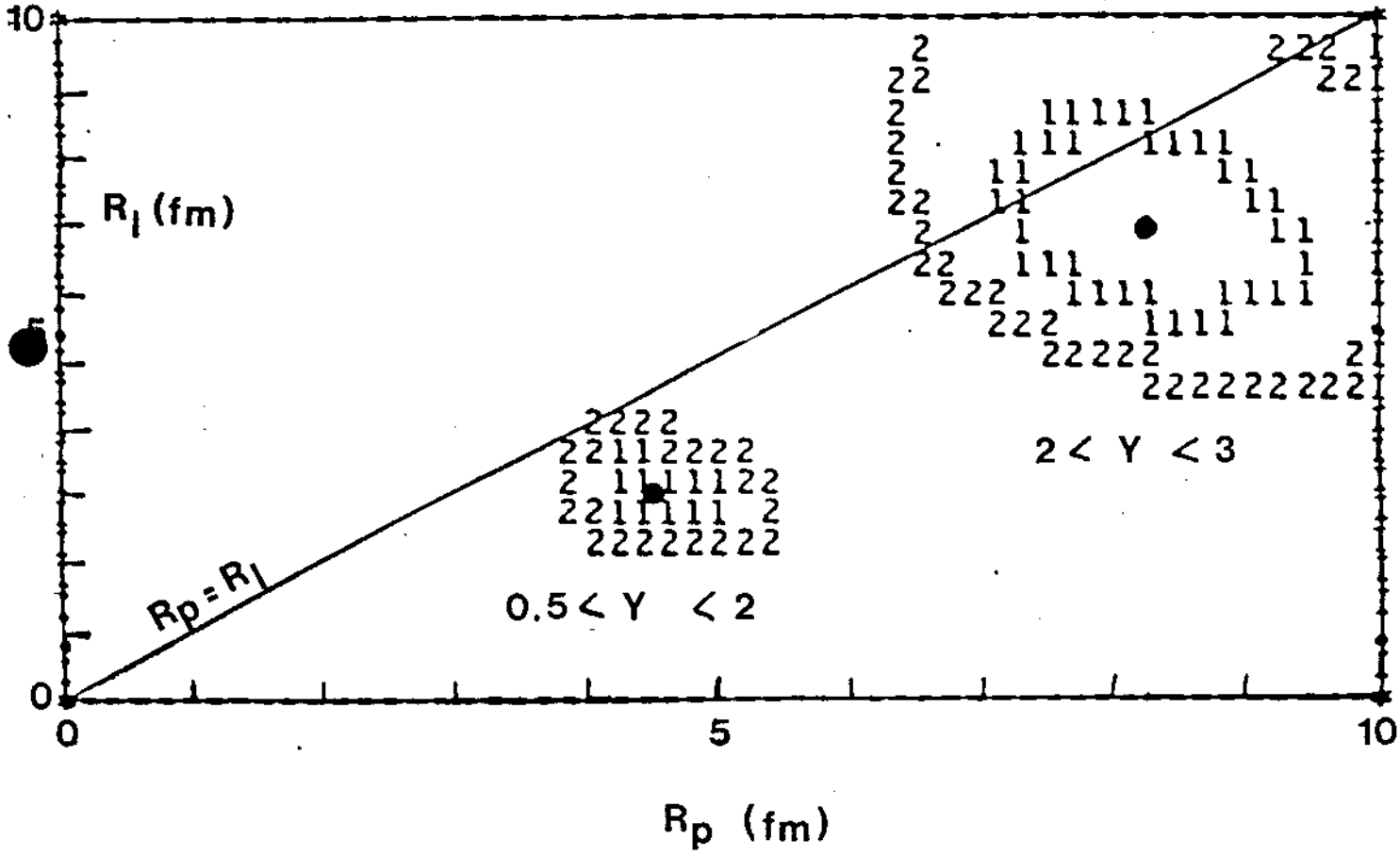

FIGURE II.9.

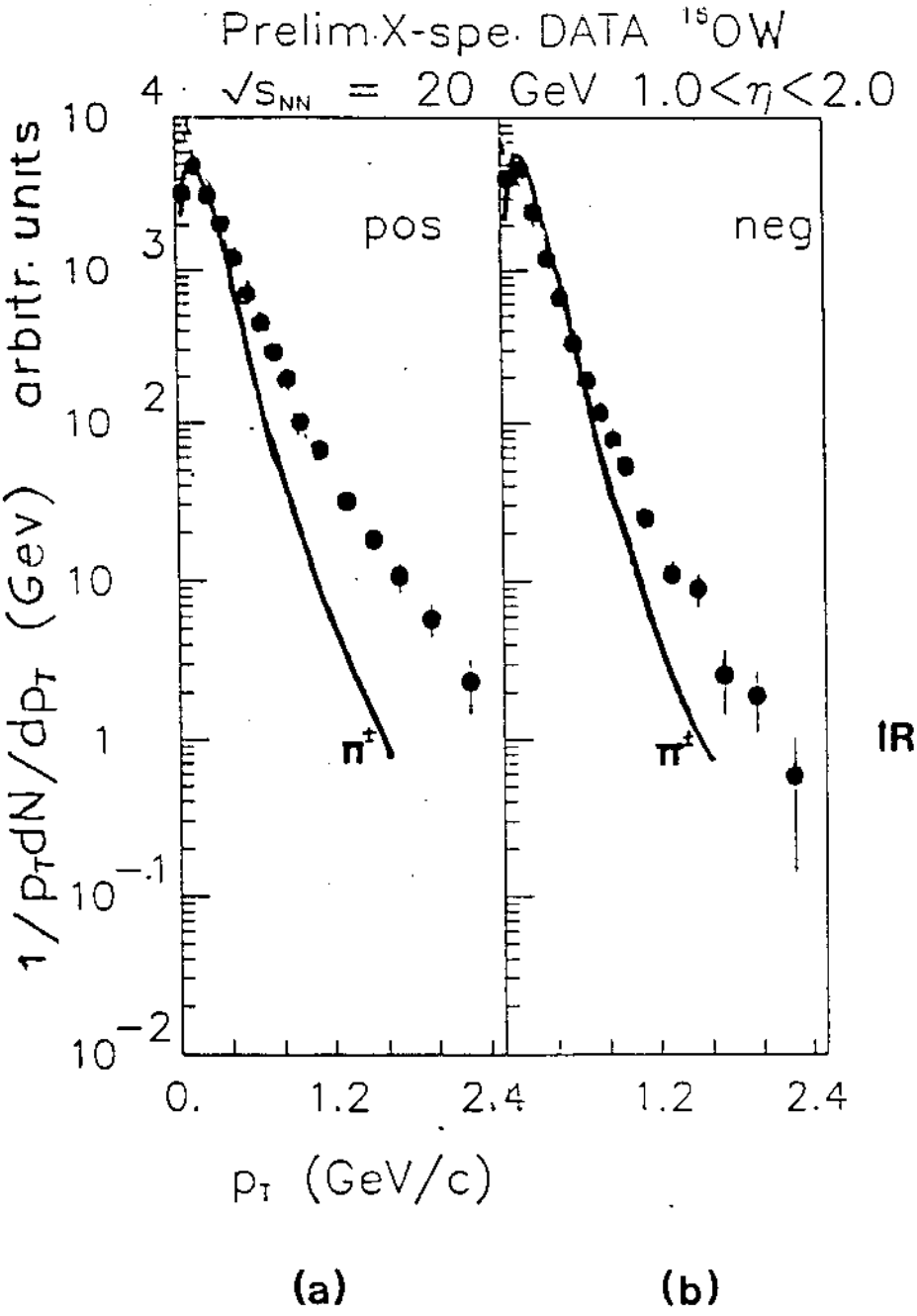
Prelim X-spe. DATA ^{16}OW
$\sqrt{s_{NN}}$ = 20 GeV 1.0<η<2.0
pos
neg
π^+
π^+
$1/p_T dN/dp_T$ (Gev) arbitr. units
p_T (GeV/c)
0.
1.2
2.4
1.2
2.4
IRIS
(a)
(b)

FIGURE II.10.

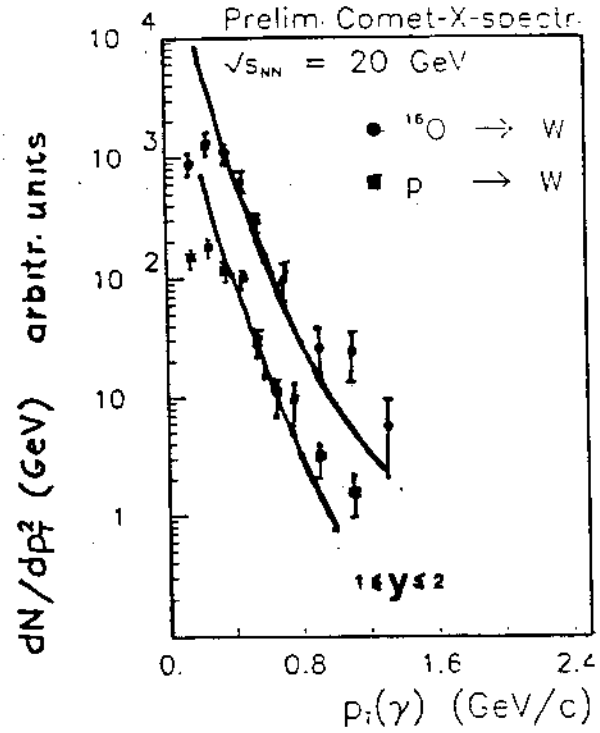

(a)

— IRIS ^{16}O-W

p - Pb

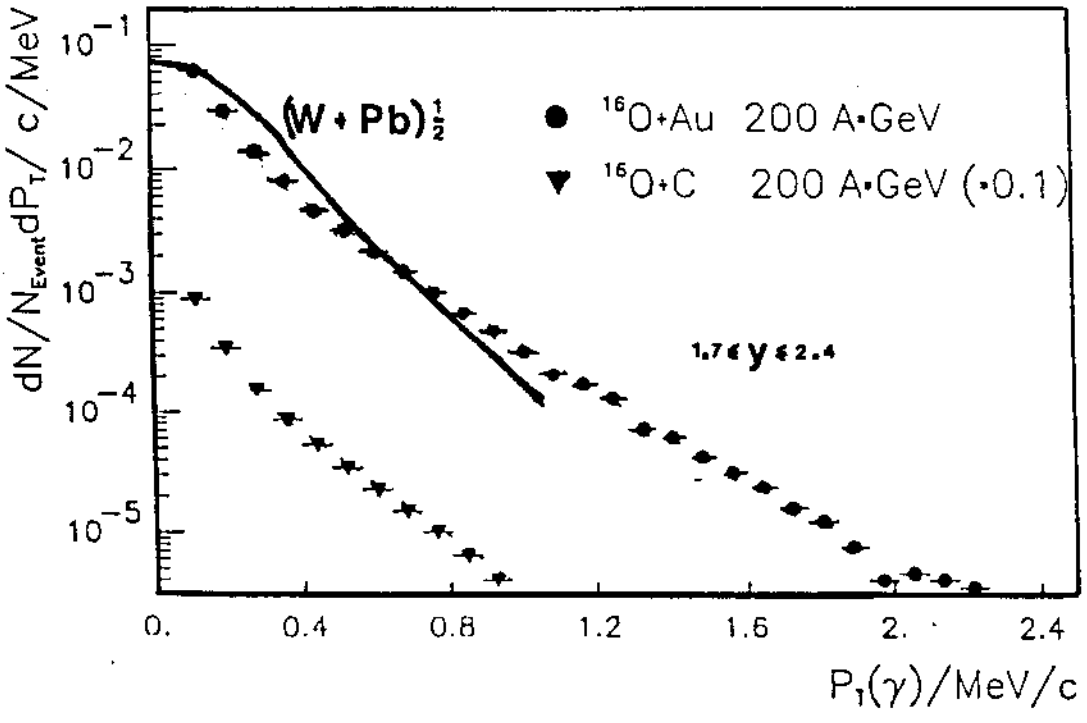

(b)

FIGURE II.11.

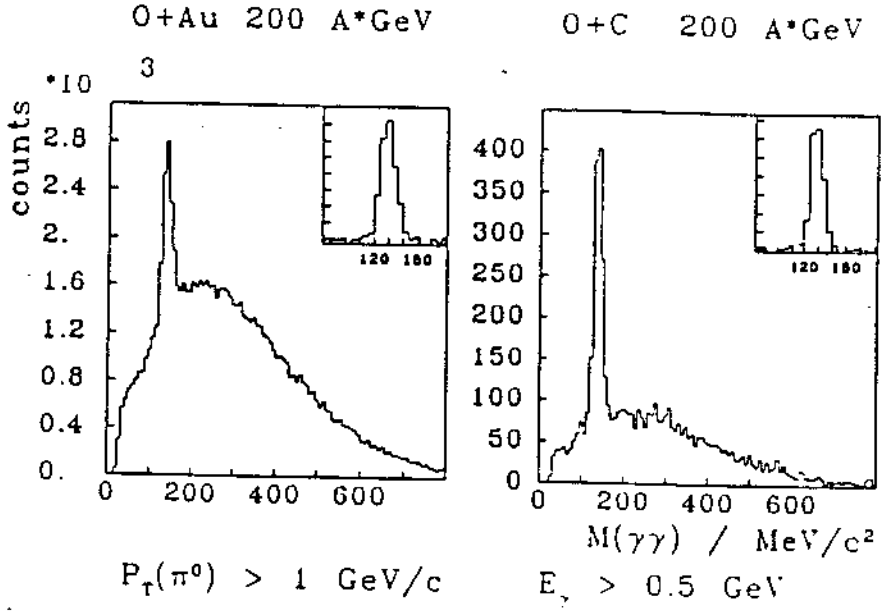
O+Au 200 A*GeV
O+C 200 A*GeV
*10 3
counts
2.8
2.4
2.
1.6
1.2
0.8
0.4
0.
0 200 400 600
120 180
400
350
300
250
200
150
100
50
0
0 200 400 600
120 180
M(γγ) / MeV/c²
P_T(π⁰) > 1 GeV/c
E_γ > 0.5 GeV

(a)

—— IRIS ^{16}O-W

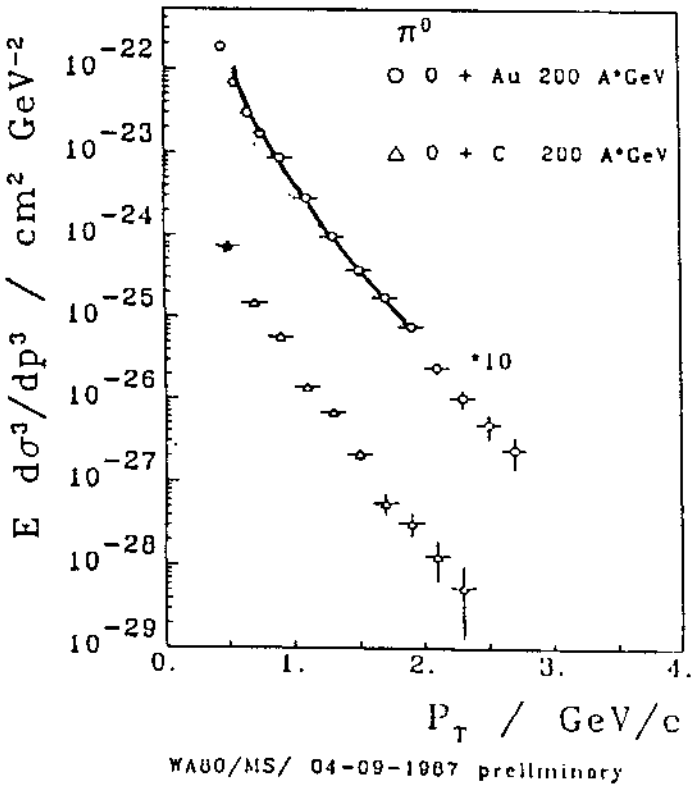
π⁰
O 0 + Au 200 A*GeV
△ 0 + C 200 A*GeV
*10
E dσ³/dp³ / cm² GeV⁻²
10⁻²²
10⁻²³
10⁻²⁴
10⁻²⁵
10⁻²⁶
10⁻²⁷
10⁻²⁸
10⁻²⁹
0. 1. 2. 3. 4.
P_T / GeV/c
WA80/MS/ 04-09-1987 preliminary

(b)

^{16}O - W

Charged Particles

$1.15 \leq \eta \leq 1.65$

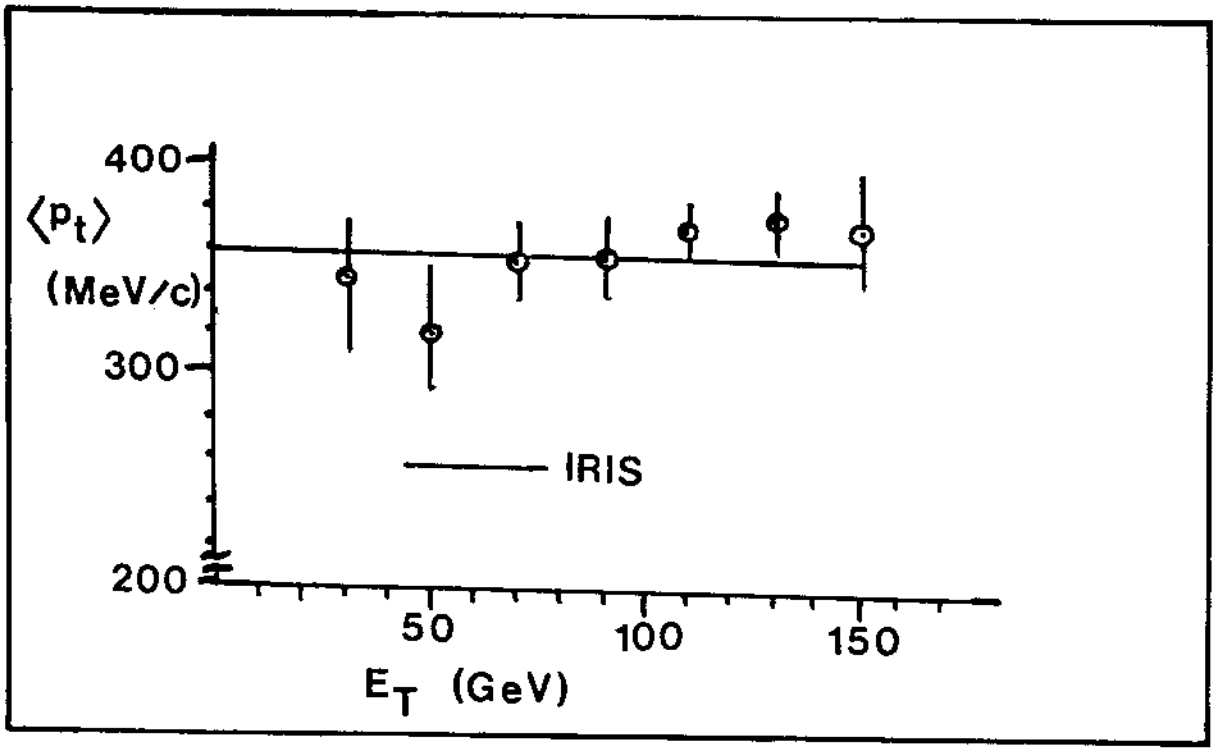

FIGURE II.13.

^{16}O-Au

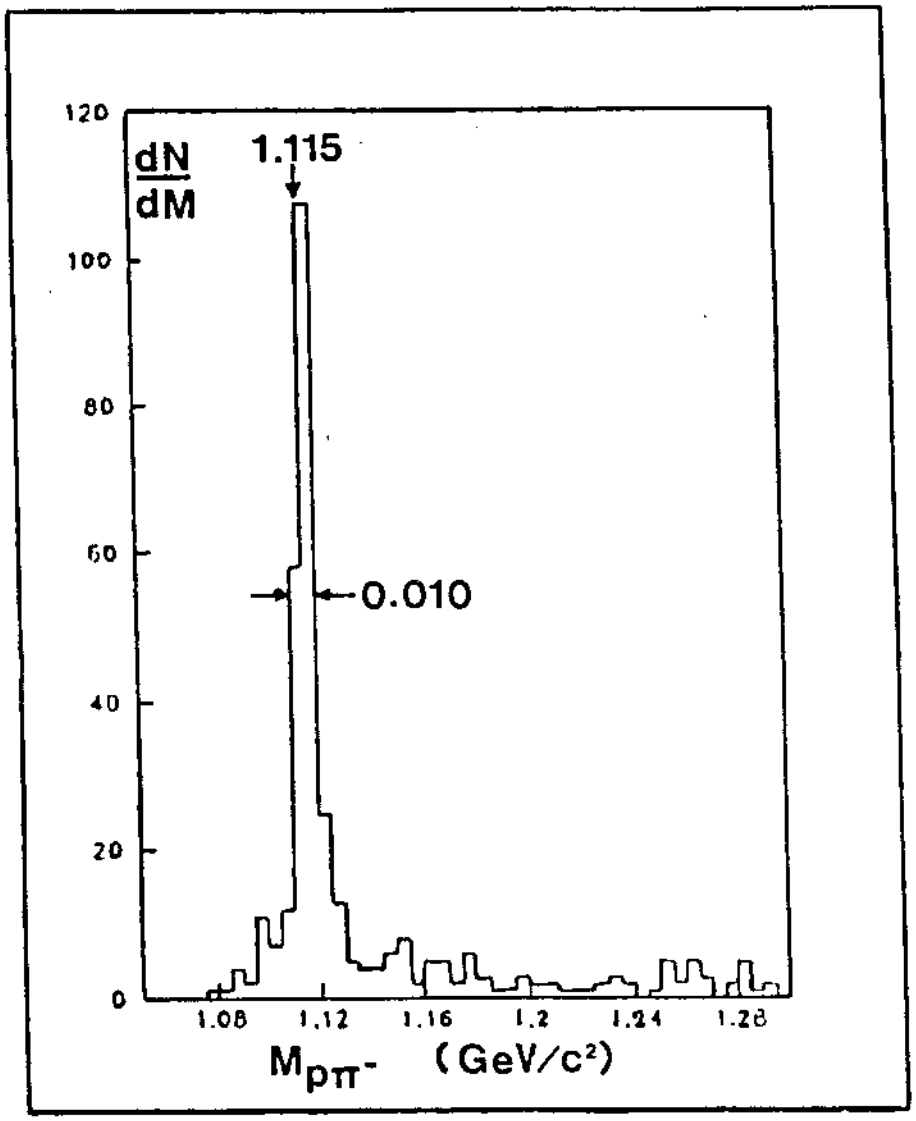

FIGURE II.14.

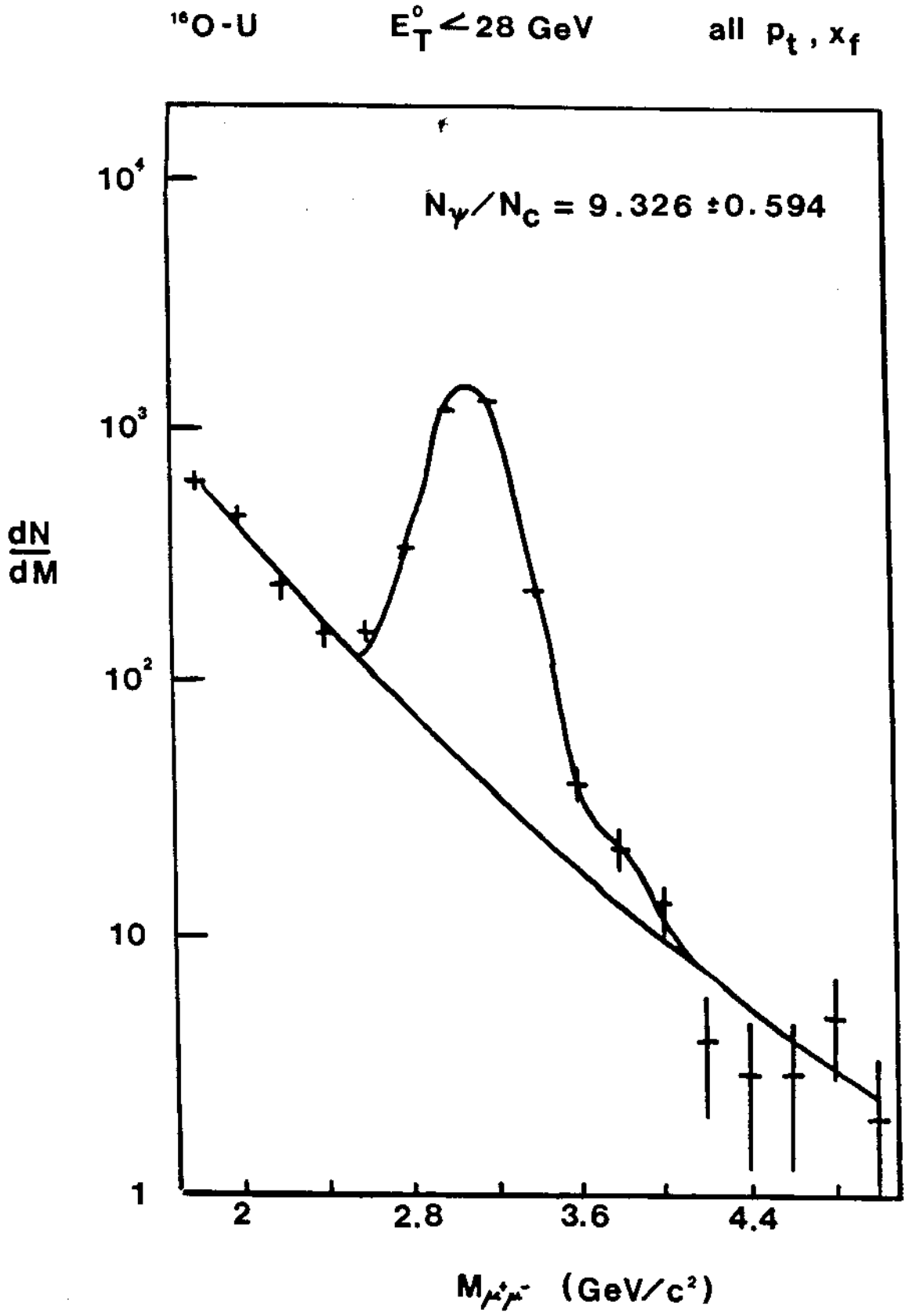

(a)

FIGURE II.15.

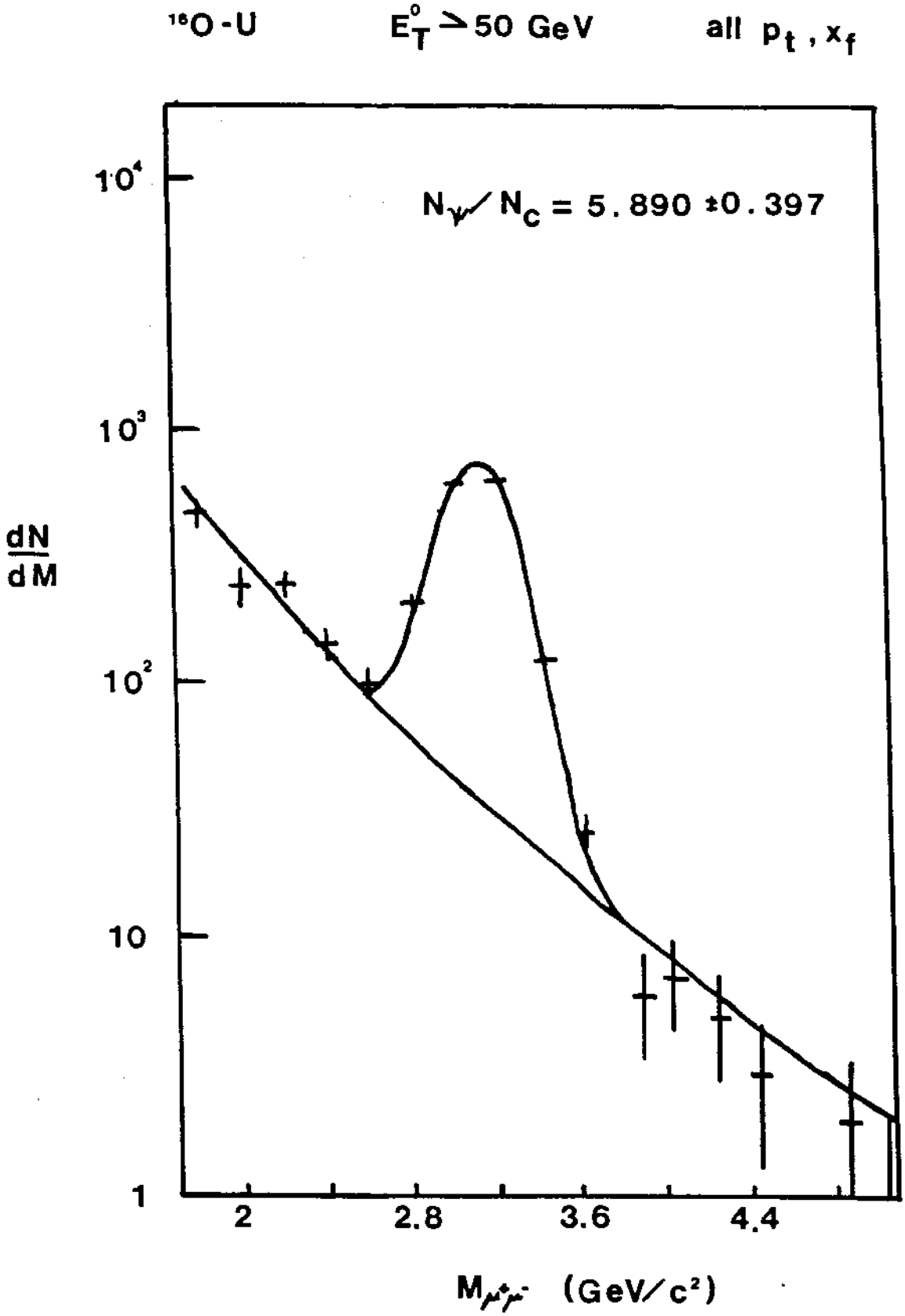

(b)

FIGURE II.15.

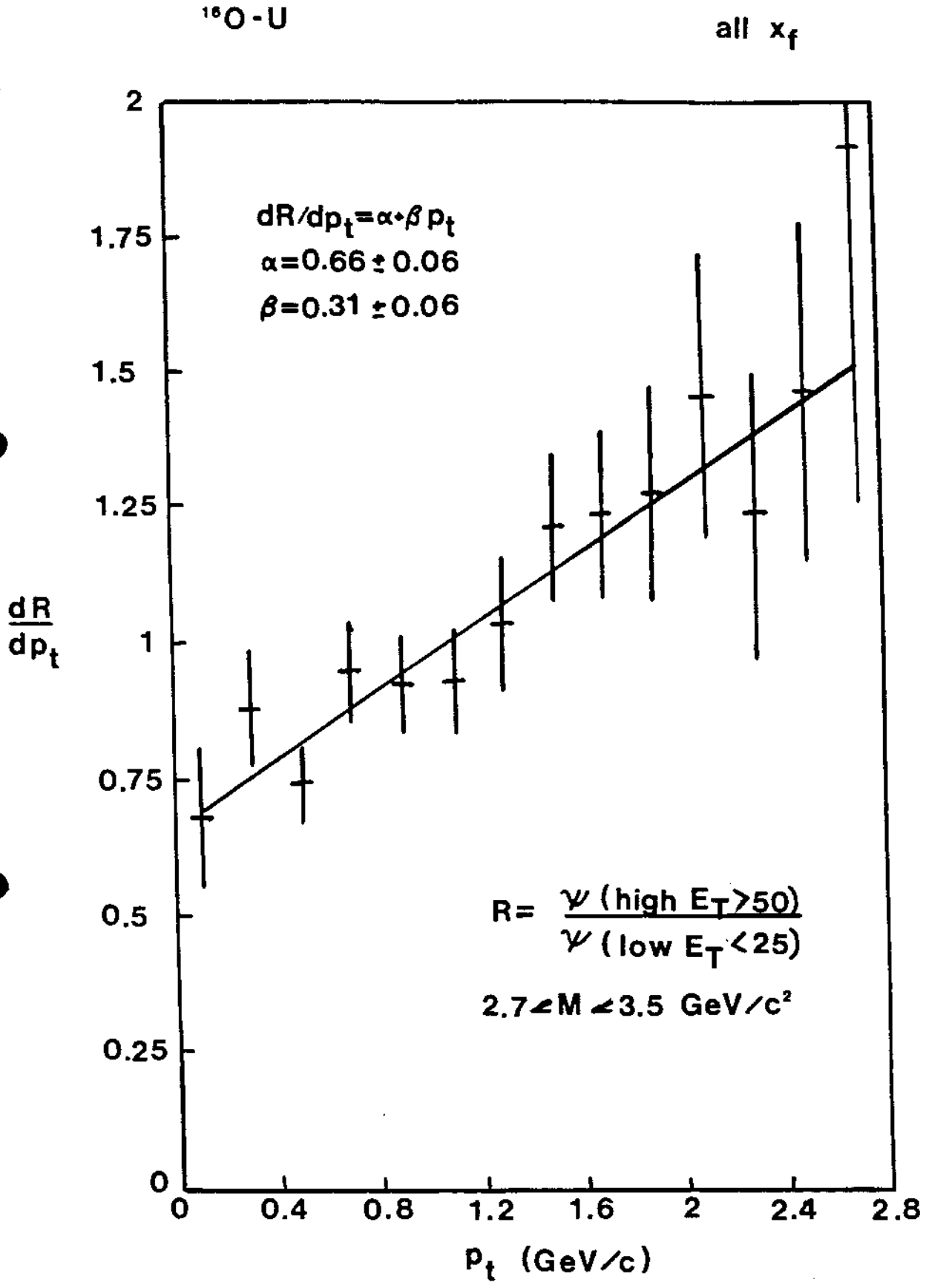
^{16}O - U
all x_f
$dR/dp_t = \alpha + \beta p_t$
$\alpha = 0.66 \pm 0.06$
$\beta = 0.31 \pm 0.06$
$R = \frac{\psi (\text{high } E_T > 50)}{\psi (\text{low } E_T < 25)}$
$2.7 < M < 3.5$ GeV/c^2
$\frac{dR}{dp_t}$
p_t (GeV/c)
0
0.25
0.5
0.75
1
1.25
1.5
1.75
2
0.4
0.8
1.2
1.6
2.4
2.8

FIGURE II.16.

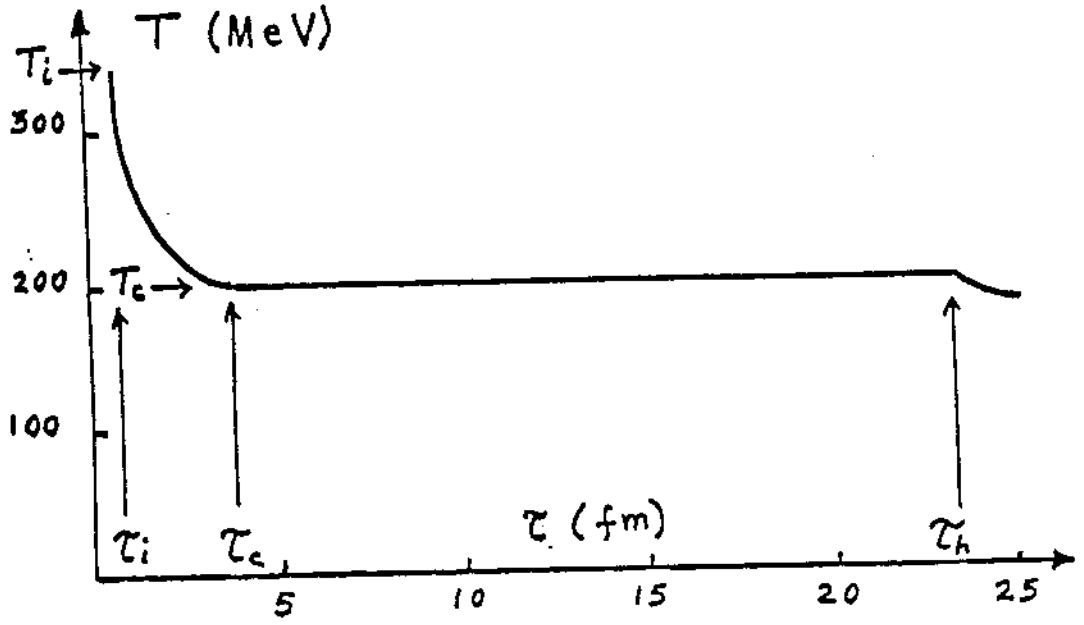

FIGURE III.1.

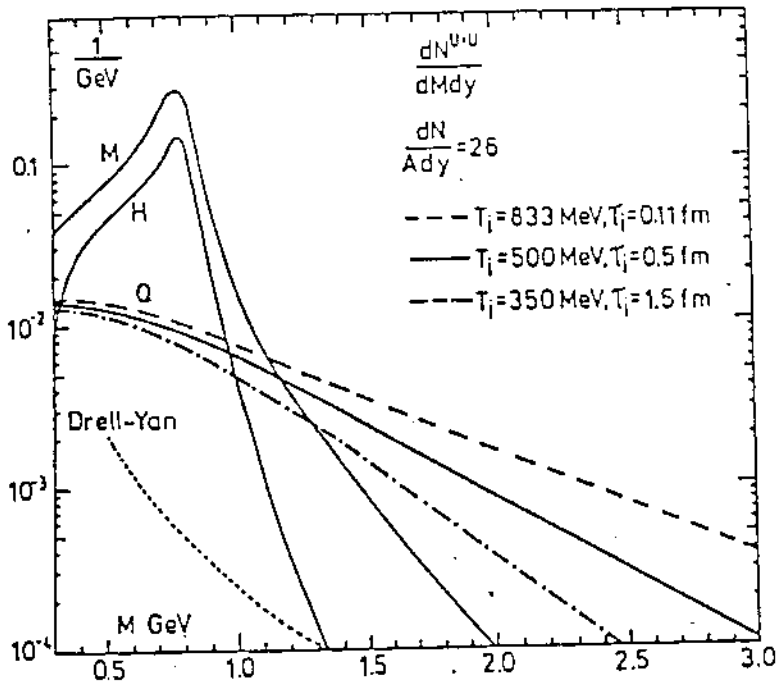

FIGURE III.2.

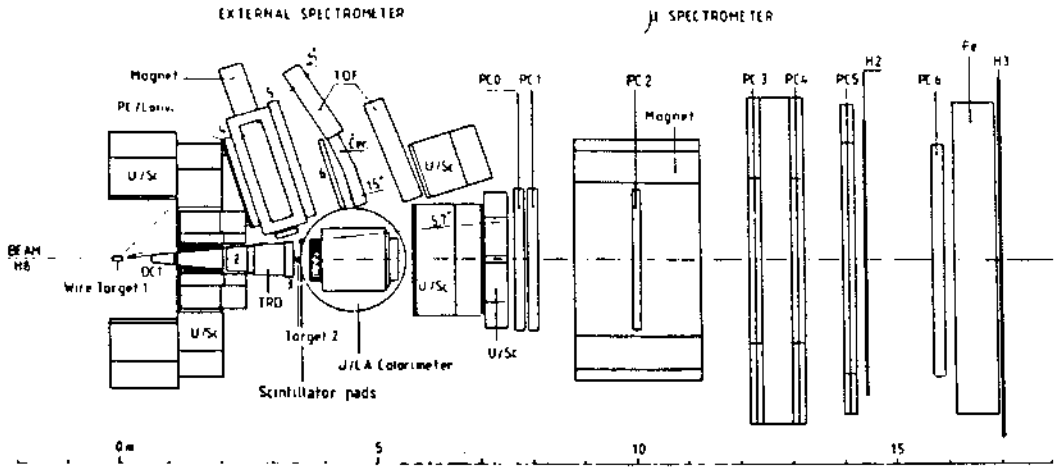

(a) Experiment NA34/2: Study of High Energy Densities over Extended Nuclear Volumes via Nucleus-Nucleus Collisions at the SPS

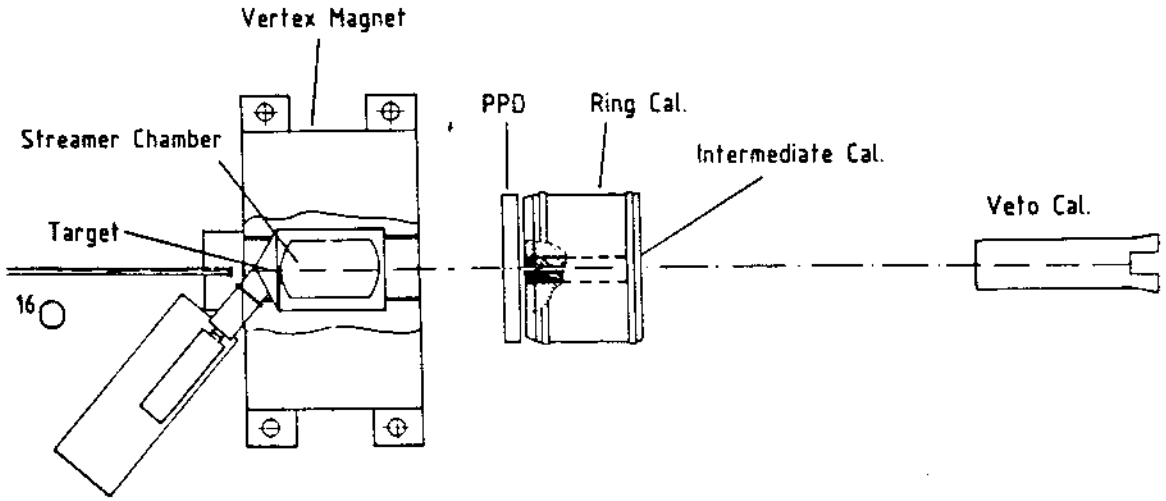

(b) Experiment NA35: Study of Relativistic Nucleus-nucleus Collisions

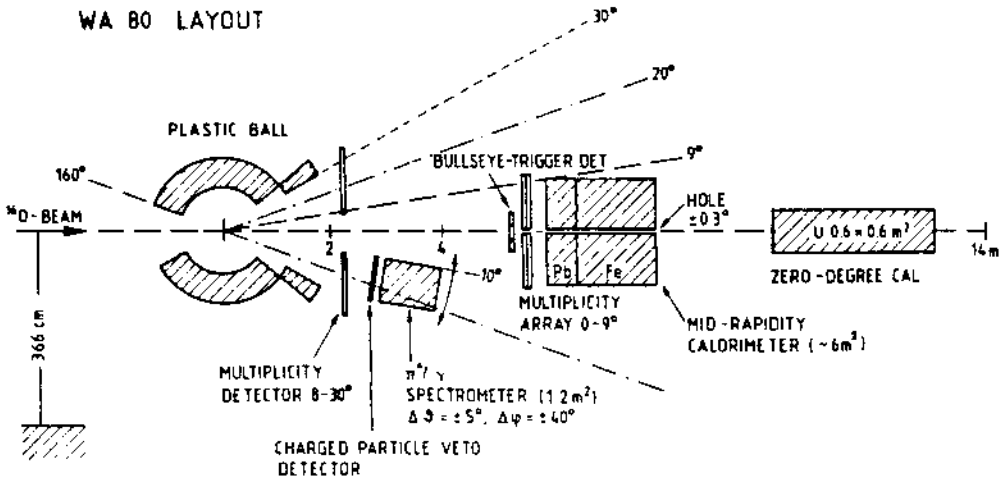

(c) Experiment WA80: Study of Relativistic Nucleus-Nucleus Collisions at the CERN SPS

FIGURE IV.1.

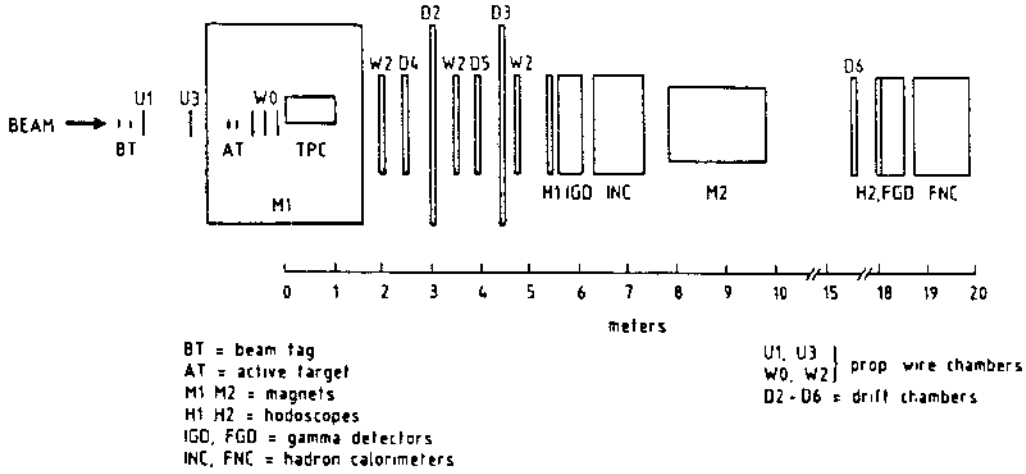

(d) Experiment NA36: Production of Strange Baryons and Antibaryons in Relativistic Ion Collisions

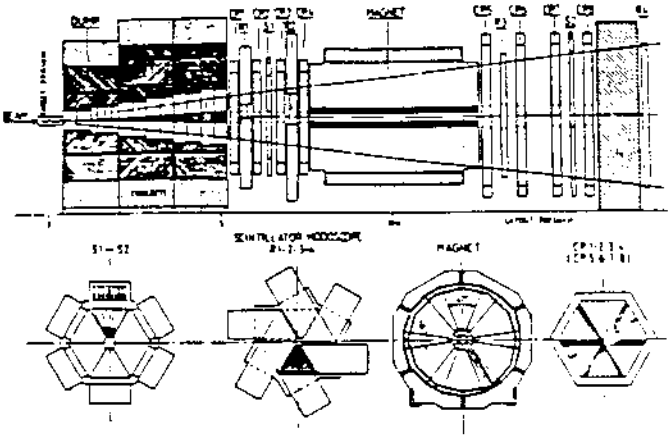

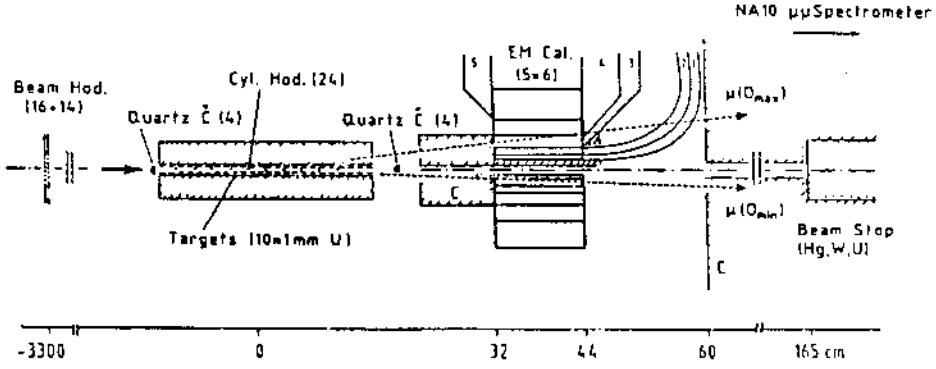

The proposed layout: the NA10 spectrometer (top), front view of its main components (middle), target region (bottom — note scale! C = quartz, Ph/Sc are Pb and scintillating fibre structures).

(e) Experiment NA38: Study of High-Energy Nucleus-Nucleus Interactions with the Enlarged NA10 Dimuon Spectrometer

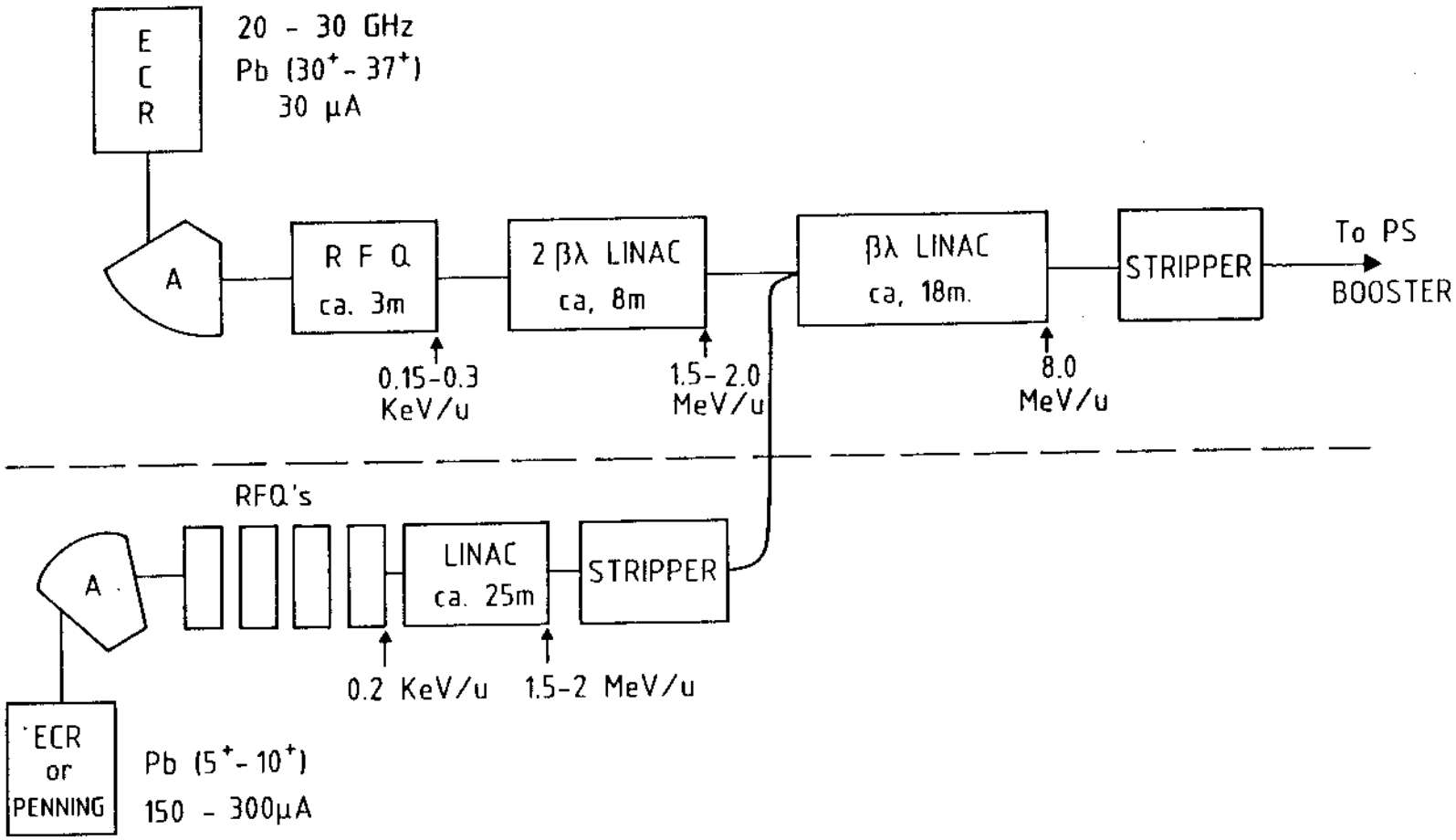
E
C
R
20 - 30 GHz
Pb (30⁺ - 37⁺)
30 μA
A
R F Q
ca. 3m
2 βλ LINAC
ca, 8m
βλ LINAC
ca, 18m.
STRIPPER
To PS
BOOSTER
0.15-0.3
KeV/u
1.5- 2.0
MeV/u
8.0
MeV/u
RFQ's
A
LINAC
ca. 25m
STRIPPER
0.2 KeV/u
1.5-2 MeV/u
ECR
or
PENNING
Pb (5⁺ - 10⁺)
150 - 300μA

FIGURE V.1.

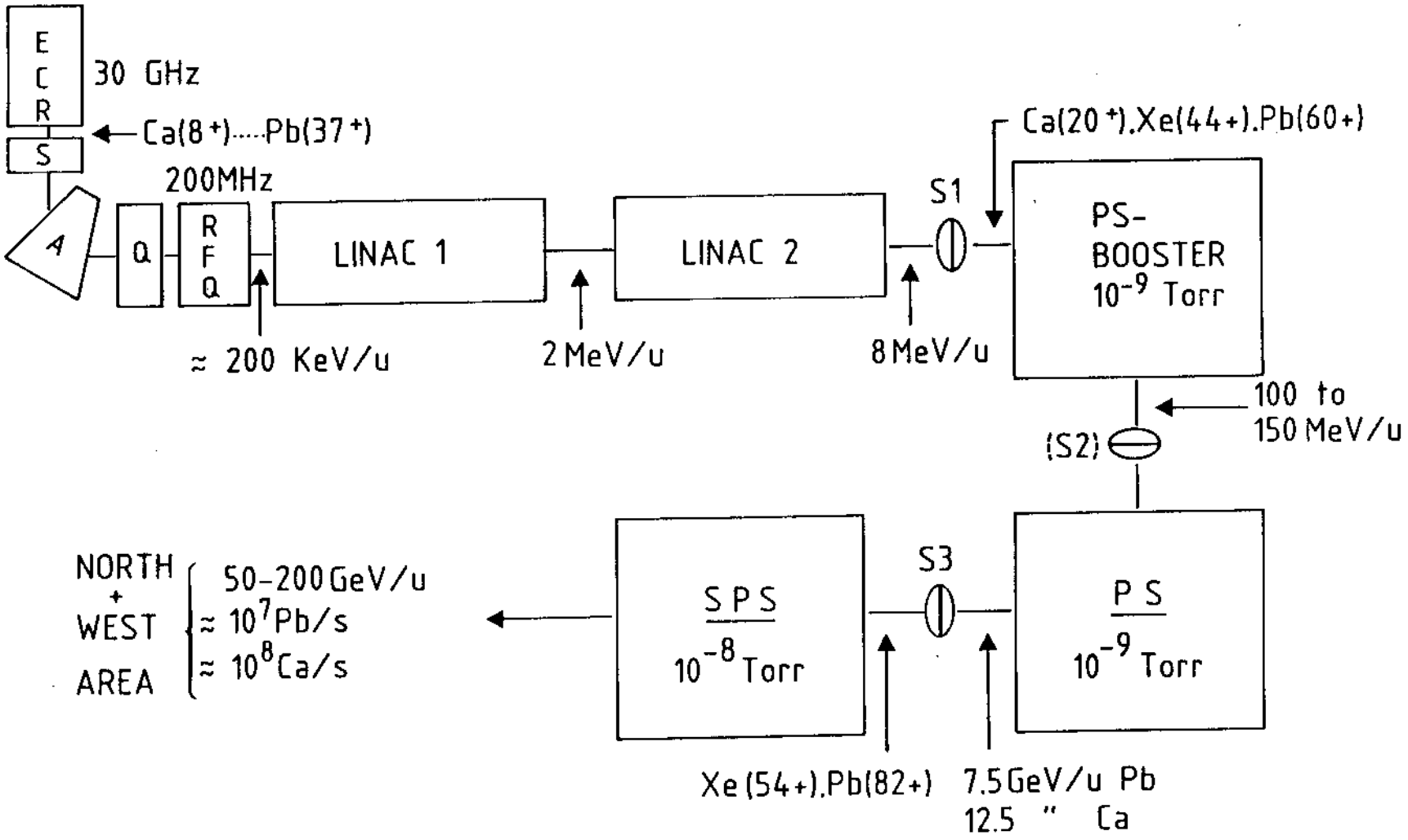
E
C
R
S
30 GHz
Ca(8+)....Pb(37+)
200MHz
A
Q
R
F
Q
LINAC 1
LINAC 2
S1
Ca(20+).Xe(44+).Pb(60+)
PS-
BOOSTER
10-9 Torr
≈ 200 KeV/u
2 MeV/u
8 MeV/u
100 to
150 MeV/u
(S2)
NORTH
+
WEST
AREA
50-200 GeV/u
≈ 10^7 Pb/s
≈ 10^8 Ca/s
SPS
10-8 Torr
S3
PS
10-9 Torr
Xe(54+).Pb(82+)
7.5 GeV/u Pb
12.5 " Ca

FIGURE V.2.

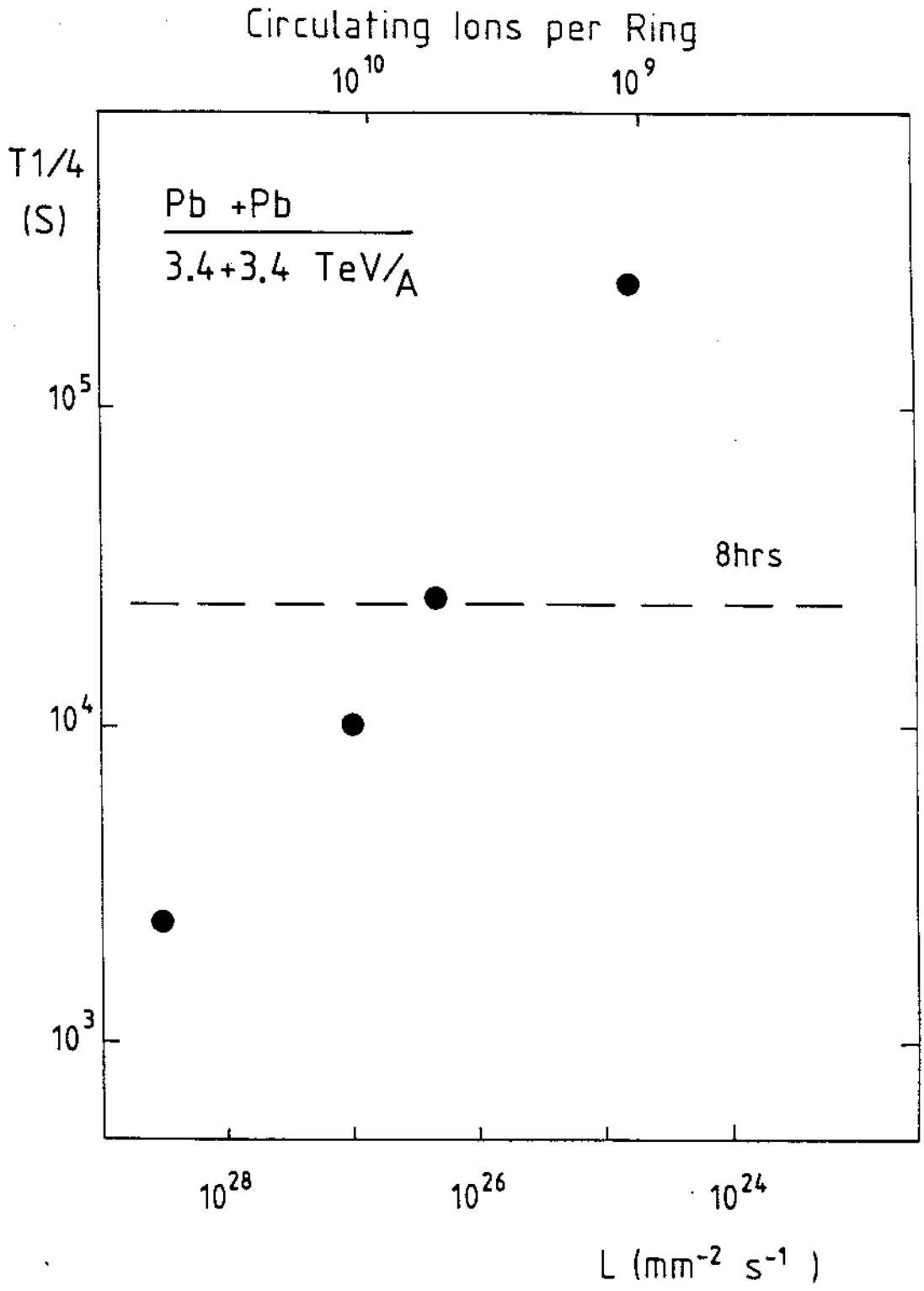
Circulating Ions per Ring
10^{10}
10^{9}
T1/4
(S)
Pb +Pb
3.4+3.4 TeV/A
10^{5}
8hrs
10^{4}
10^{3}
10^{28}
10^{26}
10^{24}
L (mm^{-2} s^{-1})

FIGURE V.3.

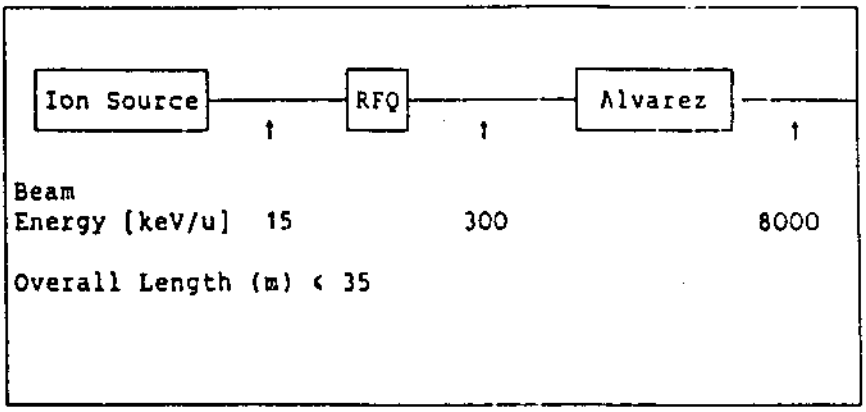

FIGURE V.4.

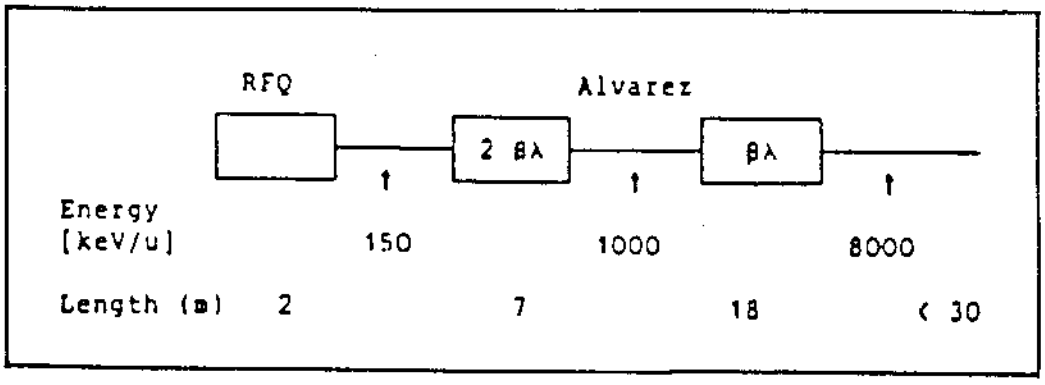

FIGURE V.5.